Elucidating the Role of WDR47 in Regulating Neuronal migration, Autophagy, and Tubulin Dynamics
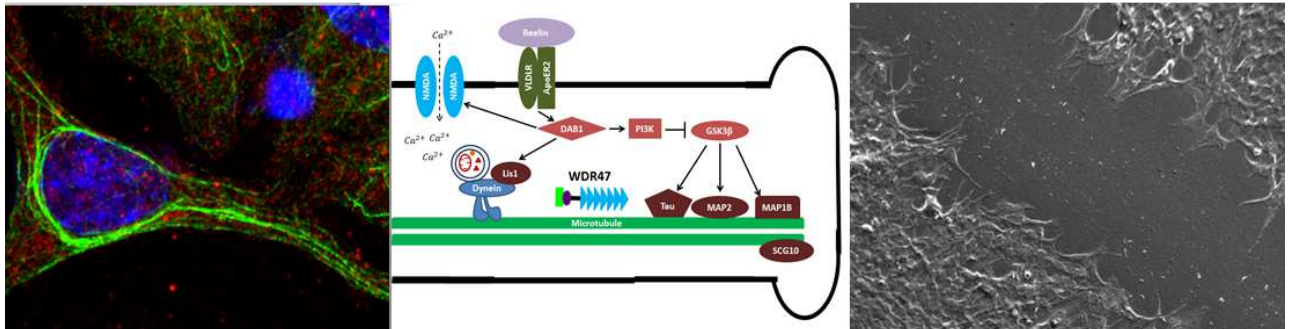
By

Marna Roos

Thesis presented in partial fulfilment of the requirements for the Degree of Masters of Science in Physiological Sciences at Stellenbosch University

Supervisor: Dr Ben Loos

Co-supervisor: Dr Craig Kinnear

....)

Elucidating the Role of WDR47 in Regulating Neuronal migration, Autophagy, and Tubulin Dynamics

September 2014

Declaration

I, the undersigned, hereby declare that the work contained in this thesis is my own original work, that no plagiarism was committed, and that I have not previously in its entirety or in part submitted it at any university for a degree.

Signature: …………………………………………..

Date: …………………………………………..

o   y

Abstract

Introduction

Normal cerebral cortex development depends on extensive neuronal migration during embryogenesis, permitting the formation of accurate synaptic circuits and a highly ordered laminar neocortex. The motility of a migrating neuron is achieved by a dynamic microtubule cytoskeleton that alternates between states of stabilization/lengthening and destabilization/shortening. This dynamic instability of the microtubule cytoskeleton is controlled by numerous microtubule-stabilizing and -destabilising proteins that bind directly to microtubules.

Autophagy ("self-eating"), a major bulk intracellular degradation system, involves the fusion of autophagosomes with lysosomes, followed by proteolysis and recycling of cellular constituents. Like neuronal migration, autophagy is a microtubule-dependent process. The dynamic microtubule network serves as a track for autophagosomes to be transported to the lysosomes.

WDR47 is a protein that is expressed in the brain during development, but of which the function is largely unknown. Novel interactions have recently been identified between Reelin and WDR47 and between the microtubule-destabilising protein superior cervical ganglion 10 (SCG10) and WDR47. These findings suggest that WDR47 may be regulating microtubule-dependent processes such as neuronal migration and autophagy. We hypothesize that WDR47 may play a role in regulating neuronal migration and/or autophagy, and that this regulation may be mediated by a tubulin stability-regulating role of WDR47.

Aims and Methods

Our aims are to assess the cellular localization of WDR47 in GT1-7 cells and to determine whether WDR47 is able to influence neuronal migration, filopodia extension, surface adhesion, ultra-structure, autophagy, tubulin stability, and tau or SCG10 protein levels.

GT1-7 neuronal cells were cultured under normal conditions and transfected with WDR47 siRNA for 24 hours, followed by western blot verification of the knock-down. A 36 hour

neuronal *in vitro* cell migration assay was performed and images of the wound were captured every 6 hours; the migration distances and the wound areas for the different time points were measured and analysed. A 24 hour migration assay was performed, capturing images every hour, and the direction of migration was determined. Scanning electron microscopy (SEM) and transmission electron microscopy (TEM) were performed to analyse neuronal surface morphology and ultra-structure. Western blot analysis of SCG10, acetylated α-tubulin, Tau, LC3, and Sequestosome 1/p62 (SQTM1) protein levels was performed. Super-resolution structured Illumination microscopy (SR-SIM) three-dimensional (3-D) imaging of WDR47-YFP transfected cells, confocal microscopy of LC3 and acetylated tubulin, co-localization analysis of WDR47 and acetylated tubulin, and fluorescence recovery after photo-bleaching (FRAP) analysis were performed.

Results

WDR47 siRNA treatment significantly reduced the average migration distance and the migration velocity, resulted in fewer filopodia-like extensions as well as perturbed surface adhesion of migrating neurons, and lead to an increased presence of endoplasmic reticulum (ER) structures as well as an expanded nuclear envelope. LC3-II protein levels were significantly lower with WDR47 siRNA treatment, but were significantly increased with WDR47 siRNA treatment in conjunction with Bafilomycin A1 treatment, indicating increased autophagic flux. SCG10 protein levels were significantly decreased with WDR47 siRNA treatment. SR-SIM and confocal microscopy of WDR47 siRNA treated cells revealed a robust presence of highly convoluted acetylated tubulin in the perinuclear region as well as decreased LC3 fluorescence signal. Confocal microscopy revealed co-localization of WDR47 with acetylated tubulin.

Discussion and Conclusion

The results suggest that WDR47 is involved in regulating neuronal migration, neuronal surface adhesion and filopodia formation, microtubule dynamics, and likely also autophagic flux. Taken together, we propose that WDR47 is regulating microtubule dynamics by facilitating assembly of microtubule-regulating proteins such as SCG10, thereby affecting microtubule-dependent processes such as neuronal migration and autophagy.

Opsomming

Inleiding

Normale serebrale korteks ontwikkeling is hoogs afhanklik van neuronale migrasie tydens embriogenese, en is belanrik vir die vorming van akkurate sinaptiese netwerke en 'n hoogs geordende laminêre neokorteks. Die vermoë van 'n neuron om te migreer berus op 'n hoogs dinamiese mikrotubulien sitoskelet wat verleng/stabiliseer of verkort/destabiliseer soos tubulien-eenhede begevoeg of verwyder word. Hierdie dinamiese onstabiliteit van die mikrotubulien sitoskelet word beheer deur verskeie mikrotubulien-stabiliserende en -destabiliserende proteïene wat direk bind aan mikrotubuliene.

Autofagie ("self-eet"), 'n grootmaat intrasellulêre degradasie stelsel, behels die fussie van autofagosome met lisosome, gevolg deur proteolitiese afbraak van sellulêre organelle en proteine. Soos neuronale migrasie is autofagie 'n mikrotubulien-afhanklike proses. Die dinamiese mikrotubulien netwerk dien as 'n spoor vir die vervoer van autofagosome na lisosome.

WDR47 is 'n proteïen wat voorkom in die brein tydens ontwikkeling, maar waarvan die funksie grootliks onbekend is. Interaksies was onlangs geïdentifiseer tussen beide Reelin en WDR47 en die mikrotubulien-destabiliserende proteïen SCG10 en WDR47. Hierdie bevindinge dui daarop aan dat WDR47 n rol speel in die regulering van tubulienstabiliteit en sodoende mikrotubulien-afhanklike prosesse. Ons veronderstel dat WDR47 'n rol kan speel in die regulering van neuronale migrasie en/of autofagie en dat hierdie regulasie moontlik afhanklik is van 'n tubulien-stabiliteit-regulerende rol van WDR47.

Doelwitte en Metodes

Ons doelwitte is om die sellulêre lokalisering van WDR47 in GT1-7 neurone te evalueer en om te bepaal of WDR47 n effek het op neuronale migrasie, oppervlak adhesie en filopodia formasie, ultra-struktuur, autofagie, tubulien-netwerke en -stabiliteit, en Tau of SCG10 proteïenvlakke.

GT1-7 neuronale selle is gekweek onder normale omstandighede en vir 24 uur getransfekteer met WDR47 siRNA, gevolg deur verifikasie met Western-blot analise. 'n 36 uur neuronale *in vitro* sel migrasie toets is uitgevoer en fotos van die wond is elke 6 uur geneem. Die migrasie afstande en die wondareas vir die verskillende tydpunte is gemeet en ontleed. 'N 24-uur-migrasie toets is uitgevoer, 'n foto van die wond is elke uur geneem, en die rigting van migrasie is bepaal. Skandering elektronmikroskopie (SEM) en transmissie-elektronmikroskopie (TEM) is uitgevoer om neuronale oppervlakmorfologie en ultra-struktuur te observeer. Western blot analise van SCG10, geasetieleerde α-tubulien, Tau, LC3 en Sequestosome 1/p62 (SQTM1) proteïenvlakke is uitgevoer. Super-resolusie gestruktureerde verligting mikroskopie (SR-SIM) driedimensionele (3-D) beelding van WDR47-YFP getransfekteerde selle, konfokale mikroskopie vir visualisering van LC3 en tubulien, co-lokalisering analise van beide WDR47 en LC3 en WDR47 en tubulien, asook fluorescentie hersteling na foto-bleek (FRAP) analise is uitgevoer.

Resultate

Die gemiddelde migrasie-afstand en die migrasiesnelheid (μm/min) het beduidend afgeneem met WDR47 siRNA behandeling. SEM analise van WD47 siRNA-behandelde neurone het minder filopodia en veranderde oppervlak adhesie vertoon, en TEM analise het 'n verhoogde teenwoordigheid van endoplasmiese retikulum (ER) strukture, en 'n uitgebreide kernmembraan vertoon. LC3-II proteïenvlakke was beduidend laer met slegs WDR47 siRNA behandeling, maar beduidend hoër met WDR47 siRNA behandeling in samewerking met Bafilomycin A1 behandeling. Hierdie resultate dui aan op toeneemende autofagie met WDR47 siRNA behandeling. Verder, beduidend laer vlakke van SCG10 proteïenvlakke is waargeneem met WDR47 siRNA behandeling. SR-SIM en konfokale mikroskopie van WDR47 siRNA behandelde selle het 'n robuuste teenwoordigheid van hoogs buigende geasetieleerdetubulien in die area rondom die nukleus, 'n afgeneemde LC3 fluoressensie sein, en co-lokalisering van WDR47 met geasetieleerdetubulien getoon.

Bespreking en Gevolgtrekking

Die resultate dui daarop aan dat WDR47 betrokke is by die regulering van neuronale migrasie, filopodia vormasie, oppervlak adhesie, mikrotubuliendinamika, en waarskynlik ook autofagie. Ons stel voor dat WDR47 mikrotubuliendinamika afekteer deur die regulering van

proteïene soos SCG10, en sodoende mikrotubulienafhanklike prosesse soos neuronale migrasie en autofagie fasiliteer.

Acknowledgements

I would like to express my sincere gratitude to my supervisor, Dr Ben Loos, for his excellent mentorship, constant guidance, and note-worthy dedication in time and effort.

I wish to thank my co-supervisor, Dr Craig Kinnear, for always being available for assistance and for the excellent planning and prior research that formed the basis of this study.

I wish to thank the Department of Physiological Sciences, particularly the Disease Signalling Group (DSG), for fellowship and support, and Prof Faadiel Essop for admirable leadership as the head of the Department.

I wish to acknowledge and thank Nolan Muller for generating the transmission electron microscopy images.

I wish to thank Dr Lydia Lacerda, Dr Annadie Krygsman, Lize Engelbrecht, Rozanne Adams, and Madelaine Frazenburg for technical support.

I wish to thank the National Research Foundation for financial assistance.

Lastly, I wish to thank my parents, Ludolf and Elria Roos, and my partner, Jonathan Oettle, for love and support throughout the duration of this project.

List of Conferences

Central Analytical Facilities (CAF) Symposium (Stellenbosch University)

International Cell Death Society (ICDS) Annual Meeting

Physiology Society of South Africa (PSSA) Annual Meeting

Microscopy Society of South Africa (MSSA) Annual Meeting

Index

List of Figures

Abbreviations

3-D:	Three Dimensional
AEP:	Anterior Entopeduncular Area
AMPK:	AMP-activated protein kinase
ApoER2:	Apolipoprotein Receptor 2
Beclin 1:	BCL2 Interacting Protein 1
BSA:	Bovine Serum Albumine
CDK:	Cyclin-Dependent Kinase
CP:	Cortical Plate
CO_2:	Carbon Dioxide
CTLH:	C-Terminal to LisH Domain
Dab-1:	Disabled-1
dH_2O:	Distilled Water
DMEM:	Dulbecco's Modified Eagle's Medium
DMSO:	Dimethyl Sulfoxide
DNA:	Deoxyribonucleic Acid
DCX:	Doublecortin
ECL:	Enhanced Chemiluminescence
EDTA:	Ethylenediaminetetraacetic Acid
ER:	Endoplasmic Recticulum
CRP:	CREB-binding Protein
FAS:	Foetal Alcohol Syndrome
FBS:	Foetal Bovine Serum
FMR1:	Fragile X Mental Retardation Protein 1
FRAP:	Fluorescent Recovery after Photo-Bleaching
GSK3β:	Glycogen Synthase Kinase
HC:	Heavy Chain
IZ:	Intermediate Zone

JNK:	C-Jun NH2-terminal kinase
LAMP-2A:	Lysosomal-Associated Membrane Protein-2A
LC:	Light Chain
LC3:	Microtubule-Associated Protein 1 Light Chain 3
LC3-PE:	Microtubule-Associated Light Chain 3-Phosphatidyl Ethanolamine
LisH:	Lissencephaly-1 Homology Domain
MAP:	Microtubule Associated Protein
MAPK:	Mitogen-Activated Protein kinase
MGE:	Medial Ganglionic Eminence
MZ:	Marginal Zone
mRNA:	Messenger Ribonucleic Acid
MTOR:	Mammalian Target of Rapamycin
NE:	Nuclear Envelope
NP:	Neural Progenitors
PAGE:	Polyacrylamide Gel Electrophoresis
PCR:	Polymerase Chain Reaction
PE:	Phosphatidylethanolamine
PI3P:	Phosphatidyl-Inositol-3-Phosphate
PI3K:	Phosphatidylinositol 3-Kinase
PKA:	Protein Kinase A
PKB:	Protein Kinase B
PP:	Preplate
PS:	Pial Surface
PVDF:	Poly-vinylidene Fluoride
PMSF:	Phenylmethylsulfonyl Fluoride
RanBPM:	Ran-Binding Protein in the Microtubule-Organizing Centre
RNA:	Ribonucleic Acid
RIPA:	Radio-immunoprecipitation

ROI: Region of Interest

SBH: Subcortical Band Heterotopia

SC: Short Chain

SCG10:   Superior Cervical Ganglion 10

SDS: Sodium Dodecyl Sulphate

SDS-PAGE: Sodium Dodecyl Sulphate

SEM: Scanning Electron Microscopy

SENDA: Static Encephalopathy of Childhood with Neurodegeneration in Adulthood

Shh: Sonic Hedgehog

shRNA: Short Hairpin RNA

siRNA: Small Interfering RNA

SP: Subplate

SQSTM1:   Sequestosome 1 (P62)

SR-SIM: Super-Resolution Structured Illumination Microscopy

SVZ: Sub-Ventricular Zone

TBS-T: Tris-Buffered Saline and Tween 20

UVRAG: UV Radiation Resistance-Associated Gene

VLDL-R: Very Low Density Lipid Receptor

VZ: Ventricular Zone

WDR47:   WD Repeat Domain 47

WHO: World Health Organization

Units of Measurements

A: ampere

%:   percentage

˚C: degrees Celcius

µl: microliter

µg: microgram

µm: micrometer

µM: micromolar

g: gram

kDA: kilodalton

l: litre

M: molar

mg: milligram

ml: millilitre

nM: nanomolar

Motivation

WDR47 (WD40 repeat domain 7) is a protein of unknown function that is expressed predominantly in the brain during development (Wang *et al.,* 2012). Our colleagues from a collaborative laboratory have recently identified novel putative interactions between WDR47 and Reelin, a key regulator of neuronal migration (Kinnear, 2007), as well as between WDR47 and SCG10, a potent microtubule-destabilizing protein (McGillewie, 2009). These findings lead us to hypothesize that WDR47 may participate in regulating microtubule-dependent processes, such as neuronal migration and autophagy. Neuronal migration and autophagy are both important processes for neurodevelopment (Kwan *et al.,* 2012; Ban *et al.,* 3013), and a number of neurological disorders have been attributed to defects in WD40 repeat proteins that regulate these processes. For example, humans deficient in Lis1, a WD40 repeat protein that is crucial to neuronal migration, suffer from the severe brain malformation disorder lissencephaly (Manent and LoTurco; 2012; Moon and Wynshaw-Boris, 2013), while humans deficient in WDR45, a WD40 repeat family that has recently emerged as a key autophagy-regulating protein, suffer from static encephalopathy of childhood with neurodegeneration in adulthood (SENDA) (Saitsu *et al.,* 2013). This therefore motivated us to investigate the role of WDR47 in microtubule-dependent processes by knocking down WDR47 in GT1-7 neuronal cells and subsequently assessing neuronal migration, autophagy, and microtubule networking dynamics. Investigating the role of WDR47 in this context may contribute to the growing body of research aimed at understanding the numerous genes and proteins involved in brain formation, thereby enabling the development of successful therapeutic interventions for neurodevelopmental disorders (Collins *et al.,* 2011).

Chapter 1: Introduction

1.1 The Burden of Mental Disease

Globally, mental disease accounts for roughly 14% of disease burden (Tomlinson *et al.,* 2009; Prince *et al.,* 2007), exceeding even cardiovascular disease and cancer (Collins *et al.*, 2011). Mental disease also accounts for an astounding 28% of disability-adjusted life years, a unit for measuring the number of life years compromised by disability by adding the total years lived with disability to years of life lost. In addition, mental disease has a profound effect on mortality rates: according to the World Health Organization (WHO), approximately 1.2 million deaths result from mental disease each year. This statistic is not only related to unnatural deaths (e.g. suicides), but also to neurological complications arising from the disease pathology itself (Collins *et al.,* 2011; Prince *et al.,* 2007).

Depression, bipolar disorders, substance abuse disorders, schizophrenia, and dementias are the major contributors to the global mental disease burden (Collins *et al.,* 2011; Prince *et al.,* 2007). The burden of mental disease is exacerbated by the fact that individuals suffering from mental disorders have a greatly increased susceptibility for developing cardiovascular, endocrine, or other complications, and those suffering from poor physical health conversely have greater risk of developing mental disorders. For example, schizophrenia is particularly associated with higher morbidity and mortality rates due to a number of associated conditions including circulatory, endocrine and infectious diseases, insulin resistance, and complications with an antiretroviral treatment (ART) regime in HIV/AIDS patients (Osborn, 2001; Prince *et al.,* 2007). Depression, one of the foremost contributors to the overall global disease burden (Collins *et al.,* 2009) is particularly associated with the development of cardiovascular disease, and has been acknowledged as an autonomous risk factor for stroke (Prince *et al.,* 2007). Mental retardation, bipolar disorders, and dementias are also major role players in the development of chronic diseases and the occurrence of non-suicidal deaths (Prince *et al.,* 2007).

1.1.1 Mental Disease within the South-African Context

Research focused on mental health issues is low in proportion to the global disease burden (Collins *et al.*, 2011). This is particularly true for low and middle income countries, where

2

research is primarily focussed on disease states that contribute most to mortality rates (e.g. HIV AIDS and Tuberculosis). Collectively, low and middle-income countries contribute to roughly only 3% of neuropsychiatric research (Tomlinson *et al.,* 2009). Problematically, individuals living under impoverished conditions are particularly susceptible to the development of mental disorders. For instance, an astounding 83% of suicides committed each year occur in low and middle income countries (Prince *et al.,* 2007). Mental disease rates in South Africa are high, accounting for 5.9% of overall global disease burden (WHO, 2011). Furthermore, the burden of mental disease and the need for research in this field within the South African context is particularly emphasized by the high rates of foetal alcohol syndrome (FAS). FAS is a particularly devastating neurodevelopmental disorder of the new-born that arises from regular and excessive maternal alcohol consumption during pregnancy. Mental retardation and aberrant brain structural abnormalities (such as microencephaly), facial and body dimorphisms, and hindered growth are prominent features of the disease (Kumada *et al.,* 2006; May *et al.,* 2007). Astonishingly, the Western Cape Province of South Africa holds the highest reported rates of FAS globally. A cohort study based on a Western Cape community reported a rate of 68.0 – 89.2 per 1000 first grade learners to be sufferers of FAS (May *et al.,* 2007). Although the underlying mechanisms of how alcohol consumption affects brain development remain largely unclear, it is known that alcohol can affect several molecular aspects such as voltage-gated ion channels, signal transduction, and transcription of numerous genes. One of the major molecular contributors to the disease is defective neuronal migration during neurodevelopment (Kumada *et al.,* 2006).

The high rates of mental disease (particularly in low and middle income countries), the currently inadequate understanding of molecular mechanisms controlling brain development, and the lack of treatment and cures for neurological disorders highlight the necessity for research in the neuropsychiatric field to be prioritised (Collins *et al.*, 2011).

1.1.2 Molecular Studies for the Successful Treatment of Neurodevelopmental Disorders

The majority of mental disorders fall under the category of neurodevelopmental disorders, conditions that arise from molecular deficits (e.g. dysfunction of certain signalling pathways) that lead to structural brain abnormalities (Collins *et al.*, 2011; Kwan *et al.,* 2012; Lee *et al.,*

2013). Identification and treatment of the dysfunctional molecular mechanisms associated with a mutated gene can greatly improve the pathology and associated behavioural deficits characteristic of a particular disease. An example of the successful implementation of a molecular-based therapeutic intervention is Rubinstein-Taybi syndrome (RTS), a neurodevelopmental disorder associated with mutated CREB-binding protein (CRP). A mouse model of RTS demonstrates long-term memory deficits, which is restored with pharmacological up-regulation of the expression of CREB (Ehninger *et al.,* 2008). Another example of a molecular-based therapeutic intervention is subcortical band heterotopia (SBH), a neuronal migration disorder resulting from a mutated DCX (Doublecortin) gene. Re-expression of *DCX* after birth allows abnormally positioned neurons in SBH rat brains to re-enter the migration phase, improving structural abnormalities in affected cortical regions (Wynshaw-Boris, 2010).

It is therefore conceivable that a holistic understanding of the genes, proteins, and signalling pathways involved in neurodevelopment may ultimately transform the prevention and treatment of various neuropsychiatric disorders, by way of pharmacological and molecular interventions. However, the respective roles of numerous neurodevelopmental genes and proteins remain largely unclear (Ehninger *et al.,* 2008; Manent and LoTurco, 2012), and therefore forms part of the here conducted study.

The development of the mammalian brain remains to be one of the most complex and challenging questions faced by scientists (Gaspard and Vanderhaeghen, 2010). We will discuss only the development of the cerebral cortex, the area responsible for higher order functions and therefore the most relevant in the context of mental disease.

1.2 The Mammalian Cerebral Cortex

The cerebral cortex is an extensive sheet of highly convoluted neural tissue that represents the most superficial part of the mammalian forebrain. This structure is responsible for managing complex cognitive and emotional processes, such as spatial reasoning, sensory perception, conscious thought, emotions, and language acquisition. The neocortex represents the most recently evolved part of the mammalian forebrain and occupies most of the human cerebral cortex (Kwan *et al.,* 2012).

The formation of an extensively laminated and highly ordered neocortex is amongst the most intricate biological processes known to man, and the most complex aspect of embryonic development (Gaiano, 2008). Post-mitotic neuronal migration, differentiation, and the formation of functional neuronal networks are the major processes that govern corticogenesis (Figure 1.1) (Kwan *et al.,* 2012; Moon and Wynshaw-Boris, 2013).

The brain and spinal cord develop from an embryonic structure known as the neural tube. Development of the cerebral cortex during embryogenesis begins with mitotic cell division of neural progenitors (NPs) in the ventricular zone (VZ), the area in closest proximity to the walls within the ventricles of the neural tube. Cortical neural precursors specifically are born from the pseudostratified epithelium at the border of the ventricular zone. Within the VZ, neural precursors take part in the cell cycle to give rise to daughter progenitor neurons, which will eventually take part in asymmetric cell division to produce neurons that will migrate in consecutive cohorts to respective final destinations (Ayala *et al.,* 2007; Moon and Wynshaw-Boris, 2013).

1.2.1 The Formation of Cortical Layers and Functional Neural Networks

The neocortex consists of six distinct layers (L1 – L6), and the formation of these layers is referred to as cortical lamination. Each of these layers is functionally and structurally unique, housing distinct cell types with diverse roles. The six layers are formed in an 'inside-out' fashion: L6, the innermost layer, forms first, followed by L5 - 2, and then L1, the most superficial layer closest to the skull, forms last. This implies that later-born neurons need to migrate through previously formed layers in order to reach their destinations. Migrating neurons are believed to receive important regulatory and guidance signals secreted from cells in previously formed layers (McGillewie, 2009; Kwan *et al.,* 2012).

Formation of the cerebral cortex begins with the first cohort of neurons migrating toward the pial surface (PS) of the brain to form a structure known as the preplate (PP). The PP represents the earliest born cortical neurons and houses a cell type referred to as Cajal-Retzius cell, which produces Reelin, a crucial role-player in controlling neuronal migration (section 1.4.4). After formation of the PP, the next post-mitotic wave of neurons will migrate to the PP to split it into two layers: the marginal zone (MZ), the most superficial layer which

will eventually become L1, and the deeper subplate (SP). Collectively, the MZ and the SP are referred to as the cortical plate (Marín *et al.,* 2010). With each successive wave of post-mitotic neurons migrating to their final position, the cortical plate will develop into the six layers of the neocortex (Ayala *et al.,* 2007; Kwan *et al.,* 2012; Moon and Wynshaw-Boris, 2013), with the MZ housing the Cajal-Retzius cells and remaining the most superficial layer, and the SP remaining the deepest layer. Each neuron therefore migrates past the SP, but not past the MZ, and the space between the VZ and MZ increases with each consecutive wave of migrating neurons (Gaiano, 2008; Marín *et al.,* 2010). In other words, the MZ moves outward as the cerebral cortex expands, and the later-born neurons travel longer distances than earlier-born neurons to reach their destinations near the PS (Figure 1.1). Neuronal birth date therefore plays a significant role in determining the layer-specific identity of each migrating neuron, as neurons born at a specific time point will eventually settle in a specific layer. This is one of the primary means by which a highly organized and laminated neocortex is achieved (Lakatosova and Ostatnikova, 2012; Marín *et al.,* 2010).

The vast quantity of neurons constituting the cerebral cortex form extensive connections, either with neurons from the same hemisphere (intracortically) or with neurons from the opposite hemisphere by projecting through either the corpus callosum or the internal capsule (Richards, 2002). Inaccurate positioning of neurons due to defective migration interferes with brain architecture and electrophysiology (Kwan *et al.,* 2012; McGillewie, 2009; Moon and Wynshaw-Boris, 2013).
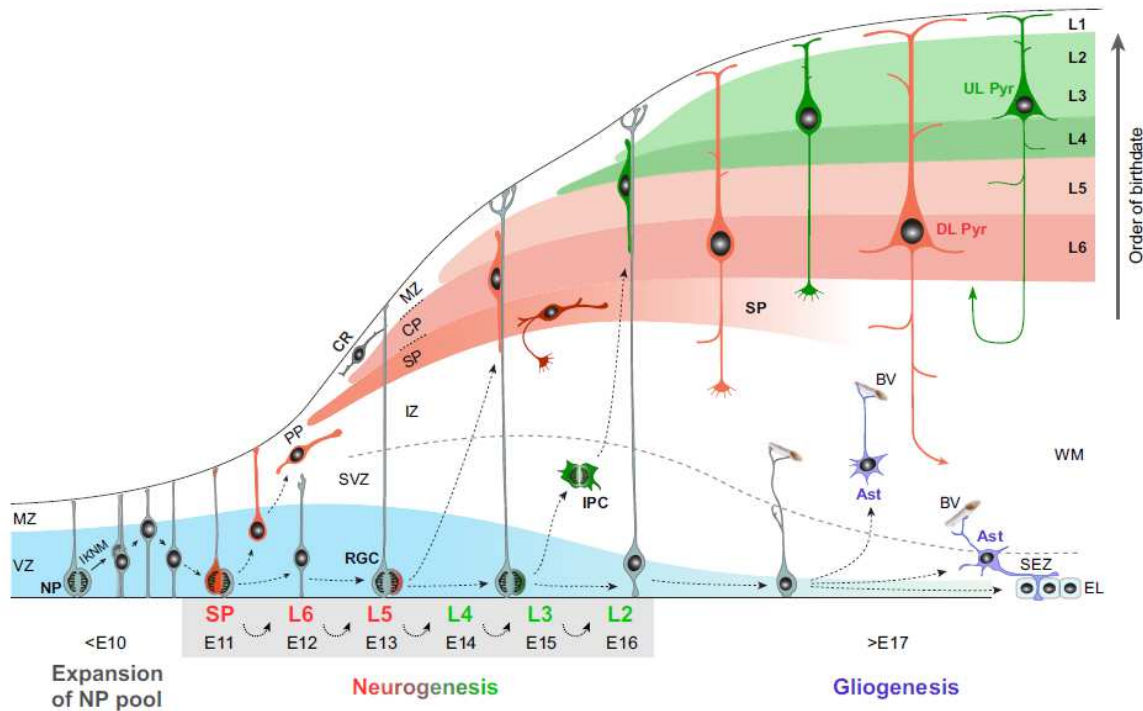
Figure 1.1: Formation of the six-layered mammalian cerebral cortex. The first phase of neurogenesis consists of neural progenitors (NPs) undergoing mitosis in the VZ (blue) to expand the progenitor pool. When the NP pool is substantially large, cells begin to divide asymmetrically to give rise to daughter neurons that migrate in successive cohorts to form the six layers of the cortex. The first group of migrating neurons settle to form the PP. The next group of migrating neurons split the PP into the MZ and the SP. L6, the innermost layer, forms first, followed by L2 – L5, and lastly, L1. Later-born neurons thus need to migrate past previously settled neurons to reach their respective destinations in more superficial layers before neurons can differentiate to assume their layer-specific identities (Kwan *et al.,* 2012). MZ: marginal zone; VZ: ventricular zone; SVZ: sub-ventricular zone; IZ: intermediate zone; SP: subplate; CP: cortical plate.

1.2.2 Classification of Cortical Neurons

Roughly 80% of neurons within the neocortex are projection neurons (also called pyramidal neurons due to their characteristic pyramid-shaped cell bodies), with the remaining 20% consisting of interneurons. The former are excitatory (glutamatergic) neurons while the latter are inhibitory (GABAergic) neurons. Projection neurons have numerous dendrites sprouting in different directions as well as a single apical dendrite directed towards the pial surface, and an extended axon which usually reaches to far intracortical or subcortical locations. Interneurons vary greatly in structure and morphology and extend their axons locally over shorter distances (Kwan *et al.,* 2012; Moon and Wynshaw-Boris, 2013).

1.2.3 Molecular Complexity of the Developing Cerebral Cortex

The neocortex accommodates a vast quantity of neurons, each of which must migrate in a highly orchestrated manner over tens to hundreds of cell body distances and past earlier born cells to a precise final destination (Tsai and Gleeson, 2005). A developing neuron typically possesses a number of neurites (extended processes) that differentiate into an axon and several dendrites once the neuron has reached its destination in the cortex. The axon grows faster and extends over a longer distance than the dendrites, responding to environmental signals to guide its direction of extension until a central or peripheral connection is formed, a process referred to as axonal pathfinding. The dendrites branch and extend over short distances to form pre-determined synaptic connections with other neurons (Poulain and Sobel, 2010; Richards, 2002). The development of the six layered neural network is consequently an intricately well-organized and highly ordered process dependent on two key processes: the migration of post mitotic neurons to their respective final destinations and the achievement of specific neuronal networks. The achievement of neuronal networks is highly dependent on neurite pruning, which has recently been shown to rely on protein degradation pathways such as autophagy (Lee *et al.,* 2013). Both neuronal migration and neural network formation are regulated by various complex molecular signalling pathways involving numerous genes and proteins, many of which the respective roles in neurodevelopment are still to be elucidated (Kwan *et al.,* 2012). It is therefore our main aim to introduce and discuss the complex regulation underlying two processes: neuronal migration (section 1.3; below) and autophagy (section 1.5).

1.3 Neuronal Migration

The journey of neurons from their place of origin to their respective final locations within the cortex lays the foundation for proper brain structure and function (Ayala *et al.,* 2007). Each individual migrating neuron repeatedly alternates between two broad phases: first, the neuron extends a highly dynamic structure known as the leading process (phase 1; lengthening of the leading process). Next, a swelling forms between the nucleus and the leading process, the centrosome is positioned in the swelling, and then the nucleus translocates into the swelling toward the centrosome (phase 2; termed nucleokinesis) while the leading process retracts. These two phases constitute one migratory cycle, and occur in

a salutatory manner instead of a smooth and continuous motion (Marín *et al.,* 2010; Schaar and McConnel, 2006; Solecki *et al.,* 2004; Tsai and Gleeson, 2005).

Neurons utilize two main modes of migration, namely radial migration and tangential migration (Figure 1.2). The mode of migration is sub-population dependent, but some neurons make use of both modes, altering their morphologies to switch from radial to tangential migration and vice versa. This suggests that common regulatory mechanisms govern different forms of neuronal migration (Schaar and McConnel, 2005). Both modes will be briefly discussed.

1.3.1 Radial Migration

Radial migration is the chief means by which hippocampal development and cortical lamination occurs, accounting for roughly 85% of cortical migration. Radially migrating neurons are mainly excitatory projection (pyramidal) neurons, which are born in the VZ and migrate perpendicularly from the VZ to the CP (Marín *et al.,* 2010; Moon and Wynashaw-Boris, 2013). Two types of radial migration have been identified: firstly, somal translocation, a glial-independent mode in which the leading process reaches all the way to the pial surface, followed by repeated translocations of the cell body, and secondly, locomotion (or glial-dependent migration) in which the leading process extends over a short distance before the cell body follows. These different modes of radial migration are not dependent on cell type, and migrating neurons often switch between locomotion and somal translocation for the final short distance to the pial surface. The majority of radially migrating neurons make use of radial glial cells to translocate toward the CP. Radial glial cells stem from the same neural progenitors as the migrating neurons, but their cell bodies remain in the ventricular zone whilst they extend a long process toward the most superficial part (the PS) of the developing cerebral cortex. Glial-dependent radially migrating neurons extend and retract their leading processes along the glial cells to propel themselves toward a final resting destination (Ayala *et al.,* 2007; Marín *et al.,* 2010).

1.3.2 Tangential Migration

Tangential migration is the mode by which inhibitory interneurons, born in the medial ganglionic eminence (MGE), the lateral ganglionic eminence (LGE), or the anterior

entopeduncular area (AEP) reach their positions within the cortex. These neurons do not follow a straight-forward path of migration, but instead migrate at a tangent to a circular route. Interneurons also do not exhibit the same bipolar morphology of radially migrating neurons, but instead extend multiple processes and transit between different states of polarity. Some interneurons migrate tangentially for the majority of their specific routes, and then switch to a bipolar morphology and radial migration for the short distance to their final destination (Kwan *et al.,* 2012; Marín *et al.,* 2010; Moon and Wynshaw-Boris, 2013).
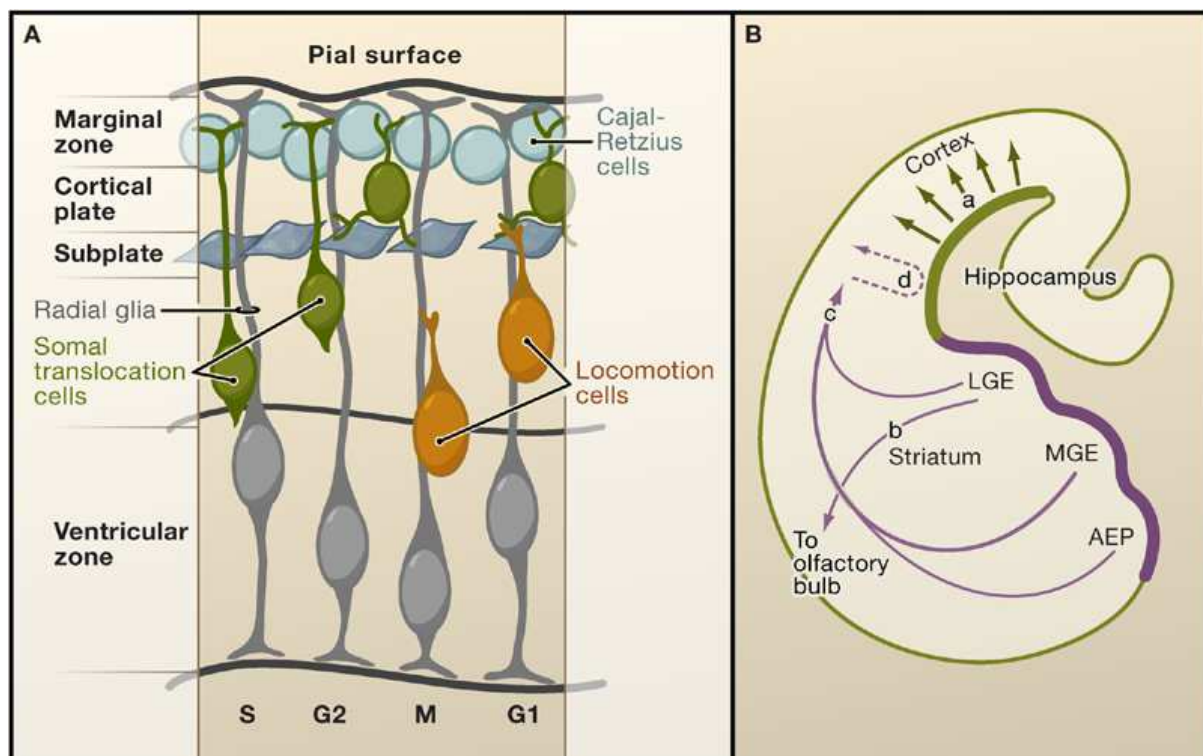
Figure 1.2: Modes of neuronal migration. A: Excitatory pyramidal (projection) neurons are born and proliferate in the VZ, after which they migrate radially to the CP by adhering to radial glia. B: In contrast to radially migrating projection neurons (a), inhibitory interneurons are born in the MGE, LGE, or AEP and follow a circular route to migrate tangentially to their respective final destinations (b,c). After migrating tangentially for long distances, some interneurons switch to radial migration for the final distance before reaching the CP (d) (Ayala *et al.,* 2007).

1.3.3 Morphological and Dynamic Features of the Migrating Neuron

Neuronal cells are highly polarised in nature, a property that is vital for directed migration and synapse formation (Ban *et al.,* 2013; Tsai and Gleeson, 2005). This polarity is achieved when neurons send forth both a longer leading process and a shorter trailing process, the latter of which eventually becomes the axon. The leading process of a migrating neuron

generally extends over a relatively long distance from the cell body and nucleus, a feature that distinguishes neurons from other migrating cells. The leading process undergoes constant remodelling, a property that allows this structure to guide the migrating neuron towards the cortical plate. The growth cone is a structure situated at the tip of the leading process and is responsible for detecting guidance signals (Heng, 2009; Marín *et al.,* 2010; Schaar and McConnel, 2005). The growth cone reaches to the migration region and consists of filamentous actin fibers that play a role in surface adhesion (Moon and Wynshaw-Boris, 2013). Upon detecting guidance signals, the growth cone is able to induce process extension/retraction, pauses, or changes in migration direction (Morri *et al.,* 2006).

Projection neurons typically extend a single leading process toward the CP. However, the leading process often undergoes morphological changes as the neuron migrates through different cortical zones. For example, as the neuron migrates through the sub-ventricular zone (SVZ), the leading process transits briefly between a bipolar and multipolar state. The bipolar morphology is established again as the neuron continues to migrate to the cortical plate, and is seen throughout the majority of the projection neuron's journey. Furthermore, radially migrating neurons often temporarily pause or even reverse as they migrate past precursor neurons (Kwan *et al.,* 2012; Marín *et al.,* 2010).

In contrast to projection neurons, interneurons display a branched leading process. This multipolar morphology allows the migrating neuron to alter its direction of translocation in response to environmental signals. The leading process of the interneuron will typically consist of two branches that dynamically explore the environment until the neuron 'chooses' a direction to follow, after which only one of the branches will continue to extend. Subsequently, the interneuron will undergo nucleokinesis and the next cycle of migration will ensue (Marín *et al.,* 2010).

The nucleus of a migrating neuron is much larger compared to that of a non-migrating cell, and is enclosed by a microtubule-rich cage. The leading process contains prolonged microtubule filaments that originate at the microtubule organising centre (MTOC), also known as the centrosome, positioned adjacent to and ahead of the nucleus of the migrating cell (Moon and Wynshaw-Boris, 2013; Solecki *et al.,* 2004; Tsai and Gleeson, 2005). The centrosome plays an important role in either anchoring or releasing microtubules according

to cellular requirements (Mètin *et al.,* 2008). In addition, migrating neurons typically possess numerous membrane protrusions called filopodia. Filopodia are extensions of the actin cytoskeleton situated below the neuronal membrane, and are important for key aspects of migration such as micro-environment sensing, surface adhesion, directed migration, neuronal process extension and branching (Guerrier *et al.,* 2009; Schaar *et al.,* 2005). Figure 1.3 summarizes the morphological features of a migrating neuron.
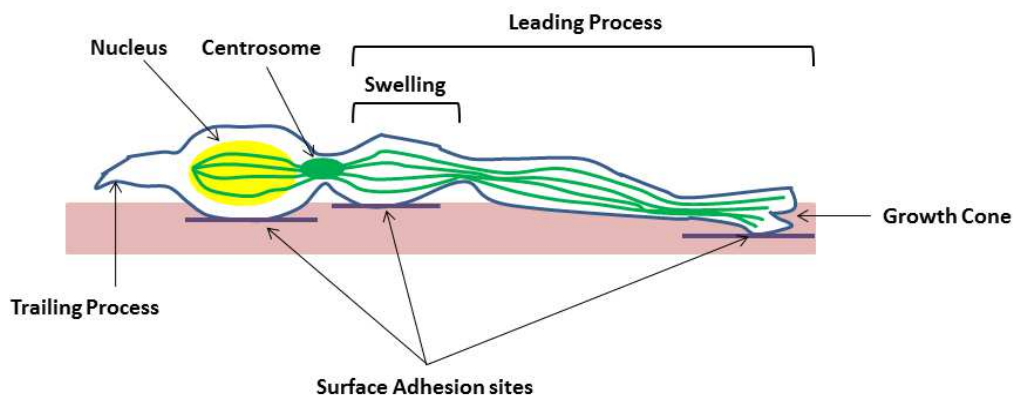
Figure 1.3: Morphological features of a bipolar migrating neuron. The neuron possesses a large nucleus and sends forth a long leading process in the direction of migration. A short trailing process follows the nucleus and cell body. Microtubule filaments originate at the centrosome, form a cage around the nucleus and extend throughout the leading process. The growth cone is situated at the tip of the leading process and senses the microenvironment. Several regions of surface adhesion exist, where filopodia (not shown) play an important role. A swelling in the leading process precedes nucleokinesis.

1.4 The Microtubule Cytoskeleton

A key regulatory component of neuronal migration is the cytoskeleton. The neuronal cytoskeleton consists of two major components: actin filaments and microtubules. Actin and microtubule networks have both distinct and synergistic intracellular roles, but the interaction between these two systems is not well understood (Ayala *et al.,* 2007; Heng *et al.,* 2009). For the purposes of this study, we will focus mainly on the regulation and function of the microtubule component of the cytoskeleton. Microtubules are highly

dynamic polymers constituted of heterodimers of non-covalently bounded α- and β-tubulin building blocks. Microtubules undergo rapid polymerization and depolymerisation in living cells, and also display several dynamic features such as bending, buckling, and looping. The relevance of and mechanisms behind microtubule dynamics remains poorly understood (Bicek *et al.,* 2009).

1.4.1 Biological Functions of Microtubules

The microtubule cytoskeleton plays a vital role in various cellular processes, such as maintaining structural integrity of cells, signal transduction, force production, cell cycle regulation, and differentiation, and migration (Al-Bassam and Corbett, 2012; Ayala *et al.,* 2007; Heng *et al.,* 2009). Additionally and of particular interest is the role microtubules play in facilitating intracellular transport of organelles (e.g. autophagosomes and mitochondria). This transport is mediated by motor proteins such as dynein and kinesin (Ayala *et al.,* 2007). The complex role that the microtubule cytoskeleton plays in facilitating neuronal migration is most relevant here. Several components of the migration process are dependent on microtubule dynamics, including nucleokinesis, membrane remodelling, and process extension (Ayala *et al.,* 2007; Heng *et al.,* 2009; Wang *et al.,* 2012). The role of the microtubule cytoskeleton in enabling these processes is briefly described.

1.4.1.1 Microtubules Facilitate Nucleokinesis

The microtubule cage that surrounds the nucleus of the migrating neuron is tightly associated with the nuclear envelope (NE). The microtubules stretch over the nucleus, join at the centrosome, and extend throughout the leading process (Figure 1.3). Nucleokinesis is preceded by the formation of a swelling in the leading process and subsequent centrosome positioning. The nucleus is then pulled in the direction of the centrosome and into the swelling through a force generated by dynein motors and microtubules (Kato and Dobyns, 2003; Schaar and McConnel, 2005; Tsai and Gleeson, 2005). The role of dynein in centrosome positioning and nucleokinesis is further described in section 1.4.3.

1.4.1.2 Microtubules Regulate in Membrane Remodelling

Microtubule regulation is linked to neuronal membrane morphology, such as filopodia formation, and this is believed to function as one of the ways in which the microtubule

13

network facilitates neuronal migration (Guerrier *et al.,* 2009). Filopodia extend and retract in response to extracellular guidance signals to enable growth cone motility. Filopodia extension occurs in response to an attractive guidance signal and stimulates the growth cone to turn in the direction of extension, while filopodia retraction occurs in response to a repellent guidance signal and stimulates the growth cone to turn away from the signal (Geraldo and Gordon-Weeks, 2009).

Microtubules interact with the actin filaments present in filopodia, and play a role in regulating filopodia formation (Geraldo and Gordon-Weeks, 2009; Myers *et al.,* 2006; Schober *et al.,* 2007). Schober *et al.* (2007) demonstrated a potential role for microtubules in regulating the density of filopodia by dissociating microtubules and filopodia with the microtubule depolymerizing reagent nocodazole. The treatment inhibited the merging of filopodia, resulting in a significantly increased filopodia density. Interestingly, siRNA knock-down of dynein heavy chain inhibits microtubules from entering filopodia and results in defective growth cone turning, suggesting that dynein is involved in the transport of short microtubules into filopodia (Myers *et al.,* 2006). The formation of filopodia, the interaction between microtubules and actin filaments in filopodia, and the regulation of this interaction are topics that remain largely unclear (Geraldo and Gordon-Weeks, 2009; Schober *et al.,* 2007).

1.4.1.3 Microtubules Enable Neurite Extension and Retraction

Microtubules are nucleated at the centrosome (Malikov *et al.,* 2004), a feature that enables neuronal polarity and directed migration. The plus end of the microtubule is directed towards the growth cone of the migrating neuron, and the minus end is directed towards the nucleus. Typically, tubulin units are added to or sequestered from the growing microtubule at the plus end. Stabilisation or lengthening occurs with microtubule polymerization, and destabilisation or shortening occurs with microtubule depolymerisation. This oscillation between lengthening and shortening of the microtubule is termed dynamic instability (Figure 1.4) and enables the extension and retraction of the leading process during neuronal migration. This dynamic instability also allows the microtubule to explore three-dimensional space, enabling growth cone turning to effectively control the direction of migration (Mori *et al.,* 2006; Schober *et al.,* 2007; Vega *et al.,* 2006).
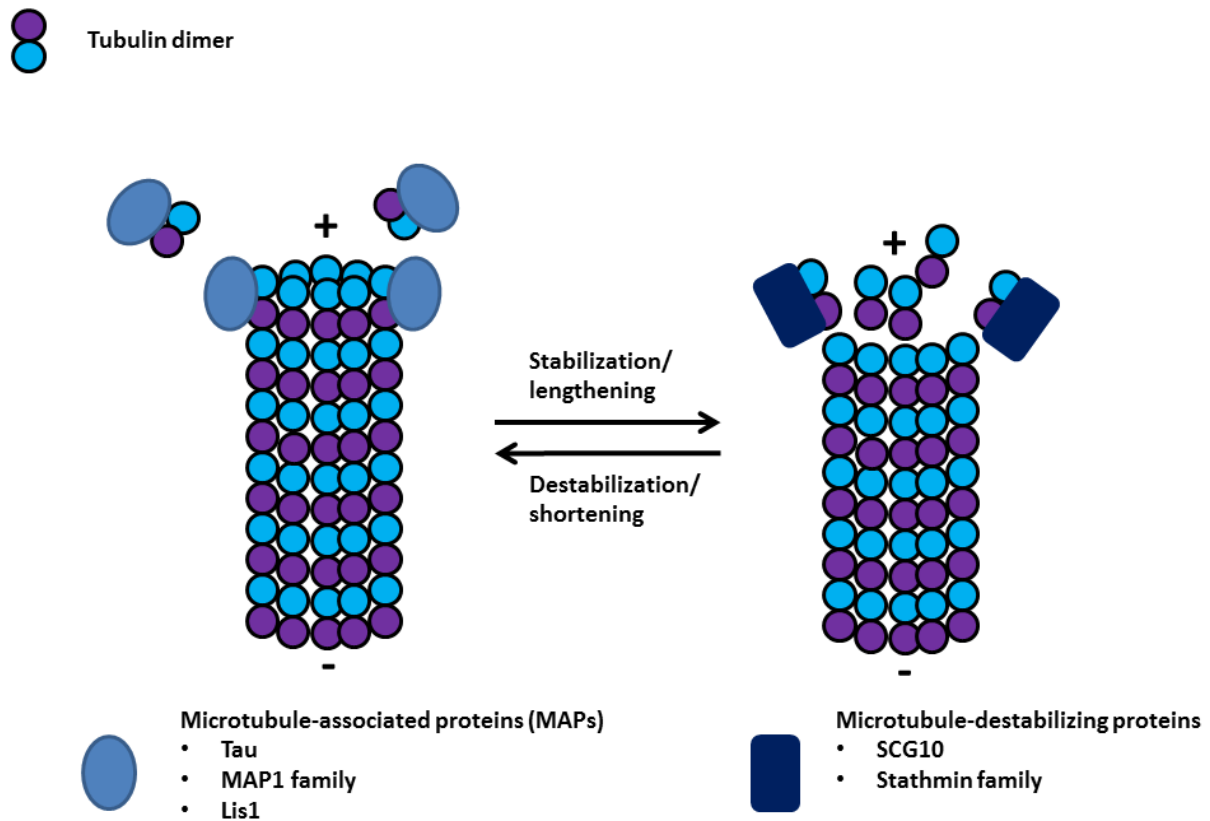
Figure 1.4: Dynamic instability of the microtubule polymer. Dimers of tubulin are typically added to or sequestered from the plus end of the microtubule to stabilize (lengthen) or destabilize (shorten) the microtubule. Various MAPs and microtubule–destabilizing proteins facilitate this dynamic state.

1.4.2 Regulation of the Microtubule Cytoskeleton

The extension and retraction of the leading process is dependent on the addition or removal of tubulin dimers to or from the microtubule cytoskeleton. This dynamic state of microtubules is regulated by various microtubule associated proteins (MAPS) and microtubule destabilising proteins that add or remove tubulin units to or from the microtubule. These MAPs and microtubule-destabilising proteins are in turn regulated by signalling cascades consisting of protein scaffolds that bind to and recruit other proteins, and by various regulatory kinases/phosphatases that activate/deactivate other microtubule-regulating proteins (Heng *et al.,* 2009; Wang *et al.,* 2012). Additionally, microtubule stability is also dependent on several tubulin post-translational modifications, such as tyrosination and acetylation. The reversible acetylation of α-tubulin at the lys-40 residue is linked to

stable microtubules (Al-Bassam and Corbett, 2012; Tȍkèsi *et al.,* 2010), while tyrosination is linked to younger and more dynamic microtubules (Poulain and Sobel; 2010).

It should be noted that microtubule regulation is multi-faceted, and one defective microtubule-regulating protein may set off a cascade of effects. Actin and microtubule networks are functionally inseparable, so interfering with a protein involved in microtubule regulation usually also affects actin regulation and vice versa. Additionally, an increase in the number of MAPs binding to the microtubule is known to interfere with dynein/kinesin motor-based transport, and this has been suggested to be as a result of the MAPs acting as "road blocks" (Baas and Qiang, 2005). Therefore, inhibition or up-regulation of a particular microtubule-regulating protein may indirectly affect aspects of actin regulation (e.g. filopodia extension) as well as organelle transport (e.g. autophagosomal or mitochondrial transport).

1.4.3 Microtubule-Regulating Proteins

Key examples of proteins directly involved in regulating microtubule stability are briefly summarized, followed by an introduction to Reelin, a major role player in controlling microtubule stability through affecting the activity of several MAPs.

1.4.3.1 Tau

Tau is a MAP of particular relevance in neuronal migration studies. Dephosphorylation and subsequent activation allows Tau to bind to tubulin dimers and stabilize the microtubule. Tau is important for development as the activation of this MAP not only regulates microtubule stability, but also plays an essential role in processes such as dendritic spine formation, synaptic plasticity, and neurite and axon outgrowth. However, no apparent phenotypic abnormalities are observed in Tau knock-out mice, suggesting that Tau deficiency can be compensated for by other MAPs (Lakatosova and Ostatnikova, 2012; Poulain and Sobel, 2010).

Tau is not only involved in neurodevelopment, but also in the survival of mature neurons. Microtubule-regulation defects may result in the inability of Tau to bind to the microtubule, leading to a phenomenon where Tau becomes hyper-phosphorylated. Hyper-

phosphorylated aggregates of Tau are a common feature of neurodegenerative diseases (e.g. Alzheimers), collectively referred to as Tauopaties (Vega *et al.,* 2006).

1.4.3.2 SCG10 (Super Cervical Ganglion 10)

SCG10 is a potent microtubule destabilising protein that belongs to the stathmin family of proteins and that is exclusively expressed in neurons. This protein is predominantly expressed during development, is enriched in the growth cones of developing neuronal processes, and recruits membranous vesicles from the Golgi apparatus to the growth cone. SCG10 is constituted of three functional domains: A distinctive hydrophobic N-terminal domain that allows SCG10 to localize to growth cones and to associate with vesicle membranes originating from the Golgi apparatus (Alves *et al.,* 2010), a central domain consisting of phosphorylation sites that regulates SCG10 activity, and a stathmin-like domain at the C-terminus that allows SCG10 to interact with and sequester tubulin dimers from microtubules (Li *et al.,* 2008; Morii *et al.,* 2006).

By binding to and sequestering tubulin dimers from the microtubule, SCG10 enhances microtubule dynamics and facilitates neurite outgrowth in undifferentiated neurons (Alves *et al.,* 2010; Bondallaz *et al.,* 2006; Vega *et al.,* 2006). It has been demonstrated that SCG10 gene silencing in rat hippocampal neurons inhibits neuronal process outgrowth, while protein transduction to increase SCG10 expression enhances process outgrowth, suggesting that SCG10 enhances microtubule remodelling and enables growth cone motility (Morii *et al.,* 2006). Furthermore, SCG10 not only regulates process outgrowth of undifferentiated neurons, but also plays an important role in differentiation by facilitating axon lengthening (Li *et al.,* 2009).

The destabilizing activity of SCG10 is regulated by phosphorylation events, and protein analysis of SCG10 reveals different molecular weight species representing different phosphorylation states (Vega *et al.,* 2006). Protein kinase A (PKA), mitogen-activated protein kinase (MAPK), cyclin-dependent kinase (CDK), and C-Jun NH2-terminal kinase 1 (JNK1) have all been reported to phosphorylate specific residues of SCG10 (Bondallaz *et al.,* 2006; Vega *et al.,* 2006; Westerlund *et al.,* 2011), and this phosphorylation reduces neuronal migration rate (Westerlund *et al.,* 2011). Four phosphorylation sites of SCG10 have been recognized. PKA has been reported to phosphorylate Ser-50 and Ser-97, while MAPK and JNK1 have

been reported to phosphorylate Ser-62 and Ser-73 (Li *et al.,* 2009). Furthermore, SCG10 activity may be regulated by events not related to phosphorylation. For example, it has been shown that over-expressing the microtubule-stabilising protein Tau in neuroblastomas and PC12 cells results in a significant reduction of SCG10 levels. A similar reduction in SCG10 levels is seen when treating cells with Taxol (a microtubule-stabilising agent), suggesting that microtubule stabilisation regulates SCG10 expression (Vega *et al.,* 2006).

1.4.3.3 Lis1 (Lissencephaly 1)

The Lis1 gene was the first gene identified to play a role in neuronal migration disorders. Lis1 is a 45kDa evolutionarily conserved protein belonging to the WD40 repeat family of proteins (section 1.6). Lis1 is a microtubule associated protein which stabilizes microtubules by binding to tubulin as well as to other MAPs such as MAP1B. Lis1 function relies heavily on its interaction with subunits of dynein (section 1.4.3.4) (Moon and Wynshaw-Boris, 2013; Tsai and Gleeson, 2005), and many identical features are observed in cells where either Lis1 or dynein is inhibited (Mètin *et al.,* 2008). Cells deficient in Lis1 are characterised by increased localization of microtubules to the perinuclear region along with a decrease in localization to the leading process (Sasaki *et al.,* 2000), by reduced migration velocity, by fewer leading process filopodia (Moon and Wynshaw-Boris, 2013), and by impaired dynein motor activity (Yamada *et al.,* 2008). Inhibition of Lis1 *in vivo* leads to defective neuronal migration, miss-positioning of neurons in the cortex, and a severe cortical lamination disorder known as lissencephaly (section 1.4.5) (Moon and Wynshaw-Boris, 2013).

1.4.3.4 Dynein

Dynein, the main retrograde microtubule motor, operates by binding to and transporting intracellular components toward the minus end of the microtubule structure by interacting with its partner dynactin (Kimura *et al.,* 2008; Moon and Wynshaw-Boris, 2013; Yamada *et al.,* 2008). The minus end-directed transport of dynein enables the relocation of organelles and cytosolic contents from the growing tip of the neuronal process back to the cell body (Ahmad *et al.,* 2006). Interestingly, interfering with microtubule stability has been reported to affect motor-based transport of organelles across microtubule tracks, suggesting that microtubule stability affects dynein function (Xie *et al.,* 2010).

In addition to transporting organelles throughout the cell, dynein plays a crucial role in facilitating neuronal migration. For example, dynein interacts with microtubules and Lis1 to form a complex that generates the pulling force involved in centrosome positioning and nucleokinesis (Moon and Wynshaw-Boris, 2013; Tsai and Gleeson, 2005; Vallee and Tsai, 2006). The microtubule network surrounding the nucleus, referred to as the perinuclear cage, establishes a link between the NE and the centrosome. The dynein-Lis1 complex is believed to pull the centrosome in the direction of the leading edge of the cell, with this pulling force acting on the perinuclear microtubules and NE to enable the forward translocation of the nucleus (Mètin *et al.,* 2008; Tsai and Gleeson, 2005).

Another important role of dynein is the bidirectional transport of short microtubules across microtubule tracks. While longer microtubules are generally stationary, short microtubules may be transported rapidly from one end of the microtubule to the other to facilitate microtubule polymerization (Myers *et al.,* 2006). Dynein motors play a key role in the bidirectional transport of short microtubules. The transport of short microtubules is predominantly anterograde, thus from the dynamic plus end to the more stable minus end near the centrosome, but some microtubules are transported in a retrograde manner (Ahmad *et al.,* 2006; Myers *et al.,* 2006). Dynein motors have been proposed to move from their site of synthesis to the plus-end of the microtubule, where short, transportable microtubule fragments are loaded onto dynein, after which dynein transports these microtubule fragments predominantly towards the minus-end of the microtubule (Yamada *et al.,* 2008).

Lastly, dynein motors play a crucial role in enabling protein clearance through autophagy (section 1.5). Interfering with dynein function in glioma cells results in the accumulation of autophagosomes, suggesting that dynein motor activity is responsible for the microtubule-based transport of autophagosomes (Yamamoto *et al.,* 2010). This is further discussed in section 1.5.5.

1.4.3.5 The MAP1 Family of Proteins

Another key regulator of the neuronal microtubule system is the MAP1 family of proteins. This family forms cross-bridges between microtubules, and consists of three members: MAP1A, MAP1B, and MAP1S (also referred to as MAP8). MAP1A and MAP1B are well-

characterised as proteins that bind to and stabilise the microtubule cytoskeleton and are both key regulators of axon and dendrite formation (Bondallaz *et al.,* 2006; Morii *et al.,* 2006; Poulain and Sobel; 2010). MAP1A is highly expressed in mature neurons and localises to axons and dendrites to stabilize microtubules (Faller *et al.,* 2009). MAP1B is enriched in axons and growth cones, and plays an important role in axon lengthening. MAP1B deficient mice are characterised by abnormal axon tracts and defective cortical lamination. Cultured MAP1B deficient hippocampal neurons are characterised by a decrease in tyrosinated microtubules and a subsequent increase in detyrosinated microtubules, suggesting that MAP1B modulates microtubule dynamics. In response to treatment with the microtubule destabilizing compound nocodazole, MAP1B deficient neurons display impaired microtubule polymerization recovery compared to controls, suggesting that MAP1B enhances microtubule polymerization (Poulain and Sobel, 2010). Although the respective roles of MAP1A and MAP1B are relatively clear and well-documented, less is known about the function of MAP1S. Post-translational modification of MAP1S gives rise to multiple isoforms, including short chain (SC), light chain (LC) and heavy chain (HC) isoforms, of which the functions remain unclear (Xie *et al.,* 2011). Abnormal accretion of MAP1S results in excessively stable microtubules and impaired axonal transport. MAP1S has also been shown to regulate *in vitro* fibroblast migration (Kalny and Propst, 2008), to affect autophagy, and to interact with the N-methyl D-aspartate (NMDA) receptor (Wang *et al.,* 2012; Xie *et al.,* 2011). NMDA receptors are membrane-associated ion channels that regulate cellular calcium uptake, which is necessary for synapse formation (Lakatosova and Ostanikova). Interestingly, NMDA receptors have been reported to influence neuronal migration, though the mechanisms responsible for these affects remain unclear (Manent *et al.,* 2005). Nevertheless, the interaction of MAP1S with NMDA receptor subunits offers a potential mechanism by which MAP1S may regulate cell migration. The discussion on MAP1S function will proceed in section 1.5.5.1 after an in depth discussion on autophagy.

The microtubule-regulating proteins discussed above are of particular relevance in the context of the current study. However, it should be mentioned that various other crucial MAPs and microtubule destabilising proteins exist, such the MAP2 family, which promote microtubule stability and neurite outgrowth, doublecortin (DCX), which binds at the junction of tubulin heterodimers and inhibits microtubule depolymerisation, and microtubule

severing proteins such as katanin and spastin (Poulain and Sobel, 2010). A key regulator of the activity of several MAPs and thereby of neuronal migration is an extracellular protein called Reelin.

1.4.4 The Reelin Signalling Cascade

Before reaching a final position within the cortex, migrating neurons must pass through the MZ. In the MZ, the migrating neurons come into contact with the Cajal-Retzius cells, which generate an important regulatory signal: Reelin, a large glycoprotein that initiates an intracellular signalling cascade upon binding to trans-membrane receptors. This cascade consists of multiple components, such as kinases, phosphatases, and several MAPs that ultimately converge at the cytoskeleton (Kwan *et al.,* 2012; Lakatosova and Ostatnikova, 2012).

The Reelin cascade (Figure 1.5) is activated upon Reelin binding to the extracellular membrane receptors apolipoprotein receptor 2 (ApoER2) and very low density lipid receptor (VLDL-R), followed by dimerization of the receptors and activation of the SRK family of tyrosine kinases. This leads to tyrosine phosphorylation of disabled-1 (Dab-1; an adaptor protein). Amongst other effects, phosphorylated Dab-1 activates the phosphatidylinsositol-3-kinase (PI3K) and subsequently protein kinase B (PKB), which leads to inhibition glycogen synthase kinase (GSK3β). GSK3β is a kinase responsible for phosphorylation and regulation of several MAPs, such as Tau protein. Dab-1 also controls Lis1 complex formation and microtubule-regulating activity. The effects of Dab-1 activation therefore control the dynamic instability of microtubules (Folsom and Fatemi, 2013; Lakatosova and Ostanikova, 2012; Moon and Wynshaw-Boris, 2013). After initiating the intracellular signalling cascade, Reelin becomes internalized for lysosomal degradation (Lakatosova and Ostatnikova, 2012).
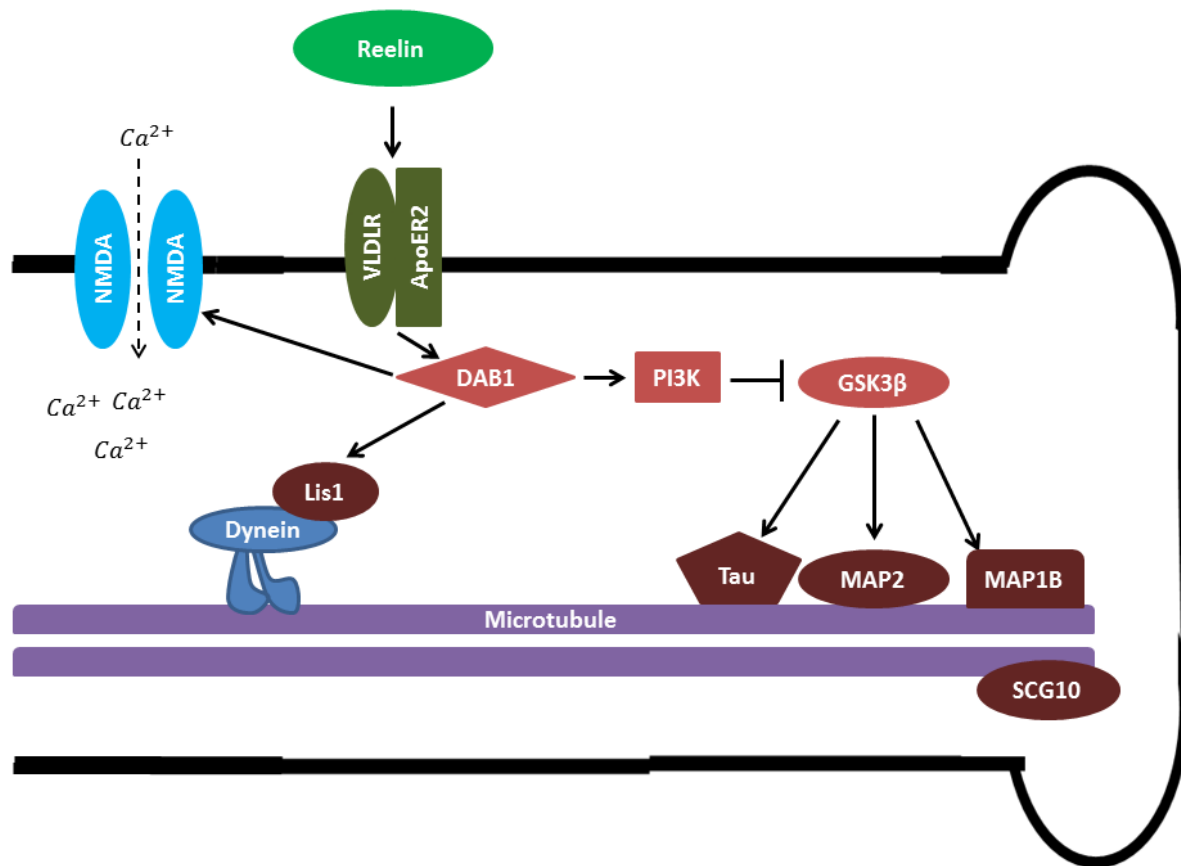
Figure 1.5: A simplified schematic of the Reelin signalling cascade. The Reelin signalling cascade is activated upon Reelin binding to ApoER2 and VLDL-R transmembrane receptors, inducing their dimerization. This leads to phosphorylation and subsequent activation of the adaptor protein Dab-1 by the SRK family (not shown), and ultimately to inhibition of GSK3β, which usually phosphorylates MAPs such as Tau. Dab-1 activation enables the interaction of Lis1 with the motor protein dynein, and also activates the NMDA receptor subunits to enable calcium influx.

Dysfunctional Reelin signalling is associated with molecular abnormalities such as the accumulation of the adaptor protein Dab-1 and/or hyperphosphorylated aggregates of Tau protein (Lakatosova and Ostatnikova, 2012). Additionally, abnormalities in actin cytoskeleton regulation and a decreased number of filopodia are observed in Reelin deficient neurons, likely because Reelin has been reported to phosphorylate the actin-depolymerizing protein cofilin. Abnormalities in actin remodelling further contribute to the neuronal migration deficits in Reelin mutants (Folsom and Fatemi, 2013; Leemhuis *et al.,* 2010; Moon and Wynshaw-Boris, 2013).

1.4.4.1 The Reeler Mouse

A mouse model lacking Reelin, the *Reeler* mouse, occurred spontaneously and was first described in 1951 (Falconer, 1951). This discovery greatly contributed to the current understanding of Reelin's role in neurodevelopment. In addition to a characteristic tremor and reeling, unsteady gait, mice lacking Reelin present with abnormal brain structure. For instance, *Reeler* mice display an underdeveloped cerebellum and severely disorganized cortical lamination (Lakatosova and Ostatnikova, 2012). In the absence of Reelin, the PP fails to split into the MZ and the SP, and neurons are incapable of migrating past earlier-born neurons within the cortex, leading to the formation of an inverted neocortex (Kwan *et al.,* 2012; Marín *et al.,* 2010). Behavioural abnormalities of *Reeler* mice include lower activity levels than littermates, crouching in the corners of cages, failure to be aroused when their cages are opened, and a reduced tendency to groom compared to wild-type mice (Falconer, 1951).

The *Reeler* mouse also greatly enhanced the current understanding of the connection between the birth date and the eventual laminar identity of cortical post-migratory neurons. Despite the inverted positioning of neurons in the *Reeler* mouse cortex, neurons conserve their birth-date specific identities. This suggests that neuronal birthdate plays a more crucial role in controlling eventual neuronal identity than does the layer-specific positioning of neurons in the cortex (Kwan *et al.,* 2012).

1.4.4.2 The Mechanisms of Reelin in Neuronal Migration and Neurodevelopment

It is evident Reelin plays an important role in controlling cortical lamination by allowing the splitting of the PP into the MZ and SP, but aspects such as the precise mechanism by which the Reelin cascade controls migration and further roles of Reelin in neurodevelopment remain unclear. Some hypothesize that Reelin acts as a chemo-attractant for migrating cells (Gaiano, 2008; Herz and Chen, 2006). A widely accepted theory is that one function of Reelin is to act as a stop signal, particularly for radially migrating neurons of the cerebral cortex and hippocampus, terminating the migration process so that neurons may settle in their positions within the cortex for terminal differentiation (Folsom and Fatemi, 2013; Lakatosova and Ostatnikova, 2012; Moon and Wynshaw-Boris, 2013). Additionally, Reelin has been shown to be involved in synapse formation and synaptic plasticity by regulating

calcium influx through the NMDA receptor (Folsom and Fatemi, 2013; Lakatosova and Ostanikova, 2012). The NMDA receptor consists of several subunits: NR1, NR2A – D, and NR3A – B (Eriksson *et al.,* 2007). Reelin binding to ApoER2 and VLDL-R receptors with subsequent activation of Dab-1 and SRK tyrosine kinases enables phosphorylation of the NMDA receptor subunits NR2A and NR2B. Phosphorylation of these subunits enables NMDA-mediated calcium uptake and initiates cascades that control synapse formation (Folsom and Fatemi, 2013; Lakatosova and Ostanikova, 2012).

1.4.4.3 Reelin in the Adult Brain

The reelin signalling pathway is not only crucial for development, but also likely plays an important role in the functioning of the adult brain (Herz and Chen, 2006; Lakatosova and Ostanikova, 2012), since it has been shown that low levels of Reelin secretion continues after birth and even throughout adulthood. The cells responsible for post-natal Reelin secretion include cerebellar granulocytes, hippocampal interneurons, and a subdivision of cortical interneurons. The binding of Reelin to ApoER2 and VLDL-R receptors is vital for the learning and memory functions of the hippocampus, and Reelin has been shown to play a role in the discharge of presynaptic neurotransmitters (Lakatosova and Ostatnikova, 2012). Furthermore, certain neurological conditions, particularly autism and psychosis associated with schizophrenia and bipolar disorder, are characterised by a 50% decrease in Reelin expression in the adult brain (Folsom and Fatemi, 2013; Lakotosova and Ostanikova; 2012).

Defects in components of the Reelin cascade are associated with several brain abnormalities, ranging from severe to mild. For example, mutations in ApoER2, VLDL-R, or Dab-1 result in a *Reeler* mouse phenotype, highlighting the crucial role of these components in Reelin signalling (Folsom and Fatemi, 2013; Gaiano, 2008; Herz and Chen, 2012). In contrast, mutations in Tau protein are not associated with obvious phenotypic abnormalities (Lakatosova and Ostatnikova, 2012; Poulain and Sobel, 2010). Generally, however, mutations in cytoskeletal components and regulators are linked to defective neuronal migration and neurological disorders such as schizophrenia, epilepsy, autism spectrum disorders, and bipolar disorder (Kwan *et al.,* 2012; Westerlund *et al.,* 2011). Mutated Lis1, for example, leads to a devastating neuronal migration disorder, termed lissencephaly, which is of particular relevance to this study.

1.4.5 Lissencephaly: a Prime Example of a Neuronal Migration Disorder

Lissencephaly, also known as "smooth brain," is clinically characterised by a severely malformed, thickened neocortex that either completely lacks convolutions (agyria) or has a greatly simplified, less convoluted appearance (pachygyria) (Marín *et al.,* 2010; Moon and Wynshaw-Boris, 2013). Affected individuals suffer from mental retardation, compromised motor function, epilepsy, and a considerably shortened life span. This severe neuronal migration disorder affects an estimated 1 in 30 000 individuals. The classical form of this disease (Type 1 Lissencephaly) is considered to be one of the most severe neuronal migration disorders, mainly results from mutations in either Lis1 or DCX, and is associated with disordered or poorly defined cortical layers (Manent and LoTurco; 2012; Moon and Wynshaw-Boris, 2013; Yamada *et al.,* 2008). Interestingly, Reelin deficiency in humans results in lissencephaly as opposed to the inverted cortex seen in rodents. The mechanisms behind this perplexing phenomenon are however not clear (Lakatosova and Ostatnikova, 2012).

Lissencephaly has received much attention due to the potential that it holds in enhancing our knowledge of the complex mechanisms underlying neuronal migration (Vallee and Tsai, 2006), because this severe cortical lamination disease can result from deficiency of a single microtubule-regulating protein (Lis1 or DCX). Lis1 has multiple binding partners, but its function is mainly dependent on interaction with microtubules and dynein motors. This re-emphasizes the profound effect of microtubule regulation on neuronal migration and brain development (Manent and LoTurco; 2012).

Taking advantage of the finding that Lis1 is proteolytically degraded by the calpain system, Yamada *et al.* (2009) demonstrated that pharmacologically increasing Lis1 protein levels by inhibiting calpain, using either calpain inhibitors or calpain siRNA, corrected the abnormal phenotype and restored the migration defects observed with heterozygous Lis1-deficient cerebellar neurons. The authors further demonstrated that neuronal migration defects, cortical architecture abnormalities, and behavioural aberrations in heterozygous Lis1-defcient mouse pups was greatly improved by pharmacological inhibition or siRNA treatment to inhibit the calpain system. This remarkable finding demonstrates that pharmacological restoration of a single protein holds potential to successfully treat neuronal

migration disorders. A clear understanding of the proteins controlling the microtubule system and neuronal migration is the key to unlocking this therapeutic potential.

The literature reviewed above summarizes the complex regulation of the microtubule system and how this affects a major aspect of corticogenesis, neuronal migration. We now proceed to review another microtubule-dependent process that has recently emerged as a crucial aspect of brain development: autophagy.

1.5 Autophagy

Autophagy (self-digestion) is a major process of bulk intracellular degradation by which cells break down long-lived cytoplasmic proteins and organelles. The ingested cargo is degraded in a lysosome-dependent manner and subsequently recycled to maintain protein homeostasis and to produce energy for the cell (Loos *et al.,* 2013; Yu, 2014).

1.5.1 Classification of Autophagy

Broadly, autophagy can be categorized either as microautophagy, chaperone-mediated autophagy, or macroautophagy. In microautophagy, cargo for degradation is delivered to lysosomes by invagination, protrusion, or separation of the lysosomal membrane. Chaperone-mediated autophagy involves the delivery of single specific intracellular proteins directly to lysosomes via the chaperone complexes Hsc70 and Lysosome-Associated Membrane Protein-2A (LAMP-2A) (Cuervo, 2004). Macroautophagy is referred to in literature as autophagy as it is the most highly characterised, best understood, and most predominantly active form of autophagy in most metabolic, cell-death related and disease-specific contexts. Macroautophagy (from here onwards referred to as autophagy) refers to bulk, non-specific autophagosomal uptake of a portion of cytoplasm and consequent fusion with lysosomes/vacuoles for degradation (Lee *et al.,* 2013; Loos *et al.,* 2013; Yu, 2014).

1.5.2 The Role of Autophagy in Health and Disease

Autophagy is important for several cellular processes, including cell survival, death, development, pathogen clearance, differentiation, and homeostasis (Ban *et al.,* 2013; Hansen and Johansen, 2011; Tanida *et al.,* 2004; Xie *et al.,* 2011; Yu, 2014). A major role of autophagy is providing cells with energy under nutrient-deprived conditions by recycling

cytosolic contents. Nevertheless, under normal nutrient conditions autophagy remains active at a basal level. This enables quality regulation of protein and organelles, shielding cells from the consequences of abnormal protein/organelle accumulation. Basal autophagy is thus important for protection from several disease states, including inflammatory diseases, cardiomyopathies, cancer, and neurodegenerative diseases (Hansen and Johansen, 2011; Klionsky, 2005; Lee *et al.,* 2013; Yu, 2014). For example inhibition of basal autophagy in mouse models consequents in protein accumulation and neurodegeneration, but inducing autophagy increases survival rates (Hansen and Johansen, 2011; Rubensztein *et al,* 2009). Autophagy also often plays a protective role in cancer by eliminating intracellular aggregates that cause oxidative stress. However, up-regulation of autophagy may contribute to disease pathogenesis in some cases. For example, autophagy may assist tumour growth by recycling and making energy available for nutrient-deprived tumours (Hansen and Johansen, 2011). Thus, an optimal balance the rate of protein degradation through autophagy, termed autophagic flux, within a particular developmental/disease-specific context is important for cell viability, and altering autophagic flux has emerged as a potential therapeutic intervention for several diseases (Yu, 2014).

1.5.3 Regulation involved in Autophagosome Formation

Autophagosomes are derived from several organelles, including the Golgi apparatus, the plasma membrane, the mitochondrial membrane, and most frequently, the endoplasmic reticulum (ER) (Bartolomeo *et al.,* 2010; Loos *et al.,* 2013; Yu, 2014). Autophagosome formation relies on four major steps: initiation, nucleation, expansion, and maturation. Once autophagy has been initiated, nucleation begins when an isolation membrane envelopes a portion of substrate-containing cytoplasm, forming the double-membrane structure known as the autophagosome. The autophagosome expands and matures, and is then transported across the microtubule cytoskeleton to fuse with the lysosome, forming an autophagolysosome, the structure responsible for degradation of the cytoplasmic components. Autophagosomes can also take a slightly different route by fusing first with endosomes to form structures called amphisomes, which then fuse with lysosomes to form autophagolysosomes (Hansen and Johansen, 2011; Lee *et al.,* 2013; Kimura *et al.,* 2008; Xie *et al.,* 2011). These steps are regulated by a host of autophagy-related genes and their

protein products (referred to ATG proteins), of which more than 30 have been identified (Klionsky, 2005; Loos *et al.,* 2013).

1.5.4 Signalling Pathways Controlling Autophagosome Initiation, Nucleation, Expansion, and Maturation

Autophagy initiation is tightly coupled to cellular energy-sensing pathways, enabling autophagy to enhance substrate availability under nutrient-deprived conditions. The mammalian target of rapamycin (MTOR) is not only a key cellular energy sensor and growth regulator (Loos *et al.,* 2013), but also a regulator of autophagy initiation. MTOR becomes activated in response to signals from either growth factors or the presence of metabolites, particularly amino acids such as leucine and isoleucine. When MTOR is activated, autophagy is inhibited. On the other hand, MTOR signalling ceases when cells are in a state of nutrient-deprivation, the inhibitory effect of MTOR on autophagy is removed, and autophagic activity increases to enhance substrate availability. Growth factor signalling inhibits autophagy by activating the MTOR- phosphatidylinositol 3-kinase (PI3K)-v-akt murine thymoma viral oncogene (AKT) pathway, while nutrients/metabolite signalling inhibits autophagy via the MTOR- serine/threonine kinase 11 (LKB1)-AMP-activated protein kinase (AMPK2). Additionally, anti-apoptotic proteins Bcl-2 and Bcl-xL recruit BCL2 interacting protein (Beclin 1) to inhibit autophagy or enhance P27 levels to activate autophagy through the LKB1-AMPK-MTOR pathway (Figure 1.6). Autophagy can also be initiated independent of MTOR signalling. Other factors that are coupled to autophagy initiation include ATP, calcium levels, and protein accumulation (Lee *et al.,* 2013; Xie *et al.,* 2011).

Nucleation, or the formation of an isolation membrane, is mediated by the Beclin1/PIK3C3 complex. This complex consists of Beclin 1, PIK3C3, AMBRA1, p150, UV Radiation Resistance-Associated Gene (UVRAG), and ATG14. Briefly, PIK3C3 enables the formation of phosphatidyl-inositol-3-phosphate (PI3P), which leads to the translocation of several ATG proteins to the isolation membrane. AMBRA-1 becomes phosphorylated, enabling PIK3C3 to be recruited from the microtubule cytoskeleton to the ER, where the isolation membrane most frequently originates from (Figure 1.6) (Lee *et al.,* 2013).

Elongation, or extension of the isolation membrane, is dependent on the ATG12-ATG5-ATG16L1 conjugation system as well as the Microtubule-associated Light Chain 3-

Phosphatidyl Ethanolamine (LC3-PE) system. The former consists of ATG12, ATG7, ATG10, ATG5, and ATG16L1, while the latter consists of LC3, ATG4, ATG7, and ATG8. The ATG12-ATG5-ATG16L1 conjugation system operates by interacting with several PI3P-recruited complexes to elongate the isolation membrane. The LC3-PE system is activated when ATG4 proteolytically modifies LC3, the mammalian homologue of yeast ATG8, into a cytosolic form, LC3-I, with an exposed C-terminal glycine residue. LC3-I then first becomes conjugated to the ubiquitin activating enzyme (E1)-like enzyme ATG7, after which it is transferred to the ubiquitin-conjugating enzyme (E2)-like enzyme ATG3. LC3-I conjugated to ATG3 is present at the autophagosome membrane initiation site, and the ATG12-ATG5-ATG16 complex accomplishes covalent conjugation of the exposed C-terminal glycine residue to phosphatidylethanolamine (PE) to form membrane-bound LC3-II (Figure 1.6). Thus, the amount of LC3-II correlates with the degree of autophagosome formation; LC3-II is often used as a marker for autophagosome formation and autophagy (Kimura *et al.,* 2008; Lee *et al.,* 2013; Xie *et al.,* 2011). An increased level of LC3-I may suggest enhanced LC3-I synthesis and/or decreased conversion of LC3-I to LC3-II, while an increased level of LC3-II may suggest either an increase in conversion of LC3-I to LC3-II, and thus increased autophagic activity, or a decrease in the degradation of autophagosomes. To accurately interpret LC3 protein level analysis, Bafilomycin A1 treatment, which inhibits the H+ ATPase and subsequently the fusion of autophagosomes with lysosomes, is often made use of. Bafilomycin A1 treatment reveals the total amount of LC3-II present whilst autophagosome and lysosome fusion is blocked. An increase in LC3-II levels in the presence of Bafilomycin A1 therefore indicates an increase in autophagic flux (Xie *et al.,* 2010). P62, also known as sequestosome 1 (SQSTM1), is an adaptor molecule that binds directly to LC3 and targets poly-ubiquitinated proteins toward the autophagolysosome for degradation, thereby enabling selective autophagy (Barth *et al.,* 2010; Bjørkøy *et al.,* 2009). Along with LC3-II, P62 is often used as a measure of autophagic activity. Although changes in P62 protein levels may indicate deviations in selective autophagy of ubiquitinated proteins, P62 is itself degraded by macroautophagy (Bjørkøy *et al.,* 2009), thereby complicating the interpretation of data. Additionally, factors such as oxidative stress and the *Ras* oncogene affect the transcription of P62 (Barth *et al.,* 2010).

Maturation of autophagosomes refers to the fusion of the autophagosomes with lysosomes or endosomes (Figure 1.6). Little is known about the proteins and factors involved in the fusion process (Lee *et al.,* 2013). However, it is known that this is a microtubule-dependent process: the microtubule cytoskeleton serves as a "tract" for autophagosomes to be transported via dynein motors to the minus-end, where lysosomes are clustered (Bartolomeo *et al.,* 2010; Katsumata *et al.,* 2010; Xie *et al.,* 2011). Interestingly, LC3 was originally identified as a binding partner of the microtubule-regulating proteins MAP1A and MAP1B, and these interactions facilitate the association of LC3-I and LC3-II with microtubules, further pointing towards a role for microtubules in autophagosome formation (Xie *et al.,* 2010).
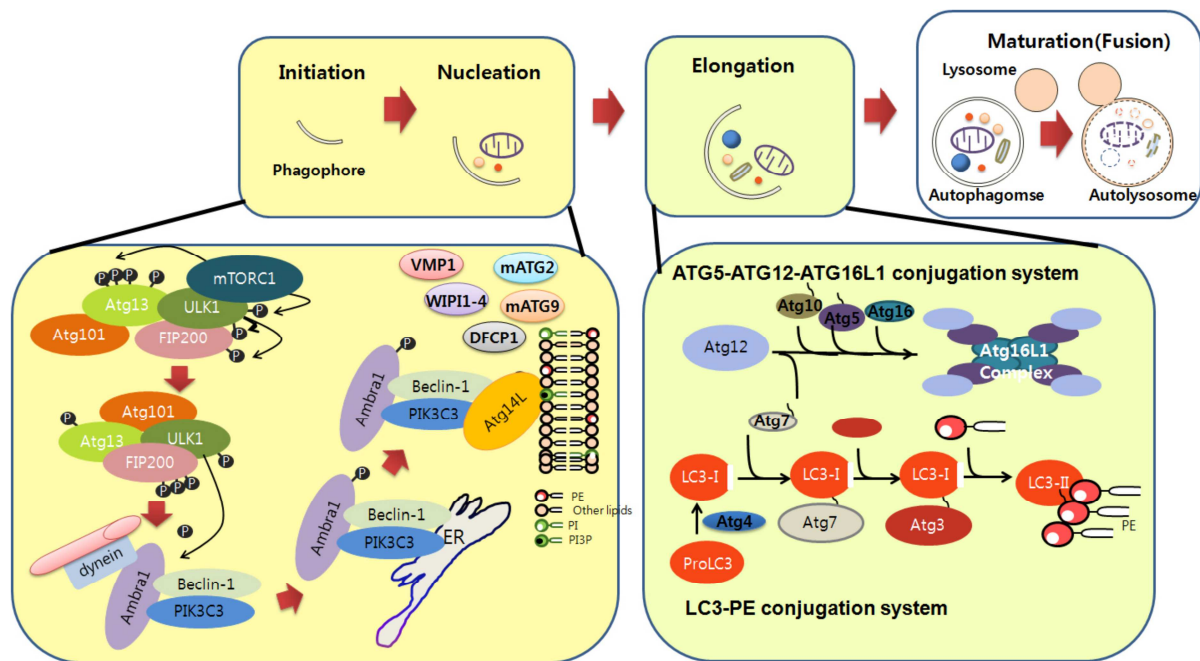
Figure1.6: Signalling cascades regulating autophagosome formation. Initiation is achieved when mTOR is inhibited and PIK3C3 translocates to the ER, Beclin1 activates PIK3C3 kinase activity, and PI3P is generated. Formation of the isolation membrane (nucleation) occurs when PI3P recruits several proteins to the phagophore. Elongation is controlled by the ATG5-ATG12-ATG16 and LC3-PE conjugation systems to generate autophagosomes with LC3-II associated to the membranes. Fusion of autophagosomes with lysosomes generates mature autophagolysosomes (Lee *et al.,* 2013).

1.5.5 The Role of the Microtubule Cytoskeleton in Facilitating Autophagy

Microtubule regulation is important for several aspects of autophagy: the initiation and maturation of autophagosomes are dependent on their association with microtubules, since they act as tracts for autophagosomes to be transported to the lysosomes and are also responsible for orchestrating the spatial order of autophagosomes, lysosomes, and cargo for degradation. The fusion of autophagosomes with lysosomes is dependent on the association with acetylated microtubules particularly, which are predominantly present near the centrosome (Xie *et al.,* 2011).

The mechanisms behind autophagosome and lysosome trafficking are poorly understood. However, it is known that autophagosomes are transported by dynein motors across the microtubule network toward the centrosome, where lysosomes are gathered (Figure 1.7) (Bartolomeo *et al.,* 2010; Katsumata *et al.,* 2010; Kimura *et al.,* 2008).
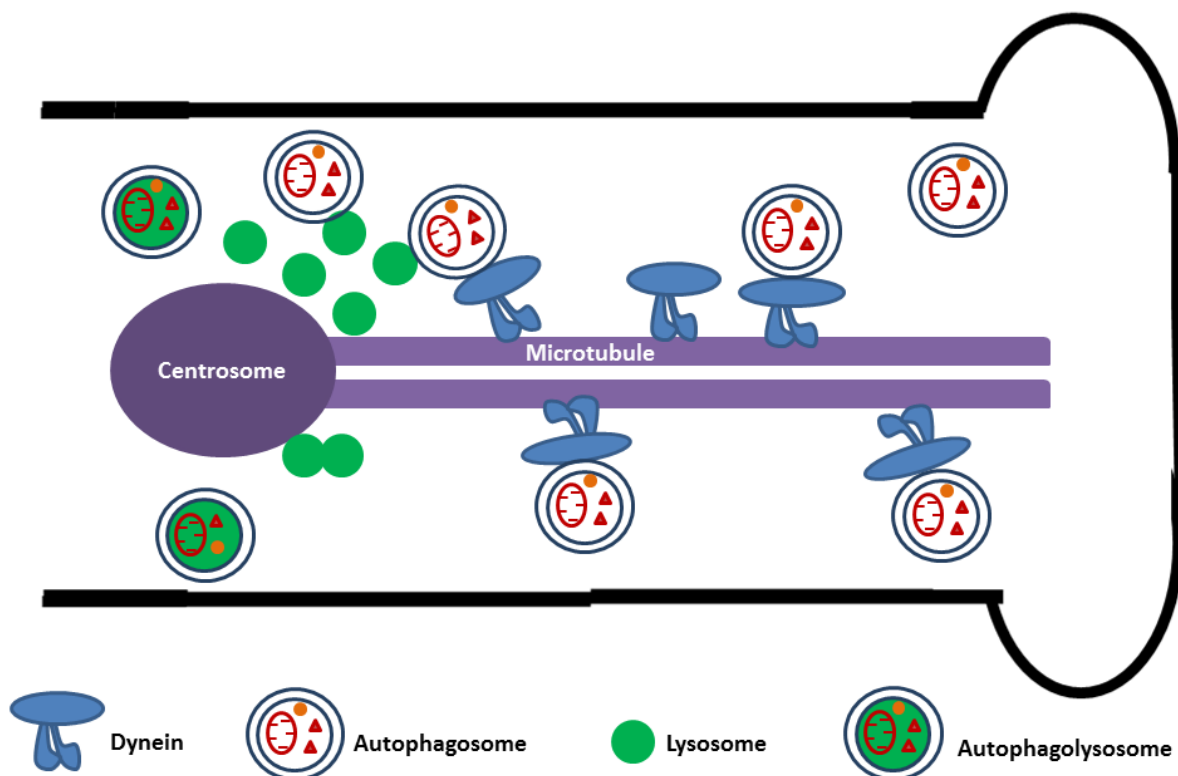
Figure 1.7: Role of the Microtubule Cytoskeleton in Autophagosome and Lysosome Fusion. Cargo-containing double-membrane autophagosomes are transported via dynein motors across the microtubule cytoskeleton, predominantly toward the centrosome where lysosomes are clustered. Autophagosomes and lysosomes fuse to enable cargo degradation

31

1.5.5.1 MAP1S: An Example of the Molecular Link between Microtubules and Autophagy

Mutations that affect microtubule regulation are often associated with alterations in autophagic activity. MAP1S, also referred to as MAP8, is a homologue of the neuron-specific microtubule-associated proteins MAP1A and MAP1B. MAP1S is a regulator of both microtubule stability and autophagy, demonstrating the synergy of these two systems. MAP1S also contains an actin binding site, suggesting that it may link the regulation of microtubule and actin networks. Additionally, MAP1S has been shown to interact with the NR3A subunit of the NMDA receptor, which regulates calcium intake by the cell to enable synapse formation (Eriksson *et al.,* 2007; Wang *et al.,* 2012; Xie *et al.,* 2011), and it has been reported to influence neuronal migration (Manent *et al.,* 2005). MAP1S isoforms interact with microtubules, but also bind to and recruit autophagosome-associated LC3-I and -II to microtubules. It was recently demonstrated that MAP1S knock-out mice display dysfunction in nutritive stress-induced autophagy and basal autophagy, and are characterised by reduced levels of Bcl-2, Bcl-xL, and P27 in brain, heart, and liver. Interestingly, no aberrant phenotypic or behavioural features are observed in MAP1S knock-out mice (Xie *et al.,* 2011). MAP1S has also been reported to affect the migration of cultured fibroblasts (Kalny and Propst, 2008). Furthermore, over-expression of MAP1S leads to extreme microtubule stabilisation and defective microtubule-associated transport. However, very little is known about the interaction of MAP1S with other proteins (Wang *et al.,* 2012).

1.5.6 Autophagy and Neurodevelopment

Neuronal cells have particularly high energy requirements paired with high rates of autophagic activity, a characteristic that is vital to preserving neural function. Neuronal autophagy plays a role in inhibiting cytotoxicity and protecting neurons from stressors such as protein accumulation, as neurons are notably sensitive to the build-up of abnormal proteins and organelles (Ban *et al.,* 2013; Lee *et al.,* 2013; Loos *et al.,* 2013). Autophagosome accumulation is evident in neurons during corticogenesis, suggesting that autophagy is actively participating in neural development. Knock-down of ATG5 or ATG7 in mice leads to atypical protein accumulation, neurodegeneration, growth delays, and behavioural abnormalities such as ataxic walking and defective reflexes, suggesting that autophagy is vital to neuronal homeostasis (Hara *et al.,* 2006; Lee *et al.,* 2013; Shehata *et*

al., 2012), and ATG7 deficiency particularly in the CNS results in premature death in mice (Komatsu *et al.,* 2006), demonstrating the crucial role of autophagy in brain development.

1.5.6.1 Potential Roles of Autophagy in Regulating Neurite Outgrowth, Neuronal Differentiation and Proliferation

Although recent literature is suggestive of a role for autophagy in neuronal protein clearance and homeostasis, other roles of autophagy in neurodevelopment remain unclear. Current research is presenting scientists with several possibilities. For example, lysosomal degradation has been linked to axon pruning, a process required for neuronal networking (Ban *et al.,* 2013; Lee *et al.,* 2013). Ban *et al.* (2013) demonstrated that suppression of autophagy by atg7 knock-down lead to abnormal lengthening of axons in cortical neurons. On the other hand, the authors demonstrated that treating cortical neurons with the autophagy-inducing agent Rapamycin lead to atypically short axonal processes. Therefore, autophagy may be a regulator of early neurite lengthening and shortening, serving as a pruning mechanism to optimize neurite morphology for neuronal network formation. Furthermore, autophagy may play a role in neuronal differentiation. Zhao *et al.* (2010) showed that inhibition of autophagy with 3-methyladenine or Bafilomycin A1 treatment disturbed the differentiation of glioma stem/progenitor cells, and that inducing autophagy with Rapamycin stimulated their differentiation. In addition, Petralia *et al.* (2013) showed that up-regulation of Sonic hedgehog (Shh), a gene involved in several neurodevelopmental aspects including presynaptic differentiation, stimulated autophagy *in vitro* in hippocampal neurons. Lastly, Cecconi *et al.* (2007) identified a potential role for autophagy in regulating the proliferation of neuroblasts during early developmental stages. The authors assessed Ambra1 in particular, a neurodevelopment-related protein known to regulate Beclin 1-mediated autophagy (Figure 1.6). Ambra1-deficient mice were characterised by hyper-proliferation of neuroblasts concurrent with decreased autophagic activity. Over-expression of Ambra1 reduced the degree of proliferation and enhanced autophagic activity.

1.5.6.2 Autophagy and Neurodevelopmental Disorders

Autophagy has been shown to play an important role in certain neurodevelopmental disorders. For example, mTOR inhibition was affected in a mouse model of autism, implying altered autophagy regulation, as mTOR inhibition is essential to autophagy initiation.

Rapamycin, an mTOR inhibitor and thereby an autophagy inducing agent, restored some of the behavioural and structural brain abnormalities associated with autism (Lee *et al.,* 2013). Fragile X syndrome is an autism spectrum disorder resulting from mutated fragile X mental retardation protein 1 (FMR1). FMR1 knock-out mice displayed increased MTOR activity as well as enhanced protein synthesis, implying that both homeostasis and autophagic activity is affected in this disorder (Lee *et al.,* 2013). WDR45, a mammalian homologue of ATG18, is a member of the WD40 repeat family of proteins that is known to be involved in autophagy regulation, though the exact mechanism of action of WDR45 remains unclear (Ozawa *et al.,*2014; Saitsu *et al.,* 2013). Interestingly, individuals with mutated WDR45 were most recently shown to suffer from a disorder known as static encephalopathy of childhood with neurodegeneration in adulthood (SENDA). This disorder is characterised by severe developmental delays in childhood along with neurodegeneration and disability in adulthood (Ozawa *et al.,* 2014). Lymphoblastoid cells isolated from individuals that are carriers of the WDR45 mutation were shown to be characterised by decreased autophagic flux and accumulation of autophagosomes (Saitsu *et al.,* 2013), demonstrating that altered autophagy can severely affect neurodevelopment.

In summary, recently generated literature is pointing towards a key role for autophagy in neurodevelopment, likely as an axonal pruning mechanism to allow accurate neuronal circuit formation and as a regulator of neuronal proliferation and/or differentiation. Defective autophagy is implicated in several neurodevelopmental disorders. Microtubule regulation affects autophagy; MAP1S is a prime example. A comprehensive understanding of the genes and proteins contributing to microtubule-dependent autophagic flux in neurons of the developing CNS may offer unique interventions for several autophagy-associated neurodevelopmental disorders (Ban *et al.,* 2013; Lee *et al.,* 2013). In this context, we now proceed to discuss WDR47, the basis of the present study.

1.6 WD Repeat Domain 47: A Protein of Unknown Function

WD repeat domain 47 (WDR47) is a recently identified protein that belongs to the highly conserved WD repeat family of proteins, a large division of functionally and structurally diverse proteins that all house the WD40 repeat domain. The members of this family of proteins have various cellular roles, including cell motility, vesicle formation, mitosis, cell

death, cytoskeletal assembly, signal transduction, cell migration, and transcription (Nocker and Ludwig, 2003; Smith *et al.,* 1999; Sun *et al.,* 2011). The function of WDR47 has not been previously investigated. WDR47 contains three functional domains: a WD repeat domain consisting of seven WD40 repeats at the C-terminal, a lissencephaly-1 homology (LisH) domain at the N-terminal, and a C-Terminal to Lis homology (CTLH) domain adjacent to the LisH domain at the N-terminal (Figure 1.8).

Figure 1.8: Functional domains of WDR47. WDR47 has a LisH domain and a CTLH domain at the N-terminal, and seven WD40 repeats at the C-terminal. This domain architecture is remarkably similar to that of Lis1, which also has a LisH domain and seven WD40 repeats.

1.6.1 WD40 repeat domain of WDR47

The WD40 domain consists of 40 – 60 amino acids and usually has a glycine-histidine (GH) dipeptide near the N-terminus as well as a tryptophan-aspartic acid (WD) at the C-terminus. Originally discovered as a subunit of the G protein transducing complex, crystal structure analysis of the WD40 domain reveals a circular seven-bladed β-propeller fold. Each WD40 repeat consists of four-stranded anti-parallel β-sheets and provides a surface for non-specific protein binding (Figure 1.9) (Stirnimann *et al.,* 2010; Wang *et al.,* 2012). In all members of this family, the WD40 domain acts as a cellular hub that enables the formation of multi-protein complexes. For example, the WD40 domain has been shown to play a scaffolding role in cytoskeletal assembly and signal transduction, two processes that depend on the interaction of various proteins and that play vital roles in neuronal migration. Although proteins possessing this domain have an underlying scaffolding role and the ability to bind to multiple proteins simultaneously, the WD40 proteins have diverse functions dependent on sequences outside of the WD repeats (Nocker and Ludwig, 2003; Stirnimann *et al.,* 2010; Sun *et al.,* 2011; Wang *et al.,* 2012). For example, the WD40 repeat proteins Ambra1 and WDR45 are both regulators of autophagy (Cecconi *et al.,* 2007; Saitsu *et al.,* 2013, respectively), and the WD40 repeat protein Lis1 plays a crucial role in controlling

microtubule dynamics to regulate neuronal migration (Manent and LoTurco; 2012; Moon and Wynshaw-Boris, 2013). Evidently, a number of severe neurological disorders are associated with proteins that have a WD40 domain (Wang *et al.,* 2012), such as SENDA, which is linked to WDR45 (Ozawa *et al.,* 2014; Saitsu *et al.,* 2013), and Lissencephaly, which is linked to Lis1 (Moon and Wynshaw-Boris, 2013; Yamada *et al.,* 2008).
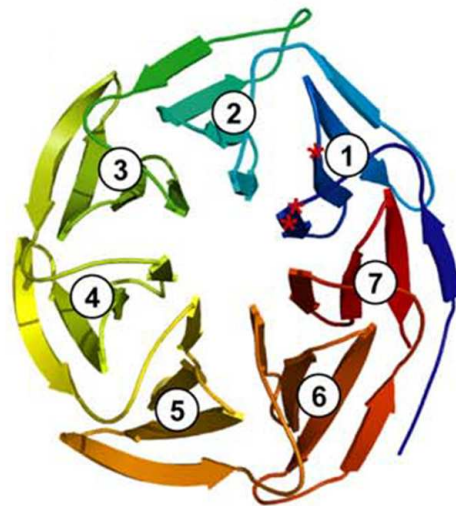
Figure 1.9: Crystal structure analysis of the WD40 domain reveals a circular seven-bladed β-propeller fold, which serves to coordinate multiple protein complex assembly in members of the WD40 repeat family (Stirnimann *et al.,* 2010).

1.6.2 LisH (Lissencephaly Homology) Domain of WDR47

The LisH domain, originally identified in the Lis1 protein that regulates neuronal migration, frequently occurs adjacent to the WD40 domain (Kinnear, 2007; Wang *et al.,* 2012). The Lis1 protein interacts with dynein, Dab1, and microtubules (Marin 2010; Wang *et al.,* 2012). WDR47 and Lis1 have remarkably similar domain structures: both proteins have a LisH domain at the N-terminal and seven WD40 repeats at the C-terminal (Kinnear, 2007; McGillewie, 2009; Wang *et al.,* 2012). The LisH domain facilitates microtubule polymerization, and seven WD40 repeats of Lis1 allow assembly and organization of dynein complexes. However, in comparison to Lis1, WDR47 has an additional functional domain, the CTLH domain. Lis1 and WDR47 share two functional domains, and it is therefore likely

that these proteins have similar functions (Kinnear, 2007; McGillewie, 2009; Wang *et al.,* 2012).

1.6.3 CTLH (C-Terminal to LisH) Domain of WDR47

The CTLH domain is conserved between yeast and mammals, but the biological function of this domain remains obscure. However, the CTLH domain shows sequence homology with Ran-binding protein in the microtubule-organizing centre (RanBPM), a protein reported to associate with the centrosome and to play a role in microtubule assembly in mammalian cells (Kinnear, 2007; Tomaštíková *et al.,* 2012).

1.6.4 Putative Interactions of WDR47 with Reelin and SCG10

Kinnear (2007) recently identified a putative interaction between WDR47 and the extracellular matrix protein Reelin using yeast 2-hybrid analysis. A Foetal brain cDNA library was screened using the N-terminal *reeler* domain of Reelin as "bait". The interaction between Reelin and WDR47 suggested a potential role for WDR47 in neurodevelopment. McGillewie (2009) proceeded with yeast 2-hybrid analysis to identify putative interacting partners for WDR47. The N-terminal of WDR47 was used as "bait", and an interaction between WDR47 and the microtubule destabilizing protein SCG10 was identified. WDR47 and SCG10 were shown to co-immunoprecipitate, supporting an interaction between these proteins. Co-localization of WDR47 and SCG10 in GT1-7 neuronal cells was confirmed, providing further support for an interaction between the proteins. The interaction of WDR47 with SCG10 suggests that WDR47 is involved in microtubule stability regulation.

1.6.5 Nemitin and WDR47: The Same Protein

Wang *et al.* (2012) reported information on a WD40 repeat protein tentatively called nemitin (neuronal-enriched MAP interacting). The authors demonstrated that nemitin plays an unknown role at the microtubule cytoskeleton. They reported that nemitin is expressed predominantly in the brain and spinal cord from embryonic day 11 (E11), and that levels continue to rise until the post-natal period is reached. Nemitin expression is highest during embryogenesis, with low levels of expression throughout adulthood, suggesting that it is most important during development. The expression of nemitin is highest in the brain, particularly in the cortex and hippocampus, although it is also detected in lung, kidney, and

heart tissue. Furthermore, nemitin is distributed diffusely in non-neuronal cells, but is localised at the microtubule cytoskeleton *in vivo* in the axons, dendrites, and cell bodies of neurons. Even more interestingly, co-expression of nemitin with the LC isoform of MAP1S allows the localization of nemitin along the microtubule cytoskeleton, suggesting that nemitin likely plays a role in facilitating MAP1S-related microtubule function. The authors showed by affinity pull-down analysis that the WD40 repeat domain of nemitin interacts with the N-terminal of MAP1S.

Nemitin and WDR47 have identical functional domain structures: seven WD40 repeats, a LisH domain and a CTLH, as well as the same molecular weight (102kDA). This presented us with the question of whether WDR47 and nemitin are in fact the same protein. In-house sequence alignments were performed, confirming that WDR47 and nemitin are different aliases for the same protein (See Figure A1 in Addendum). This paper therefore greatly enhanced our knowledge of WDR47: the results shown indicate that WDR47 is likely involved in microtubule regulation by interacting with MAP1S, a protein known to be involved in both neuronal migration and autophagy. However, whether WDR47 is involved in regulating neuronal migration and/or autophagy has not been previously investigated.

1.7 Aims and Hypothesis

In summary, we highlighted the following key observations made from the literature reviewed: Neuronal migration and autophagy are both of central importance for neurodevelopment, and both processes depend on an intricately regulated microtubule cytoskeleton. Reelin and SCG10 are both key microtubule-regulating proteins that have been shown to interact with WDR47. WDR47 and nemitin are likely the same protein, suggesting a putative interaction between WDR47 and MAP1S, a MAP that has been shown to regulate microtubule stability and to affect autophagy by interacting with autophagosome-associated LC3. The domain structure of WDR47 is indicative of a protein scaffolding role as well as a role in regulating the microtubule cytoskeleton. WDR47 and the microtubule-dynein-interacting protein Lis1 have remarkably similar domain structures, suggesting that WDR47 may affect microtubule-dependent processes by interacting with the motor protein dynein. However, the function of WDR47 has not yet been investigated. The present study thus investigated potential roles for WDR47 in undifferentiated neurons.

We hypothesized that WDR47 is playing a role in regulating microtubule-dependent processes such as neuronal migration and autophagy.

We aimed to elucidate the role of WDR47 in regulating neuronal migration, autophagy, and tubulin in GT1-7 neuronal cells. Our objectives were as follows:

- To determine whether WDR47 is playing a significant role in neuronal migration
- To determine whether WDR47 is able to influence the direction of migration
- To determine whether WDR47 is able to influence surface adhesion and filopodia extension of migrating neurons
- To determine whether WDR47 is able to influence neuronal ultra-structure
- To determine whether WDR47 is able to affect autophagy
- To determine whether WDR47 is able to affect tubulin stability and/or the expression of MAPs (tau and SCG10)
- To determine whether WDR47 is able to co-localize with LC3 and/or tubulin
- To assess the distribution and mobility of WDR47 in GT1-7 neurons

Chapter 2: Materials and Methods

2.1 Reagents and Consumables

2.1.1 Cell Line and General Cell Culture Reagents

Rat GT1-7 hypothalamus-derived neuronal cells were a kind gift from Dr Pamela Mellon, University of California, San Diego, USA. Dulbecco's modified Eagle's medium (DMEM), Penstrep antibiotics, and Trypsin were purchased from Life Technology (41965062, 15140122, and 25200072, respectively), and foetal bovine serum (FBS) was purchased from Scientific Group (BC/50615-HI). 15 ml and 50 ml Falcon tubes were purchased from Biocom Biotech (50015 and 50050, respectively). 25 cm^2 polystyrene non-pyrogenic cell culture flasks were purchased from Whitehead Scientific (500033) and 75 cm^2 flasks were purchased from Nest-Biotechnology (708001). 10 ml serological pipettes were purchased from Biocom Biotech (PN10E1). NUNC-chamber dishes were purchased from Thermo Scientific (155411) and 6-well plates were purchased from Biocom Biotech (30006).

2.1.2 Transfection Reagents and Treatment Reagents

HiPerfect Transfection Reagent (301705), negative control siRNA (5 nM; 1027280), WDR47_1 siRNA (5 nM; SI01471911), and WDR47_5 siRNA (5 nM; SI04774770) were purchased from Qiagen. Lipofectamine 2000 transfection reagent was purchased from Invitrogen (52887). Mitomycin C and Bafilomycin A1 were purchased from Sigma-Aldrich (M4287 and B1793, respectively).

2.1.3 Western Blot Reagents

Bradford reagent and BSA (albumine bovine serum; 200µg/ml stock solution) were obtained from Sigma-Aldrich (B6196 and A9418, respectively). Mini-PROTEAN TGX gels (4 – 15%; 15 wells per gel; 15 µl wells) and Transfer-Blot Turbo transfer packs (Mini format; 0.2 µm PVDF) were supplied by Bio-Rad (456-1083 and 170-4156, respectively). An ECL (Enhanced Chemiluminescence) kit containing peroxide buffer and enhancer solution for band detection was supplied by Thermo Scientific (34095).

2.1.4 Antibodies

Primary antibodies used include anti-WDR47 (produced in rabbit) purchased from Sigma-Aldrich (R26882), anti-LC3 (produced in rabbit) purchased from Anatech (CST2775S), anti-SQSTM1 (produced in rabbit) purchased from Biocom Biotech (AB91526), anti-Tau46 (produced in mouse) purchased from Cell Signalling (#4019), anti-SCG10 (produced in mouse) purchased from Santa Cruz (SC-135620), anti-acetylated α-Tubulin (produced in mouse) purchased from Santa Cruz (SC-23950), and anti-GAPDH (produced in rabbit) purchased from Abcam (ab9483). Secondary antibodies used included anti-rabbit IgG HRP-linked secondary antibody purchased from Cell Signalling Technology (7074S), and ECL peroxidase-labelled anti-mouse secondary antibody purchased from Amersham Pharmacia Biotech (NA931VS).

2.1.5 Fluorescent Probes

pEYFP-WDR47 (clone IOH26831), which encodes the full length WD repeat domain 47 protein (WDR47) fused to an N-terminal enhanced yellow fluorescent protein, was obtained from Imagenes (Berlin, Germany). Alexa Fluor 488 donkey anti-mouse IgG (A21202), Alexa Fluor 568 donkey anti-rabbit IgG (A10042), and Alexa Fluor 568 donkey anti-mouse IgG (A10037) secondary antibodies were purchased from Life Technology. Hoechst 33342 was purchased from Sigma-Aldrich (B261).

2.2 Experimental Procedures

2.2.1 Tissue Culture of GT1-7 Neuronal Cells

GT1-7 cells were cultured at 37˚C in a humidified 5% CO_2 atmosphere in 1X DMEM (Dulbecco's modified Eagle medium) supplemented with 1% Penstrep antibiotics and 10% foetal bovine serum (FBS). Cell-containing cryovials were stored in a liquid nitrogen cell tank; each cryovial contained approximately 1 X 10^6 cells, 10 µl dimethyl sulfoxide (DMSO), and 1000 µl FBS.

2.2.1.1 Thawing and Culturing of Cells

Frozen stock was thawed by immersing the cell-containing vial in a water bath at 37°C for 3 minutes. Cells were transferred with a sterile pipette tip (P1000 micropipette) into a 25 cm^2

flask containing 4 ml of fresh pre-warmed growth medium. After approximately 8 hours the growth medium was refreshed to remove the DMSO. Growth medium was refreshed on alternate days for the duration of the culturing procedure. Cells were grown to a confluency of 70% - 80% prior to being subcultured.

2.2.1.2 Subculturing and Seeding of Cells for Experiments

The cell monolayer was rinsed with sterile 0.01 M PBS (phosphate buffered saline), after which trypsin was added to the cell monolayer and cells were placed in an incubated cell shaker (37˚C; 5% CO_2 atmosphere) for approximately 3 minutes. Cells were viewed under an Olympus CKX41 microscope to ensure dissociation from the surface of the flask, and were subsequently transferred to a 15 ml Falcon tube using a sterile 10 ml serological pipette. The appropriate amount of FBS-supplemented growth medium (2X the volume of trypsin used) was added to the cell suspension to deactivate the trypsin. Cells were centrifuged at 1500 rpm for 3 minutes at 37˚C, after which the supernatant was decanted and the cell pellet was re-suspended in 1 ml of growth medium using a sterile pipette tip (P1000 micropipette). Cells were counted with a Neubauer Improved haemocytometer (Marenfield) and were subsequently either subcultured or seeded into appropriate experimental dishes. Cells were not used at a passage > 25.

2.2.2 WDR47 siRNA Transfection Optimization

GT1-7 cells were seeded into six well plates at a density of 3 X 10^5 cells per well. Cells were incubated at 37˚C in a 5% CO_2 atmosphere and grown to approximately 80% confluency. Two different WDR47 siRNA plasmids (siRNA1 and siRNA5) were used for the initial transfection to compare WDR47 knock-down efficiency in GT1-7 cells. Cells were seeded into four groups: an untreated control group, a siRNA control group, a WDR47 siRNA1 group, and a WDR47 siRNA5 group. Several concentrations of both siRNA1 and siRNA5 were tested before it was determined that a concentration of 28 ng/μl (12 μl) of siRNA1 achieved significant knock-down of WDR47 after 24 hours of transfection. For the remainder of the experimental procedures, the chosen siRNA and the established concentration and transfection time were used. The transfection procedure was as follows: WDR47 siRNA cells were treated with a solution consisting of 12 μl of siRNA, 8 μl HiPerfect transfection reagent, and 88 μl serum-free growth medium per well. Control siRNA cells were treated with a

solution consisting of 12 µl of negative control siRNA, 8 µl HiPerfect transfection reagent, and 88 µl of serum-free growth medium per well. Solutions were added to wells each containing 2 ml fresh growth medium in a drop-wise manner, and cells were incubated at 37˚C in a 5% CO_2 atmosphere. Cells were harvested at 24 hours post transfection. Knock-down of WDR47 was verified with western blot analysis subsequent to protein extraction as described below.

2.2.3 RIPA (Radio-Immunoprecipitation) Buffer Extraction of Protein

The RIPA buffer consists of various ingredients, protease inhibitors and phosphatase inhibitors. Protease inhibitors used include PMSF (phenylmethylsulfonyl fluoride), EDTA (ethylenediaminetetraacetic acid), leupeptin, and benzamidine. Phosphatase inhibitors used include activated sodium-orthovanidate (Na_3VO_4) and sodium-fluoride (NaF). Each well of a six well plate was rinsed three times with cold 1X PBS and subsequently incubated with 100 µl of RIPA lysis buffer for 10 minutes on ice. Cell monolayers were scraped using sterile scraper (policemen) and lysates were homogenized on ice for 4 seconds at a frequency of 4 Hertz using a Misonix Sonicator (S-4000).

2.2.4 Western Blot Verification of WDR47 Knock-Down

2.2.4.1 Bradford Protein Determination

A working solution of Bradford reagent was prepared, consisting of Coomasie Brilliant blue, 95% ethanol, phosphoric acid, and dH_2O. A standard curve was obtained by preparing a range of concentrations of BSA (bovine serum albumin; 200 µg/ml stock solution) according to Table 2.1. For the samples, 5 µg of protein was diluted in 95 µl of dH_2O. 900 µl of Bradford working solution was added to each standard and each sample tube, and the tubes were mixed thoroughly and incubated for 5 minutes at room temperature. Spectrophotometric absorbance measurements were taken at a wavelength of 595 nm using a Cecil C8 2021 spectrophotometer. *Prism5* software was used to obtain a standard curve of protein concentration against absorbance values from which the unknown protein concentration of each sample was determined.

Table 2.1: Preparation of BSA solutions for Bradford standard curve

Concentration (µg/ml)	Volume of BSA (µl)	Volume of dH$_2$O (µl)
0 (Blank)	0	100
2	10	90
4	20	80
8	40	60
12	60	40
16	80	20
20	100	0

2.2.4.2 Sample Preparation

5 ml of Laemmli's loading buffer was prepared by diluting 1 ml Tris-HCL (0.5M; pH 6.8), 0.8 ml glycerol, 1.6 ml of 10% SDS (sodium dodecyl sulfate), and 0.4 ml of 0.05% Bromophenol blue in dH$_2$O. A working solution of Laemmli's loading buffer was prepared by adding 150 µl of β-mercaptoethanol to 850 µl of Laemmli's loading buffer and by mixing thoroughly. Appropriate volumes (µl) of protein sample were added to Eppendorf tubes so as to obtain 50 µg of each protein sample per tube. The appropriate volume of Laemmli's loading buffer (1/3 the volume of protein) was added to each sample. Samples were boiled for 5 minutes at 95˚C, centrifuged briefly, and placed immediately on ice.

2.2.4.3 SDS-PAGE (Sodium-Dodecyl-Sulfate-Polyacrylamide Gel Electrophoresis)

Precast Mini-PROTEAN SDS-PAGE gels were firmly secured onto an electrode assembly and placed inside a Mini-Protean Tetra cell tank. The buffer chambers were filled with 1X running buffer (10X stock diluted with dH$_2$O), and the wells of the gel were rinsed with running buffer using an insulin syringe. 4 µl of protein marker was loaded into the first well, and the respective volumes of the prepared samples were loaded onto the remainder of the wells. The electrode assembly was connected to a power supply (BIO-RAD Power Pac 1000) and proteins were separated at 120 V for approximately 40 minutes. A Trans-Blot Turbo transfer pack and a BIO-RAD Trans-Blot turbo transfer system were used to transfer the protein for 10 minutes from the gel to a PVDF (polyvinydilene difluoride) membrane. The

membrane was blocked in 5% non-fat milk in 1X TBS-T (Tris-buffered saline and 1% Tween 20) for 1 hour to reduce non-specific binding, rinsed 3 X 5 minutes in 1X TBS-T, and incubated in WDR47 primary antibody (1:1000 in TBS-T) overnight at 4°C. After rinsing the membrane in 1X TBS-T for 3 X 5 minutes, the membrane was incubated in anti-rabbit HRP-linked secondary antibody (1:5000 in TBS-T) for 60 minutes at room temperature. The membrane was treated with 1 ml of enhanced chemiluminescence (ECL) reagent (peroxide buffer and enhancer solution prepared in a 1:1 ratio), and protein signal as well as band intensities were detected with a BIO-RAD Chemidoc MP imaging system using *Image Lab* software (version 4.1). Band intensities of control siRNA- and WDR47 siRNA-treated cells were expressed as a percentage relative to band intensities of untreated control cells.

2.2.4.4 Loading Controls for Detected Bands

GAPDH was used as a loading control for all blots. Membranes were stripped for 5 minutes with 0.2 M NaOH (sodium hydroxide) and washed for 3 X 5 minutes with dH_2O. Membranes were blocked with 5% non-fat milk for 1 hour and subsequently incubated in GAPDH primary antibody (1:1000) overnight at 4°C. Membranes were incubated in anti-rabbit HRP-linked secondary antibody and developed with ECL reagents using a BIO-RAD Chemidoc system as described above.

2.2.5 Western Blot Analysis of SCG10, Tau, Acetylated α-Tubulin, LC3, and p62

Cells were transfected with WDR47 siRNA, followed by RIPA extraction of protein (24 hours post transfection), Bradford determination of protein concentration, and sample preparation as described above. Western blot analysis proceeded as described above: proteins were separated for approximately 40 minutes at 120 V, transferred for 10 minutes, and membranes were blocked for 60 minutes in 5 % non-fat milk in 1X TBS-T. Membranes were incubated overnight at 4 °C with SCG10 primary antibody (1:500 in 1X TBS-T), Tau mouse primary antibody (1:1000 in 1X TBS-T), acetylated α-tubulin mouse primary antibody (1:1000 in 1X TBS-T) LC3 rabbit primary antibody (1:1000 in 1X TBS-T), and P62 rabbit primary antibody (1:1000 in TBS-T). On the following day, membranes were incubated at room temperature with the appropriate secondary antibodies (anti-rabbit or anti-mouse; 1:5000 in TBS-T) for 1 hour, and were subsequently developed with a BIO-RAD Chemidoc system as described above. The detected bands were analysed with *Image Lab* software as

described above. Membranes were stripped with 0.2 M NaOH and re-probed for GAPDH to control for equal loading as described above.

2.2.6 Bafilomycin A1 Treatment and Western Blot Analysis of LC3 and P62

Bafilomycin A1, an antibiotic produced in *Streptomyces griseus Sulphurus*, is widely used to inhibit the fusion of the H+ATP-ase, thereby rendering autophagosomal/lysosomal fusion dysfunctional (Barth *et al.,* 2010). 10 μg Bafilomycin A1 stock was dissolved in 16.05 μl DMSO to obtain a 1 mM stock solution. 1 μl of stock solution was diluted in 1000 μl PBS to obtain a 1 μM concentration. 100 μl of the diluted stock solution was added per 1000 μl media to obtain a final working concentration of 100 nM of Bafilomycin.

GT1-7 cells were seeded into six-well plates at a density of 3 X 10^5 cells per well and incubated under normal growth conditions to 90% confluency, and siRNA transfections were performed as described above. 6 hours prior to protein extraction, cells were incubated with 100 nM Bafilomycin. RIPA extraction of protein, Bradford determination of protein concentration, sample preparation, and Western blot analysis of P62, LC3, and GAPDH was performed as described above.

2.2.7 Neuronal Migration Assay

2.2.7.1 Mitomycin C Preparation and Optimization

Mitomycin C is a commonly used antibiotic (produced in *Streptomyces caespitosus*) that inhibits the synthesis of DNA (Ueda & Komano, 1984). Mitomycin C was used to inhibit neuronal proliferation and consequently observe neuronal migration. To obtain a stock solution of 0.5 mg/ml, 10 mg of Mitomycin C was dissolved in 2 ml of sterile 1X PBS. The stock solution was stored in the fridge in a brown Eppendorf tube for no longer than one week (Mitomycin C is light sensitive and may form a toxic precipitate if stored for longer than prescribed). On the day of use, the stock solution was further diluted in growth medium to obtain the desired working concentration (described below).

Prior to the migration assay, a Mitomycin C test experiment was performed to establish a concentration of Mitomycin C that was sufficient for the inhibition of neuronal proliferation. For the test experiment, two groups were assessed: a control group and a Mitomycin C

group. The Mitomycin C group received 10 μg/ml of Mitomycin C. Prior to imaging, the nuclei of both groups were stained with Hoechst 33342 (1:200 Hoechst to media). Images were acquired at two time points (0 and 24 hours) using an Olympus Cell^R system attached to an IX 81 inverted fluorescence microscope equipped with an F-view-II cooled CCD camera (Soft Imaging Systems), a Xenon-Arc burner (Olympus Biosystems GMBH) as light source, and with 360 nm, 492 nm and 572 nm excitation filters. Emission was collected using a UBG triple-bandpass emission filter cube (Chroma), and fluorescence was collected using a 360 nm excitation filter. Nuclear counts were performed for both groups and both time points. A working concentration of 10 μg/ml was established to be sufficient to inhibit neuronal proliferation (Addendum), and was used for the duration of subsequent experimental procedures.

2.2.7.2 Experimental Groups for the Neuronal Migration Assay

Cells were divided into four groups: a control group (untreated), a Mitomycin C control group (treated with Mitomycin C only), a control siRNA group (treated with Mitomycin C and transfected with negative control siRNA) and a WDR47 siRNA group (treated with Mitomycin C and transfected with WDR47 siRNA).

2.2.7.3 Introducing a Linear Wound

GT1-7 cells were seeded into a six-well plate at a density of 3 X 10^5 cells per well and grown to approximately 90% confluency, siRNA transfections were performed as described above, and cells were incubated for 24 hours under normal growth conditions. A sterile 10 μl pipette tip was used to introduce a linear wound in each well (Liang *et al.,* 2007). Each well was rinsed with 1 ml of growth medium to remove debris and dead cells. 2 ml of fresh medium supplemented with Mitomycin C was added to the Mitomycin control, control siRNA, and WDR47 siRNA groups. Control group cells received non-supplemented growth medium.

2.2.7.4 Imaging of Neuronal Migration

Cells were transferred to an Olympus Cell^R system attached to an IX 81 inverted fluorescence microscope equipped with an F-view-II cooled CCD camera (Soft Imaging

Systems). Images were acquired using a Halogen light source and a transmission filter. The exact coordinates of the first image (time point 0) of the wound in each well were saved and used to acquire subsequent images. Images were acquired at time points 0, 6, 12, 18, 24, 30, and 36 hours. Subsequently, to determine whether WDR47 siRNA-treatment affected the direction of a neuronal migration, a migration assay was performed as described above, but for 24 hours acquiring images every hour.

2.2.7.5 Quantification of Neuronal Migration

Cell^R software was used to measure both the migration distances (from which the migration velocity (µm/min) at 24 hours was obtained) and the wound area at each time point (from which the percentage and rate of wound closure were obtained). See Figure 2.1 and Figure 2.2 for example images of distance and area measurements. The migration distances were obtained by demarcating the wound at 0 hours with straight lines and measuring the distances (in µm) of neuronal processes perpendicular to the demarcated lines for each successive time point. Approximately 10 neurons were measured on each side of the wound for each image, and the average distance for each image was determined. The migration velocity of each group was determined by dividing the average migration distances of the 24 hour time point by the elapsed time in minutes. For the percentage of wound closure, the area of the wound was measured in μm^2 at each time point. The following formula was then used:

$$Percentage\ Wound\ Closure = \frac{Wound\ Area\ (0\ hr) - Wound\ Area\ (n\ hr)}{Wound\ Area\ (0\ hr)}\ X\ 100$$

The rate of wound closure was calculated by dividing the percentage of wound closure by the time (hours) for each group (Liang *et al.,* 2007).

For the 24 hour migration assay, *ImageJ* software was used to manually track approximately 10 neurons on each side of the wound for each group with the "Manual Tracking" plugin. Rose diagrams for each group were obtained with the "Chemotaxis and Migration Tool" plugin. Rose diagrams for the different groups were qualitatively compared.
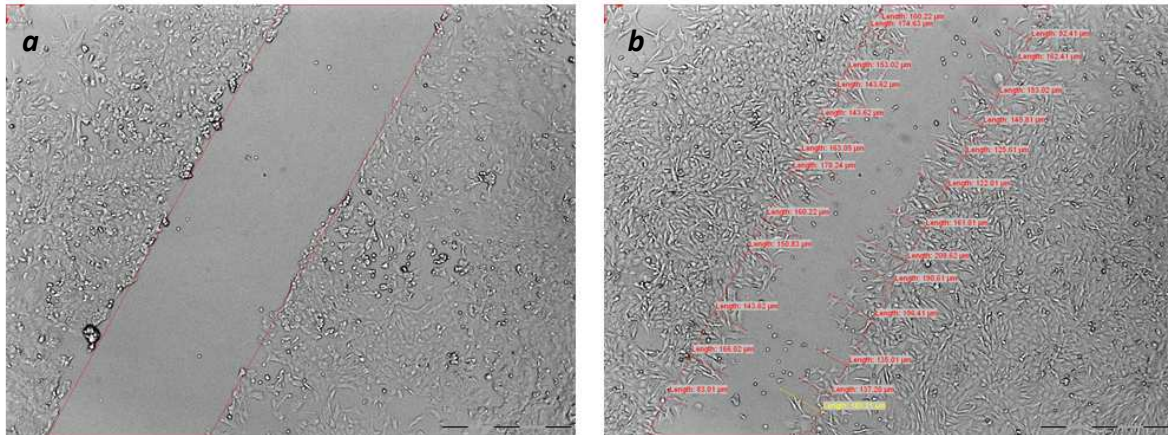
Figure 2.1: Example images of migration distance measurements as obtained with Cell^R software, from which the average migration distance and migration velocity was calculated. *a:* Demarcated wound area at 0 hours. *b:* Perpendicular distance of migration at 36 hours from demarcated wound area obtained in *a.*
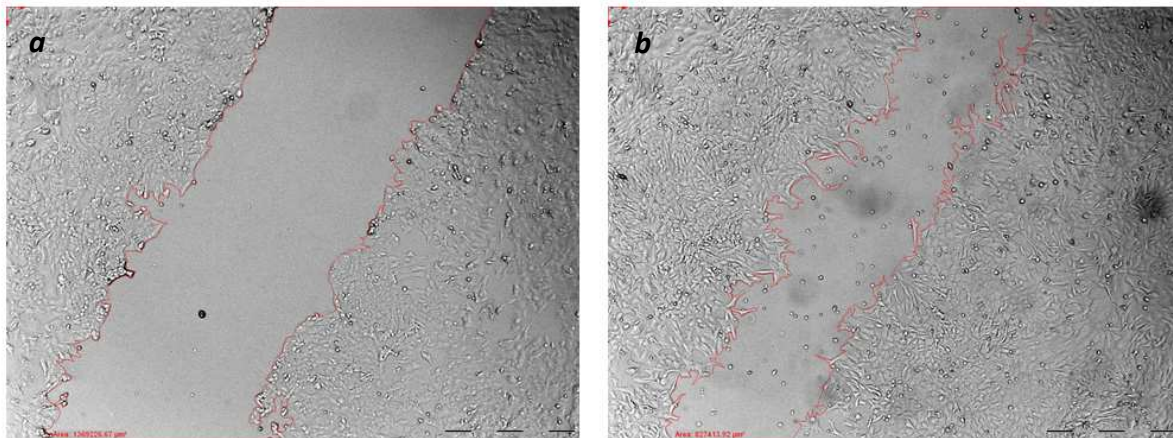
Figure 2.2: Example images of area measurements as obtained with Cell^R software, from which the percentage and rate of wound closure was calculated. *a:* Wound area at 0 hours. *b:* Wound area at 36 hours.

2.2.8 Scanning Electron Microscopy (SEM) of Neuronal Morphology in the Migration Zone

GT1-7 cells were seeded onto 12 mm cover glasses placed in 6 well plates (each well containing 2 ml of growth medium) at a density of 3 X 10^5 cells per well. Similar to the migration assay, four groups existed (control group, Mitomycin C control group, control siRNA group, and WDR47 siRNA group). Cells were incubated under normal growth conditions for 24 hours to approximately 90% confluency. siRNA control cells and WDR47 siRNA cells were transfected as described above; control and Mitomycin control cells remained untreated. Cells were again incubated for 24 hours, after which a linear wound was introduced on each cover glass using a sterile 10 µl pipette tip. The growth medium was

replaced with growth medium supplemented with Mitomycin C (10 µg/ml) for all groups except the control group. Cells were incubated for another 24 hours under normal growth conditions, after which the growth medium was removed from each well, and slides were rinsed with pre-warmed 1X PBS. 1000 µl of cold methanol-acetone fixative (1:1) was added to each well to fix cells, and cells were incubated at 4 °C for 10 minutes. The fixative was removed and the cells were allowed to air dry for 20 minutes. The cover glasses were removed from the wells and transferred to the Department of Geology, Stellenbosch University, where SEM (scanning electron microscopy) was performed: the cover glasses were mounted on a stub with double sided carbon tape and subsequently double-coated with a thin layer of gold in order to make the sample surface electrically conducting. The cover glasses were transferred to a Leo® 1430VP Scanning Electron Microscope to capture images of the surface structure of the cells. Beam conditions during surface analysis were 10 KV and approximately 1.5 nA, with a working distance of 11 mm and a spot size of 432. Images were qualitatively compared.

2.2.9 Transmission Electron Microscopy (TEM) of Neuronal Ultrastructure

2.2.9.1 Obtaining the Sample

GT1-7 cells were seeded into a 6 well plate (each well containing 2 ml of growth medium) at a density of 3 X 10^5 cells per well and were grown to approximately 90 % confluency. Three groups were assessed: a control group, a control siRNA group, and a WDR47 siRNA group. Control siRNA and WDR47 siRNA cells were transfected as described above, and control cells were left untreated. After incubation of 24 hours, each well was treated with 1 ml of trypsin for approximately 3 minutes until cells dissociated from the surface, suspensions were transferred to 15 ml Falcon tubes each containing 2 ml of FBS-supplemented growth medium, and Falcon tubes were centrifuged at 1500 rpm for 3 minutes at 37˚C. The trypsin and media was decanted and cells were re-suspended in 1X PBS to remove the trypsin and media. Cells were again centrifuged at 1500 rpm for 3 minutes at 37˚C and the PBS was decanted from the pellets. Cells were then re-suspended in 2.5 % gluteraldehyde fixative (500 µl per pellet), centrifuged, and transferred to Tygerberg Hospital where TEM analysis was performed by the National Health Laboratory Service as described below:

2.2.9.2 Preparation, Sectioning and Imaging of the Sample

The sample was cut into 1mm sections using a dissecting microscope and rinsed in Phosphate buffer. Samples were incubated in 3% osmium tetroxide for 1 hour and then stored in a 10% formalin solution to reduce the osmium tetroxide. Samples were then transferred to an automated tissue processer, and samples were immersed in different substances according to the following protocol:

1. 15 minutes in 10% urnayl acetate
2. 10 minutes in 70% alcohol
3. 10 minutes in 70% alcohol
4. 20 minutes in 10% Urynal nitrate
5. 15 minutes in 100% alcohol
6. 20 minutes in 100% alcohol
7. 30 minutes inn 100% alcohol
8. 90 minutes in half 100% alcohol and half spurr's resin
9. 60 minutes in spurr's resin
10. 60 minutes in spurs resin.

Samples were then embedded into gelatin capsules overnight at 60 °C prior to being cut into thin sections using a Leica EM UC7. Sections were stretched with Chloroform and placed onto copper grids. Images were captured with a JEOL JEM 1011 transmission electron microscope, using an ITEM soft imaging analysis program. TEM images were qualitatively analyzed.

2.2.10 SR-SIM (Super-resolution structured Illumination microscopy) of WDR47

GT1-7 cells were seeded at a density of 30 000 cells per well into an 8 chamber dish approximately 24 hours prior to transfection. Each chamber received 400 µl of growth medium (refreshed prior to transfection). For each chamber, 1600 ng of WDR47-YFP (WDR47 DNA Linked to Yellow Fluorescence Protein) made up in 50 µl serum-free growth medium was incubated with 3 µl Lipofectamine made up in 50 µl serum free growth medium for 20 minutes at room temperature. 100 µl per chamber of the solution was

51

added drop-wise into each well. Cells were incubated for 48 hours at 37˚C in a 5% CO_2 atmosphere.

Thin (0.1 µm) z-stacks of high-resolution image frames were collected in 5 rotations by utilizing an alpha Plan-Apochromat 100x/1.46 oil DIC M27 ELYRA objective, using an ELYRA S.1 (Carl Zeiss Microimaging) microscope equipped with a 488nm laser (100mW), 561nm laser (100mW) and Andor EM-CCD camera (iXon DU 885). Images were reconstructed using ZEN software (black edition, 2011, version 7.04.287) based on a structured illumination algorithm (Heintzmann & Cremer, 1999). Analysis was performed on reconstructed super-resolution images in ZEN.

2.2.11 Co-Localization of WDR47 with Acetylated α-Tubulin and LC3

Cells were seeded into NUNC-chamber dishes and WDR47-YFP transfections were performed as described above. 48 hours after the transfection, growth medium was removed and cells were rinsed with sterile 1X PBS. 1 ml of ice cold methanol-acetone fixative (1:1) was added per well, and cells were incubated for 10 minutes at 4 °C. Fixative was removed and cells were air dried for 20 minutes. After rinsing with 1X PBS, each well was incubated with 100 µl 5% donkey serum in PBS for 20 minutes at room temperature. The serum was drained, and each well was incubated with 100 µl of either LC3 (rabbit) or acetylated tubulin (mouse) primary antibody (1:50 in PBS) for 90 minutes at room temperature. Each well was rinsed with 400 µl PBS, and subsequently incubated with 100 µl of either Alexa Fluor 568 donkey anti-rabbit IgG (for LC3), or Alexa Fluor 568 donkey anti-mouse IgG (for tubulin) secondary antibody (1:200 in PBS) for 30 minutes at room temperature in the dark. 100 µl of Hoechst 33342 (1:200 in PBS) was added to each well to counterstain the nuclei, and cells were incubated for another 10 minutes at room temperature in the dark. Each well was rinsed three times with 100 µl 1X PBS. A small amount of mounting medium was added to each well. The dish was wrapped in silver-foil and stored at -20 °C. SR-SIM acquisition and processing was performed as described above.

2.2.12 SR-SIM of Acetylated Tubulin Network Arrangements and LC3 Distribution in WDR47-siRNA treated cells

Cells were seeded into NUNC-chamber dishes as described above. WDR47 siRNA transfections were performed as described in section 2.2. To obtain a concentration equivalent to previous experiments, control siRNA and WDR47 siRNA cells were transfected with 2.4 µl of siRNA and 1.6 µl of HiPerfect transfection reagent. After an incubation period of 24 hours, cells were fixed and stained as described above. However, each well was co-stained with both acetylated α-tubulin and LC3 primary antibodies. Alexa Fluor 568 donkey anti-rabbit IgG secondary antibody was used to stain LC3, and Alexa Fluor 488 donkey ant-mouse IgG secondary antibody was used to stain acetylated α-tubulin. Nuclei were counterstained with Hoechst 33342 and samples were mounted and stored as described above.

3-D Confocal microscopy was performed to assess LC3 distribution and tubulin network morphology as described. SR-SIM 3-D analysis was performed as described above to visualise tubulin network arrangements.

2.2.13 FRAP (Fluorescence Recovery after Photo-Bleaching) of WDR47

Cells were seeded into NUNC-chamber dishes and WDR47-YFP transfections were performed as described above. 48 hours after the transfection, confocal microscopy was performed as described above. Cells were selected by assessing for WDR expression. The lasers were aligned above target regions of a single cell using phase contrast optics, and two cytoplasmic regions of interest (ROI's) were bleached with a high power laser beam (100% laser power). Two unbleached ROI's, an extracellular region and a nuclear region, were used to control for background fluorescence noise. Time lapse sequences were used to measure fluorescence intensity for all regions after the bleach event, and fluorescence recovery of the bleached regions was plotted using Zen software.

2.3 Statistical Analysis

Statistical analysis and quantification of neuronal migration measurements as well as Western blot data was performed with *Prism 5* software (one way ANOVA with Bonferroni post-test). Significance was indicated at $p < 0.05$. All results are presented as means ± SE's.

Chapter 3: Results

3.1 WDR47 Knock-Down Verification

Western blot analysis was performed to verify that the established siRNA transfection protocol successfully knocks down WDR47 in GT1-7 cells. Western blot analysis reveals significant knock-down of WDR47 24 hours after transfecting cells with 12 µl of WDR47 siRNA and 8 µl of HiPerfect transfection reagent per well of a six well plate (Figure 3.1). WDR47 protein levels are significantly reduced in WDR47 siRNA-treated cells [37.3 ± 9.3 % ($P < 0.05$)] compared to control and control siRNA-treated cells (71 ± 11.9 %).
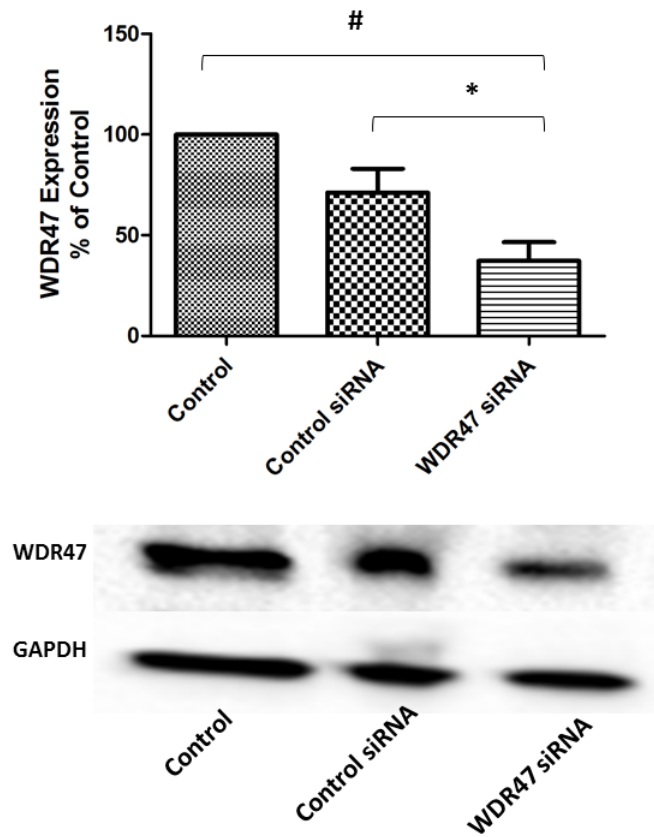
Figure 3.1: Western blot verification of WDR47 knock-down. WDR47 siRNA-treatment significantly reduces WDR47 protein levels compared to control and control siRNA-treated cells (n = 7; # $P < 0.05$ vs. control, * $P < 0.05$ vs. control siRNA).

3.2 The Effect of WDR47 siRNA Treatment on Neuronal Migration

An *in vitro* 36 hour neuronal migration assay was performed and several measurements were utilized in order to determine whether WDR7 siRNA treatment affects neuronal migration. Quantitative measurements of the migration assay include the average migration distance, the migration velocity, the percentage of wound closure, and the rate of wound closure. Significant effects of WDR47 siRNA treatment on neuronal migration are first observed at the 24 hour time point. The average migration distance is significantly reduced with WDR47 siRNA treatment [151.3 ± 4.2 µm (P < 0.05)] compared to the untreated control [184.5 ± 3.4 µm], Mitomycin control [178.5 ± 3.7 µm], or control siRNA treatment [189.6 ± 3.1 µm] at 24 hours post scratch introduction. Similarly, at 30 hours, the average migration distance is significantly reduced with WDR47 siRNA treatment [156.6 ± 4.1 µm (P < 0.05)] compared to the untreated control [198.2 ± 3.1 µm], Mitomycin control [208.0 ± 4.1 µm], or control siRNA treatment [206.6 ± 3.4 µm]. At 36 hours, the average migration distance remains significantly reduced with WDR47 siRNA treatment [163.8 ± 4.4 µm (P < 0.05)] compared to the untreated control [206.1 ± 3.9 µm], Mitomycin control [212.5 ± 5.4 µm], or control siRNA treatment [219.2 ± 4.1 µm] (Figure 3.2 *a - c*).

The migration velocity (µm/min; determined at 24 hours post scratch) is significantly reduced with WDR47 siRNA-treatment [0.11 ± 0.003 µm/min (P < 0.05)] compared to control [0.13 ± 0.002 µm/min], Mitomycin control [0.12 ± 0.003 µm/min], and control siRNA groups [0.13 ± 0.002 µm/min] (Figure 3.2 *d*).

At 24 hours post scratch introduction, the percentage of wound closure is significantly reduced with WDR47 siRNA treatment [33.7 ± 2.9 % (P < 0.05)] compared to the control group [46.1 ± 1.8 %], but not compared to the Mitomycin control [39.1 ± 3.7 %] or control siRNA groups [43.5 ± 3.1 %]. Similarly, at 30 hours, the percentage of wound closure is significantly reduced with WDR47 siRNA treatment [34.6 ± 3.1 % (P < 0.05)] compared to the control group [53.0 ± 1.3 %], but not compared to the Mitomycin control [44.0 ± 5.1 %] or control siRNA groups [45.9 ± 2.9 %]. At 36 hours, the percentage of wound closure remains significantly reduced with WDR47 siRNA treatment [35.7 ± 2.4 % (P < 0.05)] compared to the control group [59.3 ± 1.7 %], but not compared to the Mitomycin control [47.6 ± 5.9 %] or control siRNA groups [47.1 ± 3.0 %] (Figure 3.3 *a*). However, a non-significant trend for a

56

reduction in percentage of wound closure following WDR47 siRNA treatment is observed compared to the Mitomycin control and control siRNA groups.

The rate of wound closure (percentage of wound closure per hour) is significantly reduced with WDR47 siRNA treatment [1.6 ± 0.1 % / hr ($P < 0.05$)] compared to the control group [2.1 ± 0.1 % / hr], but not compared to the Mitomycin control [2.0 ± 0.1 % / hr] or control siRNA groups [2.0 ± 0.1 % / hr](Figure 3.3 *b*). However, a non-significant trend for a reduction in the rate of wound closure following WDR47 siRNA treatment is observed compared to the Mitomycin control and control siRNA groups.

In addition, several observations are made from a qualitative comparison between the control, Mitomycin control, and control siRNA groups with the WDR47 siRNA group. Cells from the control group (not treated with Mitomycin C) proliferate and rapidly close the wound area, appearing to seal the wound more effectively relative to cells from the Mitomycin control, control siRNA, and WDR47 siRNA groups (all treated with Mitomycin C). Characteristic extended processes of migrating neurons are less prominent in cells from the control group (Figure 3.9). Mitomycin control (Figure 3.10) and control siRNA-treated cells (Figure 3.11) extend relatively long, thin processes in the direction of migration, mostly perpendicular to the wound edge, to heal the wound. WDR47 siRNA-treated cells (Figure 3.12) appear to be characterised by disorganized migration, a compromised ability to extend long processes, abnormal directionality (parallel rather than perpendicular to the wound edge), and an overall compromised wound healing ability. See Figure 3.4 - 3.7 for an illustration of *in vitro* migration over time of each group individually, Figure 3.8 for a comparison of *in vitro* migration at 0 hours and 36 hours between different groups, and Figure 3.9 - 3.12 for representative images of all groups at the 36 hour time point.
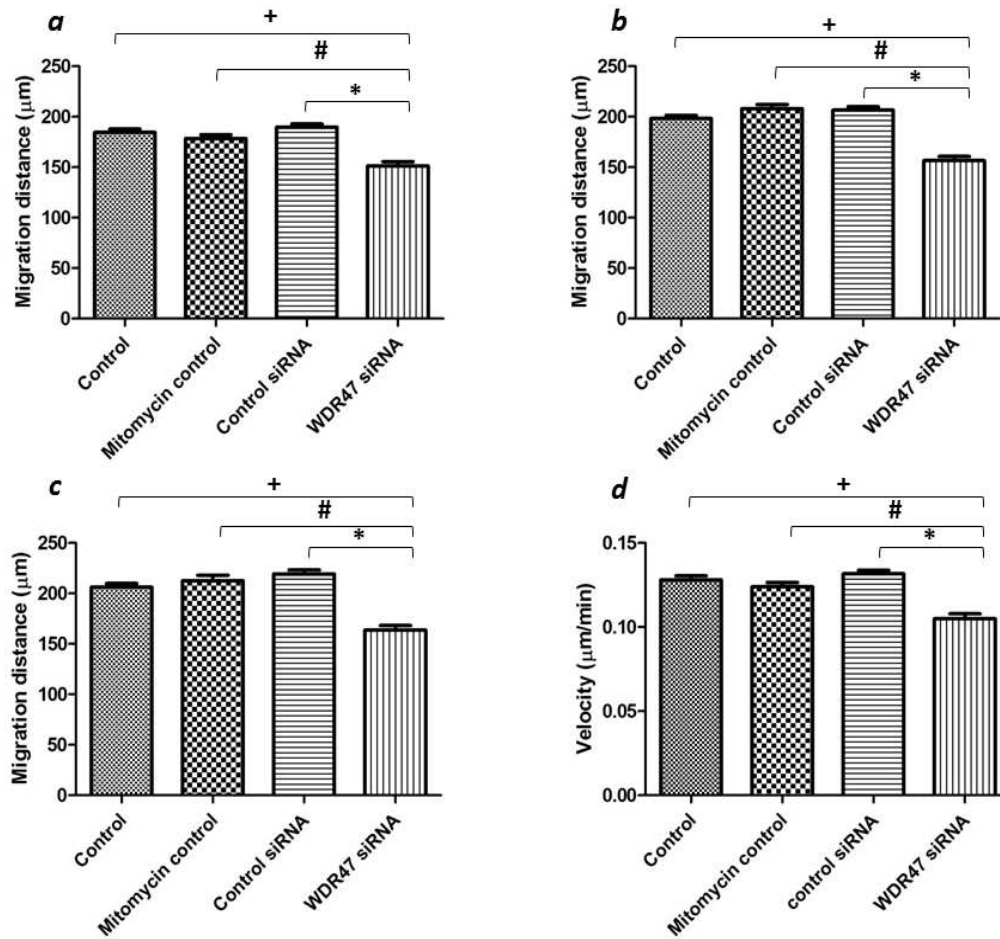
Figure 3.2: Average migration distance at 24 hours (*a*), 30 hour s (*b*) and 36 hours (*c*) as well as migration velocity (*d*). n = 4; + P < 0.05 vs control (n = 4; + P < 0.05 vs control, # P < 0.05 vs Mitomycin control, * P < 0.05 vs control siRNA).
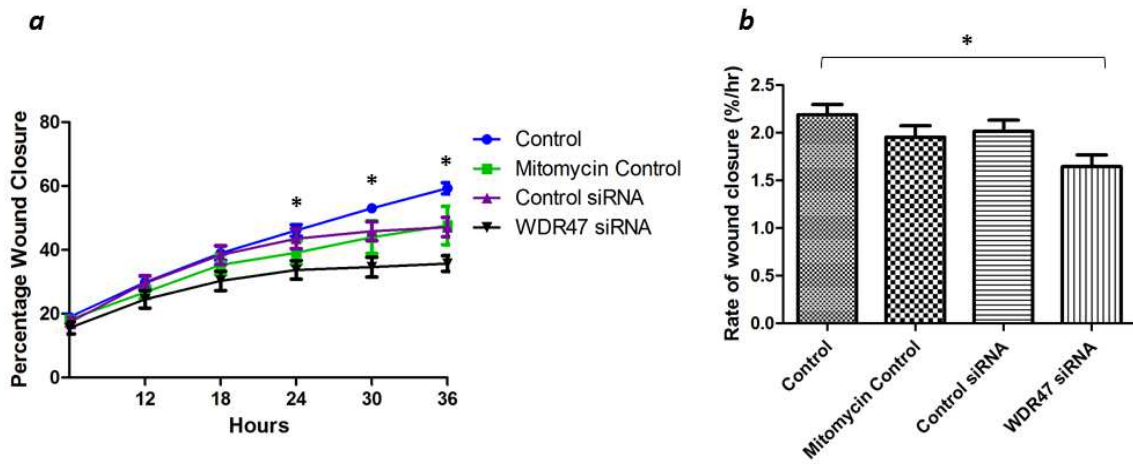
Figure 3.3: Percentage of wound closure over time (*a*) and rate (% / hour) of wound closure (*b*). n = 4; * P < 0.05 vs. control.
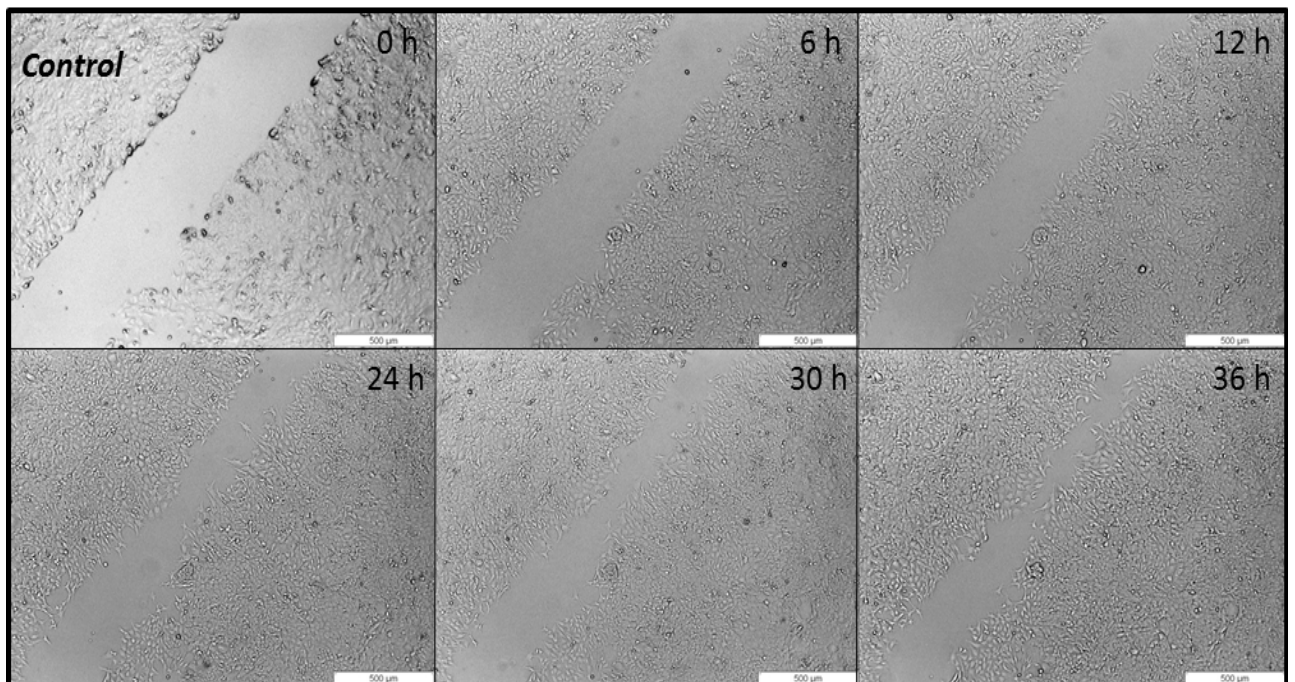
Figure 3.4: Transmission micrographs showing *in vitro* migration over time: control group. Wound closure is brought about by migration without inhibition of proliferation (scale bar: 500 µm).
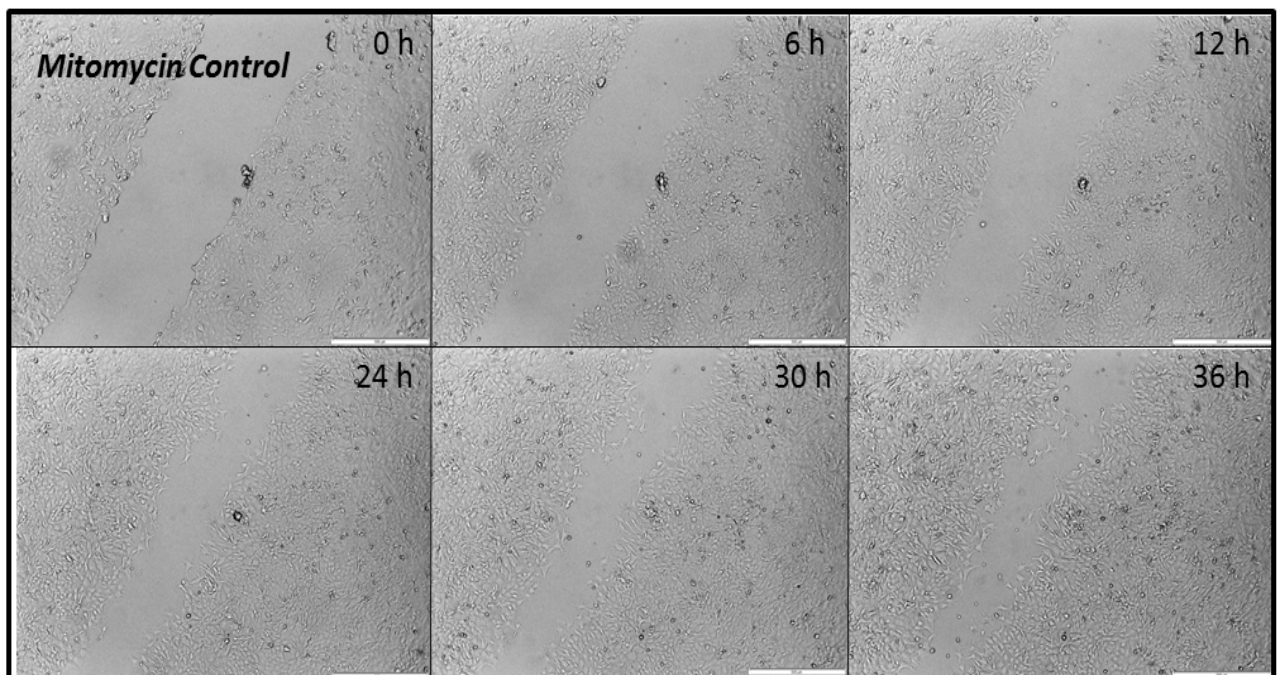
Figure 3.5: Transmission micrographs showing *in vitro* migration over time; Mitomycin control group. Wound closure is brought about by migration with inhibition of proliferation (scale bar: 500 µm).
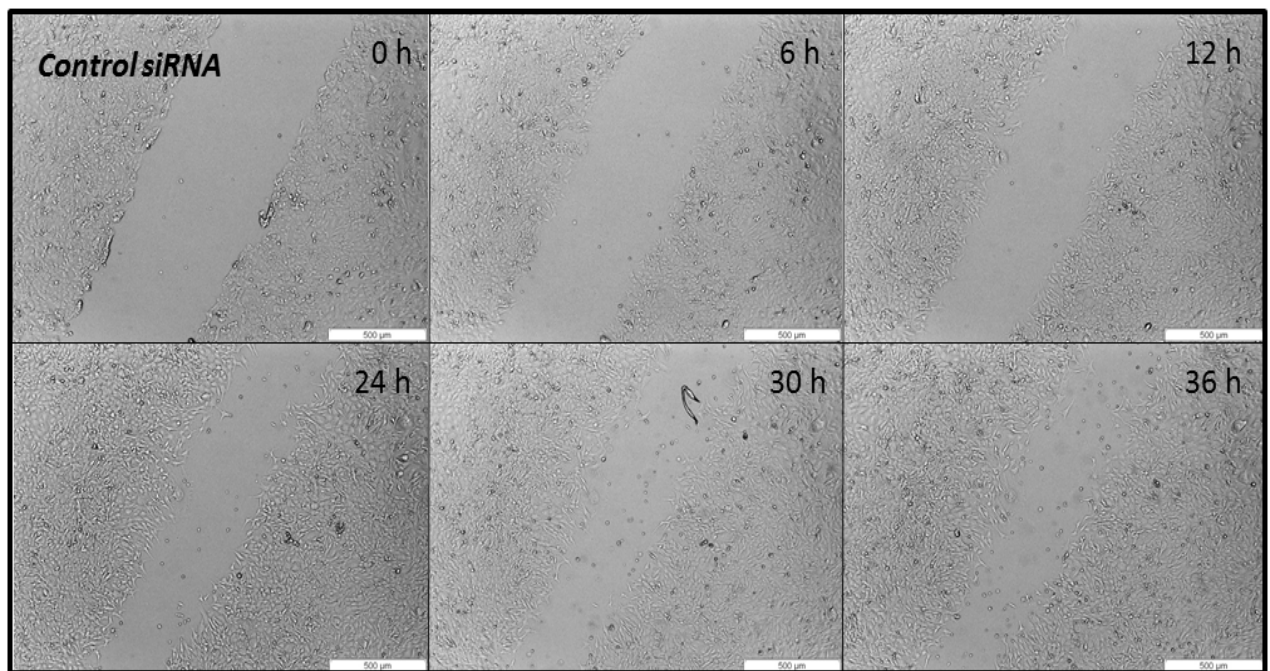
Figure 3.6: Transmission micrographs showing *in vitro* migration over time; control siRNA group, treated with Mitomycin C and transfected with control siRNA (scale bar: 500 μm).
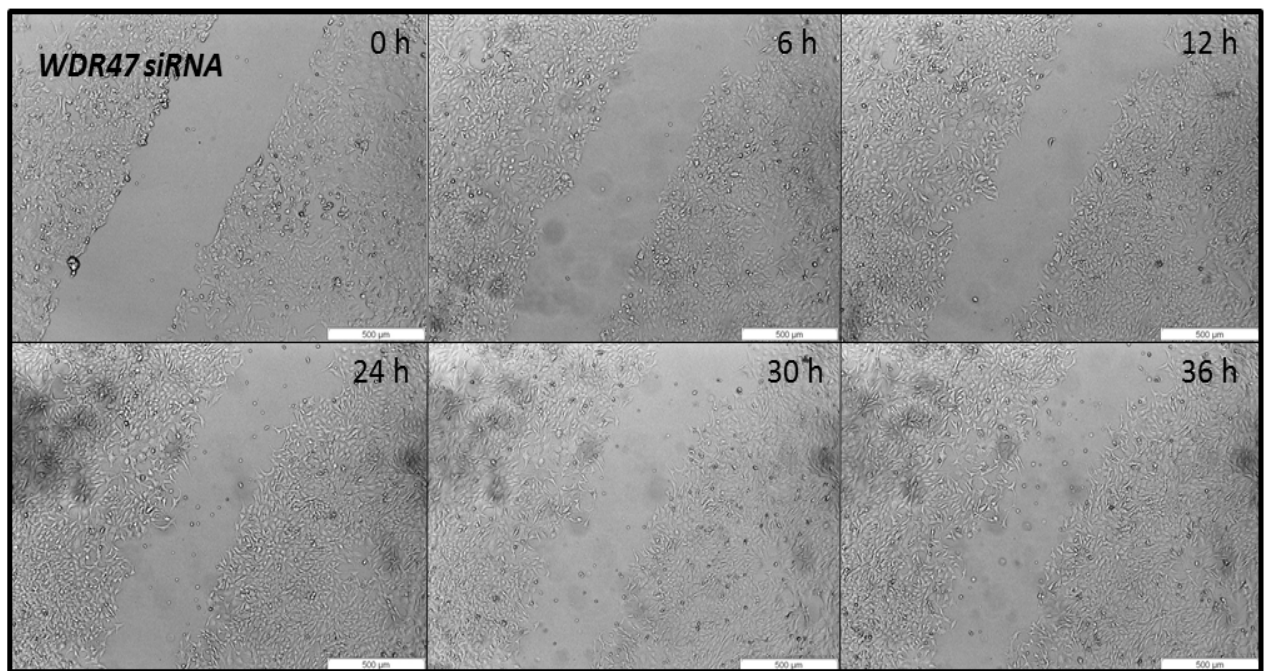
Figure 3.7: Transmission micrographs showing *in vitro* migration over time; WDR47 siRNA group, treated with Mitomycin C and transfected with WDR47 siRNA (scale bar: 500 μm).
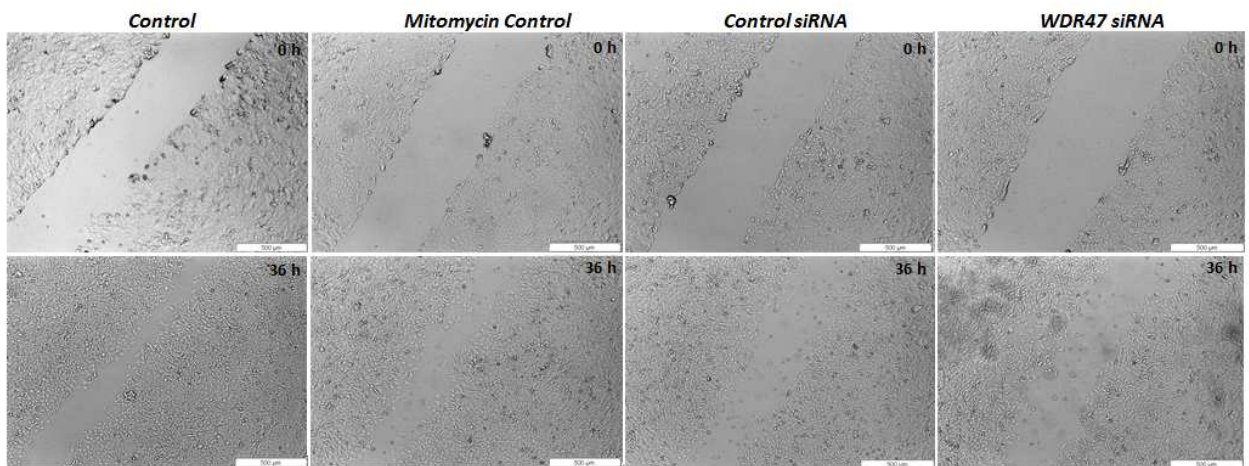
Figure 3.8: **Transmission micrographs showing** *in vitro* migration over time: comparison of control (first column), Mitomycin control (second column), control siRNA (third column), and WDR47 siRNA (fourth column) groups at 0 hours (top row) and 36 hours (bottom row) post scratch introduction. Wound healing ability of WDR47 siRNA group cells appears relatively compromised, and the area of the wound appears larger compared to other groups (scale bar: 500 μm).
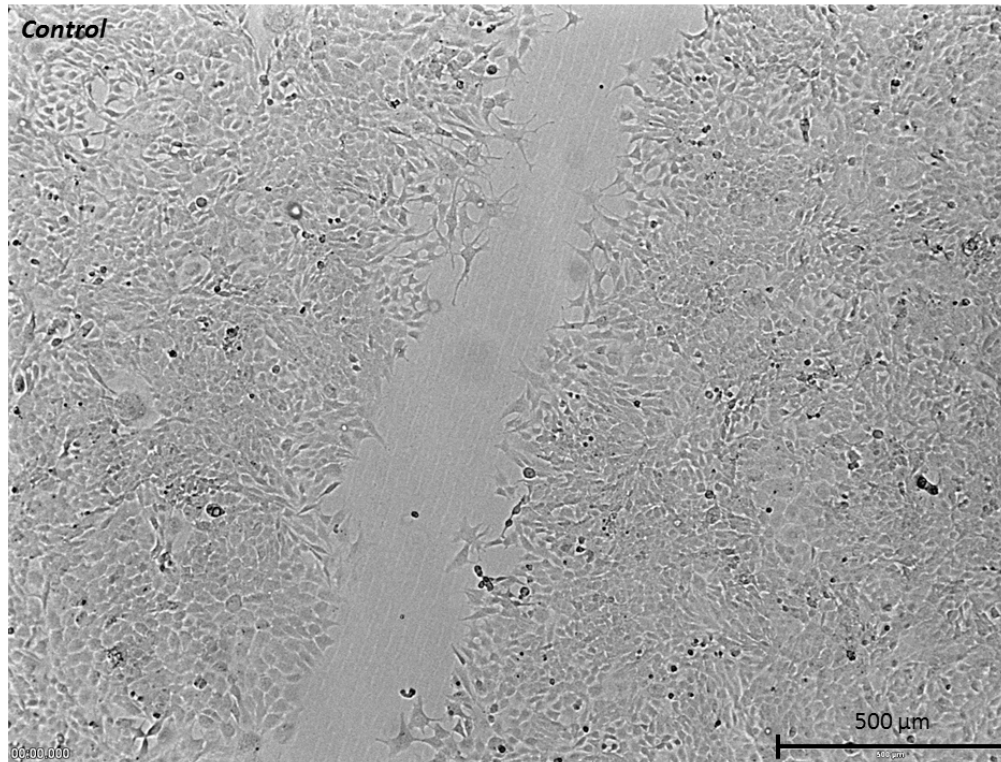
Figure 3.9: Transmission micrograph showing the control group at 36 hours post scratch introduction. Proliferating neurons closing the wound lack the distinctive extended processes of migrating neurons (scale bar: 500 μm).
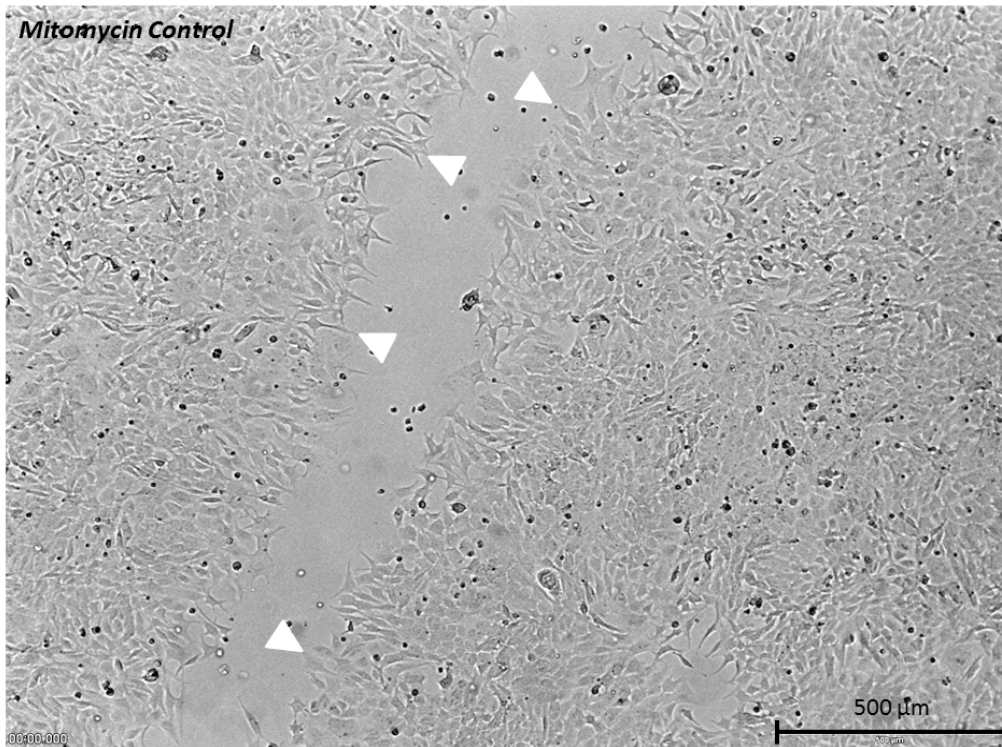
Figure 3.10: Transmission micrograph showing the Mitomycin control group at 36 hours post scratch introduction. Processes of migrating neurons extend toward the centre of the wound (scale bar: 500 μm).
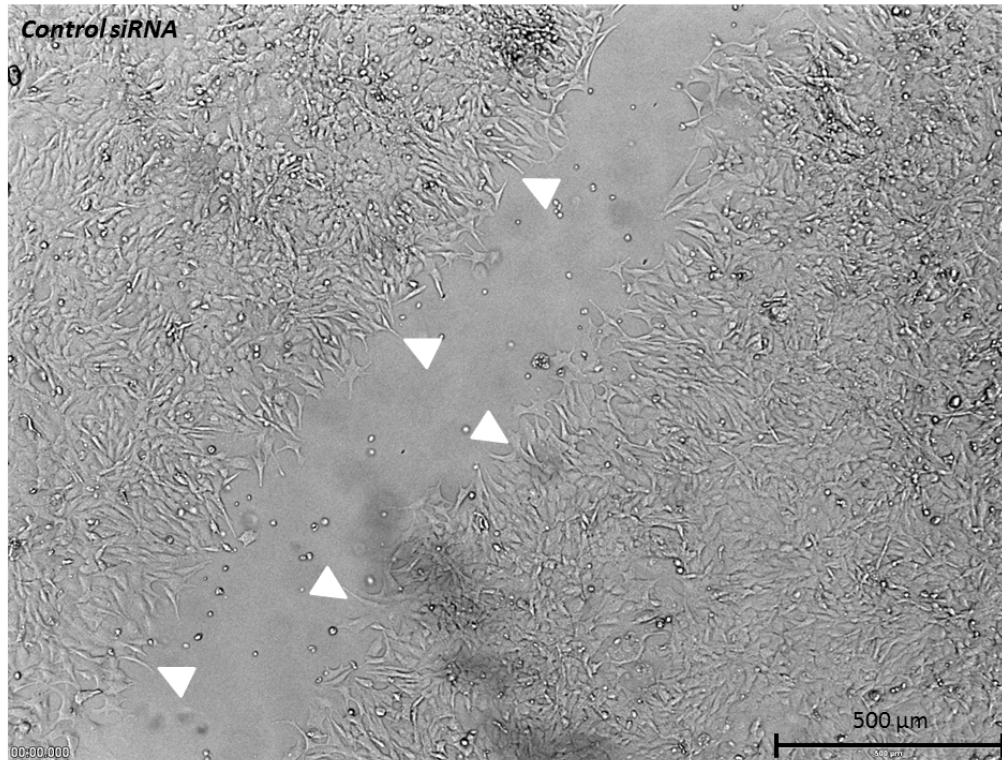
Figure 3.11: Transmission micrograph showing the control siRNA group at 36 hours post scratch introduction. Similar to Mitomycin control group cells, processes extend toward the centre of the wound (scale bar: 500 μm).
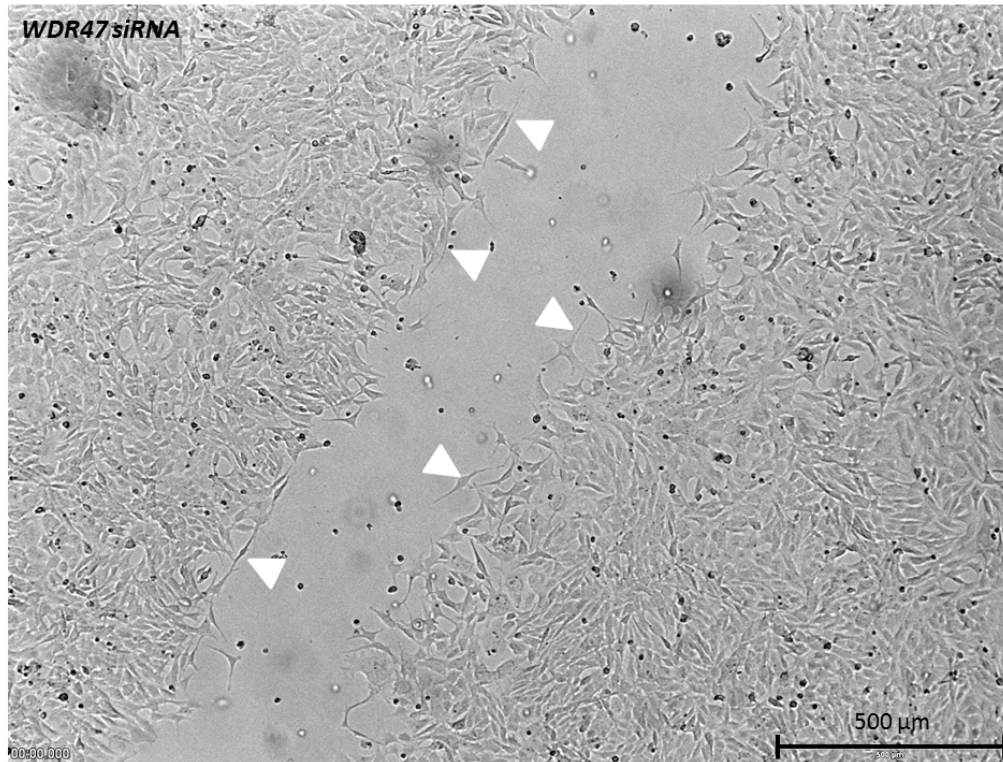
Figure 3.12: Transmission micrograph showing the WDR47 siRNA group at 36 hours post scratch introduction. Several processes of migrating neurons extend over shorter distances and lack directionality toward the centre of the wound (scale bar: 500 μm).

3.3 The Effect of WDR47 siRNA Treatment on the Direction of Migration

We speculated that WDR47 may be involved in regulating migration direction. We therefore performed a 24 hour migration assay, acquiring images every hour, and manually tracked neurons from each group to determine whether the direction of migration is affected by WDR47 siRNA-treatment. The data is displayed as a rose diagram (Figure 3.13). The distinct pattern of the quadrants represents neurons migrating to the centre from either side of the wound. The direction of migration between the different groups appears similar: rose diagrams extend primarily into the top left and bottom right quadrants. Relative to neurons from control, Mitomycin control, and control siRNA groups, rose diagrams of WDR47 siRNA-treated neurons are characterised by higher central plot density and short data points falling in distinct (top right and bottom left) quadrants.
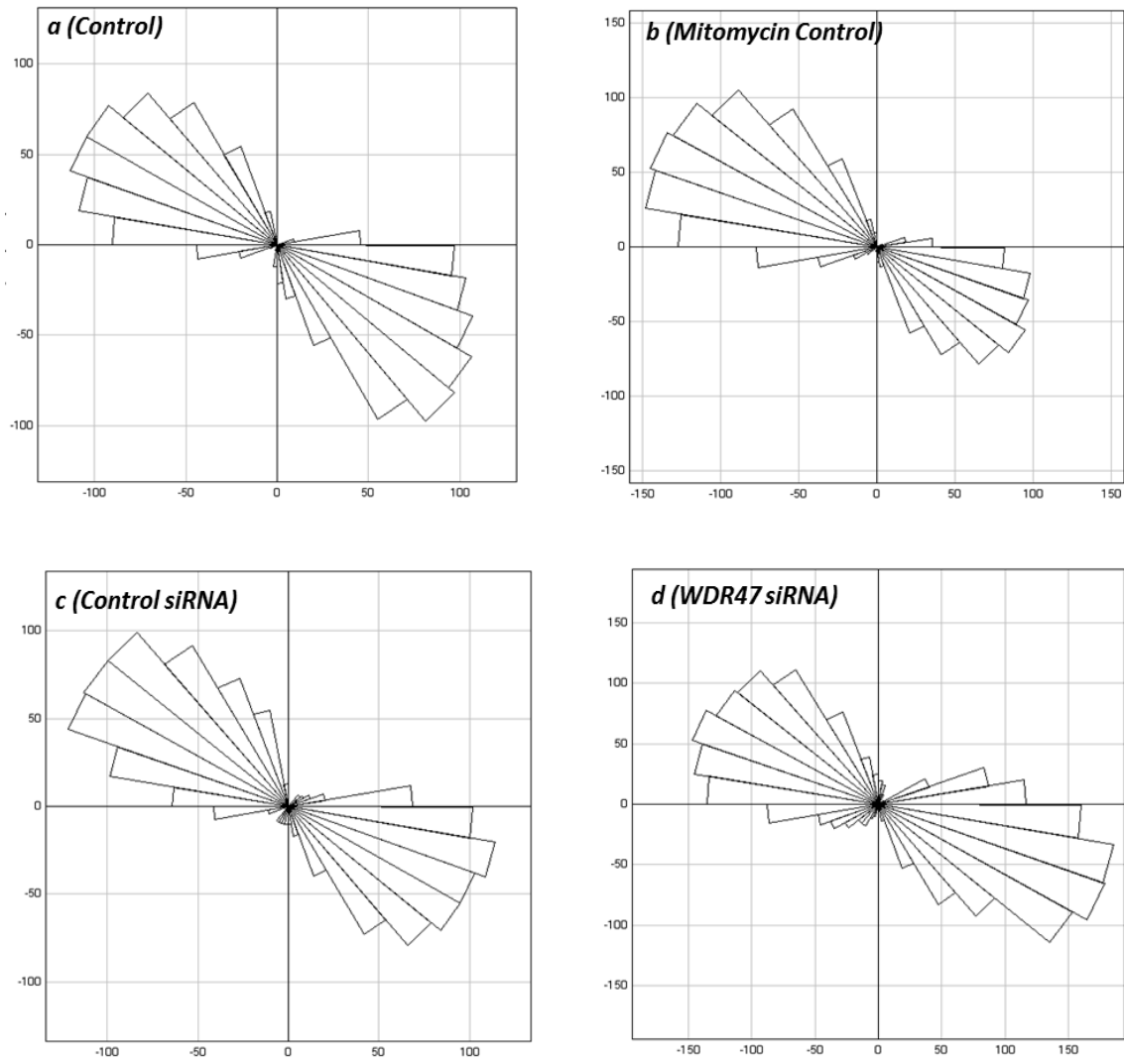
Figure 3.13: Rose diagrams representing directionality of manually tracked migrating neurons every hour for 24 hours. *a:* control neurons; *b:* Mitomycin control neurons; *c:* control siRNA cells; *d:* WDR47 siRNA cells (n = 2).

3.4 The Effect of WDR47 siRNA Treatment on Neuronal Morphology in the Migration Zone

SEM analysis of migrating neurons was performed in order to determine whether WDR47 siRNA treatment affects neuronal surface morphology, process formation, and surface adhesion. A comparison of WDR47 siRNA-treated neurons with control and control siRNA-treated neurons reveals several aberrant surface morphological features. Control and control siRNA-treated cells extend elongated, thin leading processes in the direction of migration, with defined regions of surface adhesion. Several filopodia-like extensions are observed along the processes (Figure 3.14 *a - f*). In comparison, WDR47 siRNA-treated cells are characterised by poorly defined regions of surface adhesion and intermittent loss of adhesion, with leading processes generally appearing relatively thick and short. Leading tips appear less defined, with blunted edges of a relatively large diameter. Filopodia-like extensions are absent, and the surface of the leading processes appears smooth compared to neurons from the control and control siRNA groups (Figure 3.14 *g – i*).
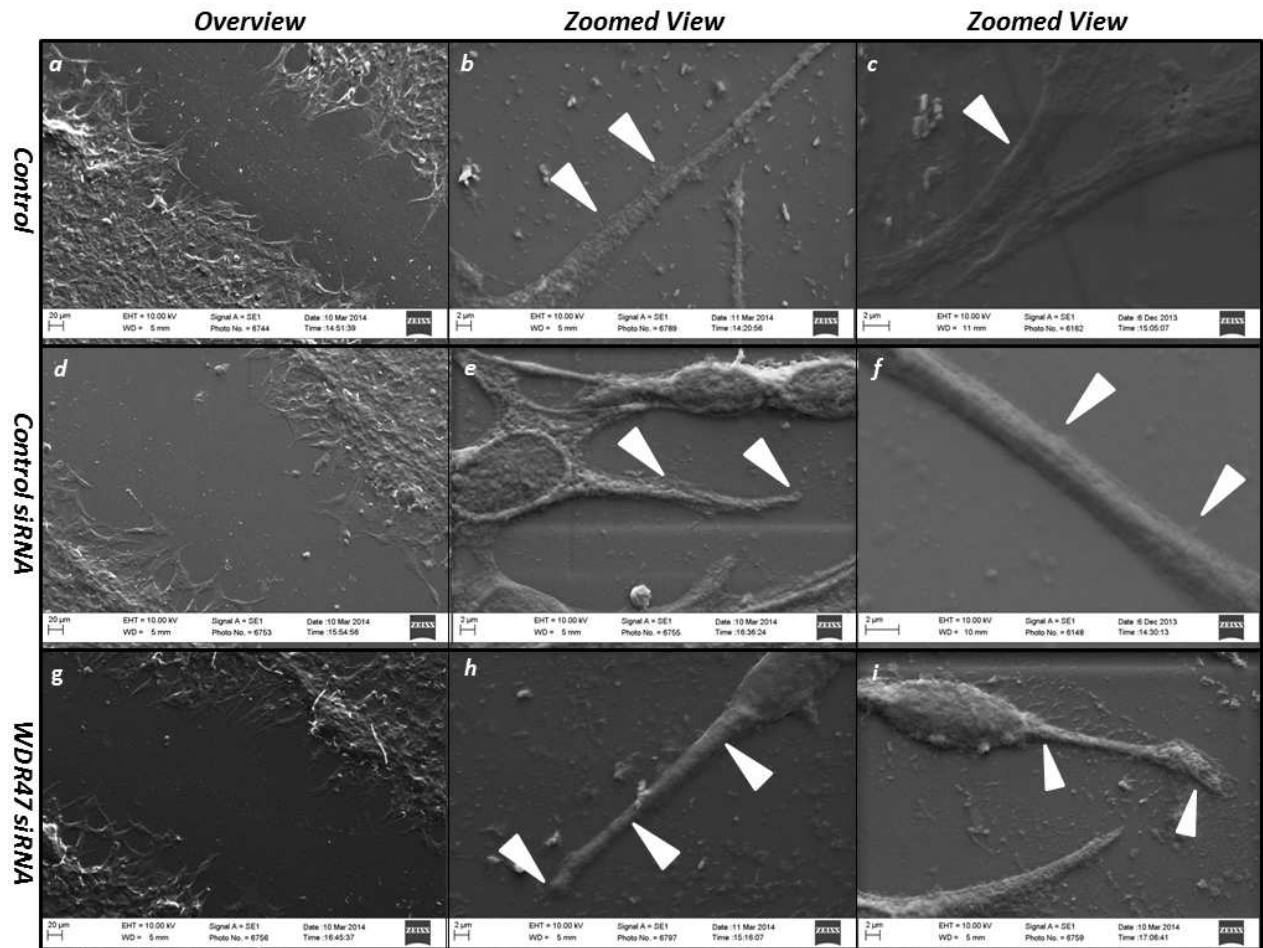
Figure 3.14: Scanning electron micrographs revealing neuronal surface morphology, process formation, and surface adhesion in the migration zone. Control neurons (*a-c*) and control siRNA neurons (*d-f*) extend a leading process characterised by filopodia-like structures and well-defined regions of surface adhesion, as well as a pointed tip. WDR47 siRNA neurons (*g-i*) extend a shorter, thicker leading process with a blunted, rounded tip, filopodia are absent, and surface adhesion appears compromised.

3.5 The Effect of WDR47 siRNA Treatment on Neuronal Ultra-Structure

TEM was utilized to determine whether WDR47 siRNA treatment affects neuronal ultra-structure. Several observations are made. Compared to control and control siRNA-treated cells (Figure 3.15 *a − h*), WDR47 siRNA-treated cells are characterised by more robust cytoplasmic membrane structures (Figure 3.15 *i*), particularly more prominent ER structures (Figure 3.15 *j*), and an expanded nuclear envelope (Figure 3.15 *k*). Mitochondria appear unaffected by WDR47 siRNA treatment: cristae are visible and mitochondria do not appear elongated, but rather characteristically oval (Figure 3.15 *l*).
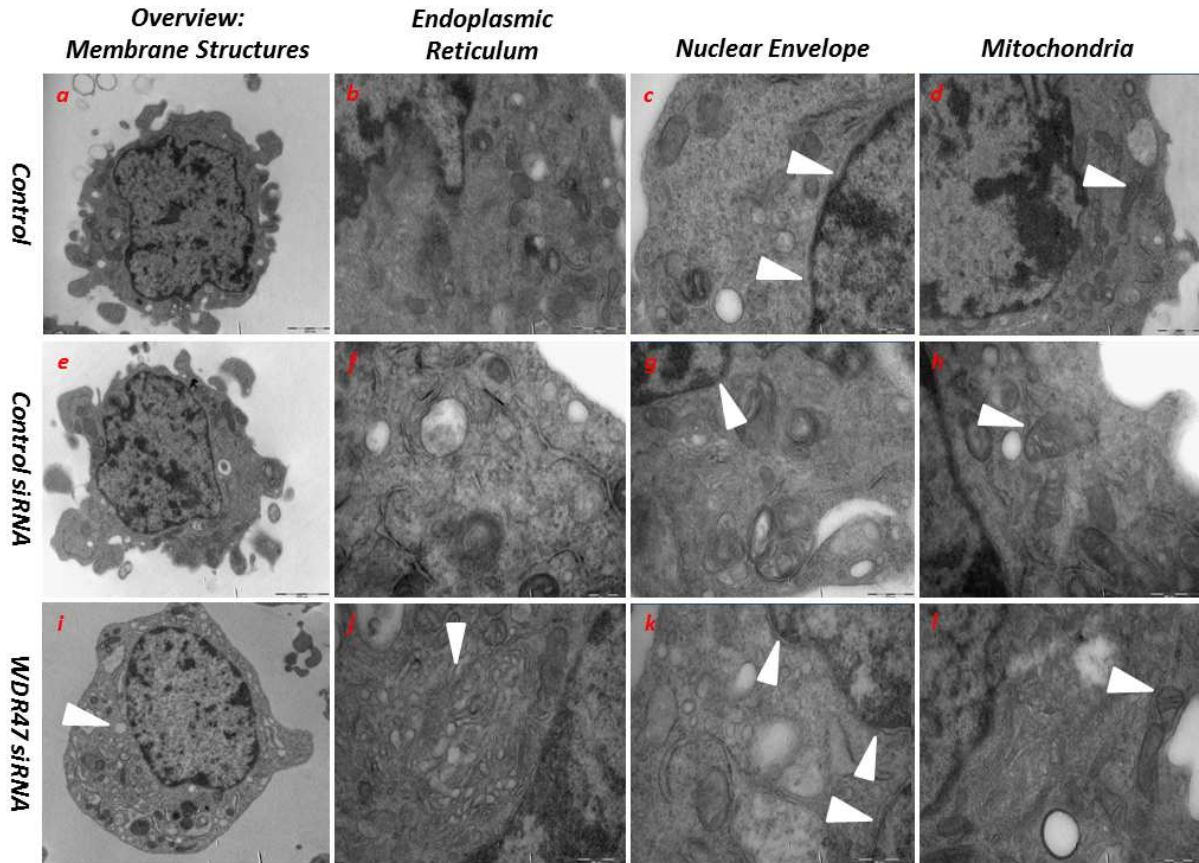
Figure 3.15: Transmission electron micrographs revealing neuronal ultrastructure. *a − d*: control; *e − h*: control siRNA-treated cell s; *I − l*: WDR47 siRNA-treated cells. Overview images (first column) reveal robust cytoplasmic membrane structures; more prominent ER structures (second column), an expanded nuclear envelope (third column) in WDR47 siRNA-treated cells compared to control and control siRNA-treated cells. No mitochondrial abnormalities are observed (fourth column) [scale bars *a,e,I:* 2000 nm; *b,c,d,f,g,h,j,k,l:* 500 nm).

3.6 The Effect of WDR47 siRNA Treatment on LC3 and P62 Protein Levels

3.6.1 LC3-I and LC3-II Relative Expression Levels

LC3 Western blot analysis was performed to determine whether WDR47 siRNA treatment plays a role in regulating autophagosome formation and autophagic flux, as LC3-II is a key marker of autophagic activity (Barth *et al.,* 2010). WDR47 siRNA treatment significantly reduced LC3-II levels [44.9 ± 6.4 % (P < 0.05)] compared to control and control siRNA-treated cells [78.6 ± 10.0 %] (Figure 3.16 *a*), indicating a decreased presence of autophagosomes. To determine whether the reduction in LC3-II levels is a result of increased autophagic flux or a result of decreased autophagosomal synthesis, we treated all groups with Bafilomycin A1, a potent inhibitor of the H+ ATPase, thereby rendering lysosomes dysfunctional with subsequent inhibition of fusion and resulting in accumulation of LC3-II-bound autophagosomes (Barth *et al.,* 2010). In Bafilomycin-treated cells (Figure 3.16 *b*), WDR47 siRNA treatment significantly increases LC3-II levels [134.0 ± 7.6 % (P < 0.05)] compared to control and control siRNA-treated cells (104.4 ± 4.7 %), indicating increased presence of autophagosomes.

75
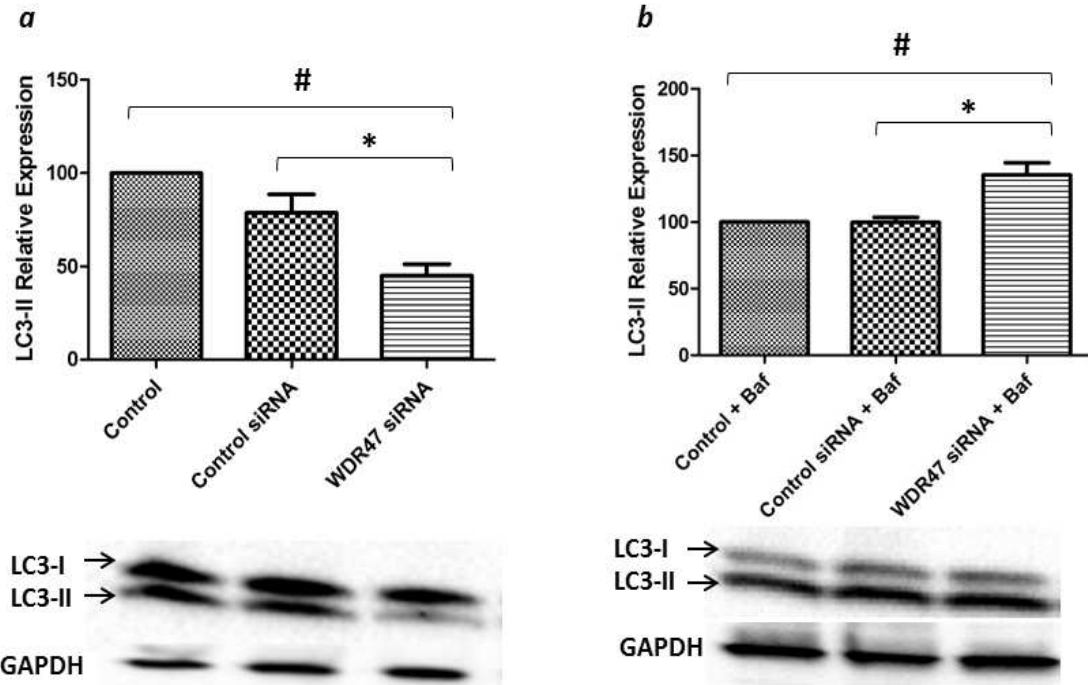
Figure 3.16: LC3-II relative expression following WDR47 siRNA treatment with and without Bafilomycin A1 treatment. *a:*WDR47 siRNA treatment significantly reduces LC3-II levels compared to control and control siRNA-treated cells (n = 8' # P < 0.05 vs control; * P < 0.05 vs control siRNA). *b:* WDR47 siRNA + Bafilomycin A1 treatment significantly increases LC3-II levels compared to control + Bafilomycin or control siRNA + Bafilomycin A1 treatment (n = 4; # P < 0.05 vs control + Baf; * P < 0.05 vs control siRNA + Baf).

3.6.2 P62 Relative Expression Levels

P62 targets poly-ubiquitinated proteins toward the autolysosome for degradation, thereby serving as a means to measure selective autophagy (Barth *et al.,* 2010). P62 Western blot analysis was performed to further determine the effect of WDR47 siRNA treatment on autophagic flux. No significant differences in P62 levels are detected between control, control siRNA-treated (105.4 ± 16.8 %), and WDR47 siRNA-treated cells [95.4 ± 13.3 %] (Figure 3.17 *a*). However, with Bafilomycin A1 treatment, P62 levels are significantly increased in WDR47 siRNA-treated cells [136.8 ± 18.2 % ($P < 0.05$) compared to control cells, but not compared to control siRNA-treated cells [86.7 ± 12.2 %] (Figure 3.17 *b*). However, a non-significant trend for increased P62 levels is observed with WDR47 siRNA treatment compared to control siRNA treated cells.
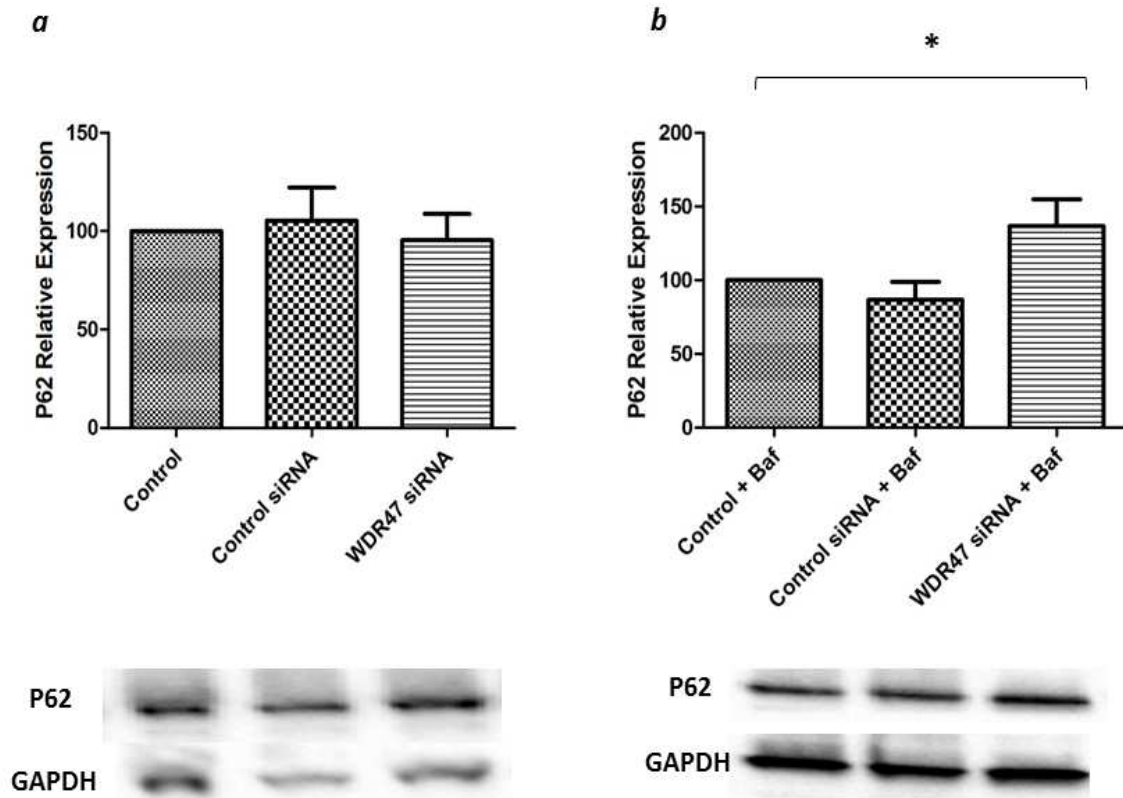
Figure 3.17: P62 relative expression following WDR47 siRNA treatment with and without Bafilomycin A1 treatment. *a:* No significant differences are detected (n = 4). *b:* WDR47 siRNA + Bafilomycin A1 treatment significantly increases P62 levels compared to control + Bafilomycin A1 treatment (n = 6; * P < 0.05 vs Control + Baf).

3.7 The Effect of WDR47 siRNA Treatment on SCG10, Tau, and Acetylated Tubulin Protein Levels

3.7.1 Total SCG10 Relative Expression Levels

Western blot analysis of SCG10 yields four bands in the molecular weight region of 20 – 25 kDa, representing distinct phosphorylation states (Bondallaz *et al.,* 2006; Westerlund *et al.,* 2011). Two major bands are detected (22 and 25 kDa). No significant differences at the 25 kDa band are observed between control, control siRNA-treated [143.9 ± 30.3%], or WDR47 siRNA-treated cells [202.4 ± 96.6 %]; however, a non-significant trend for increased 25 kDa SCG10 levels is observed with WDR47 siRNA treatment (Figure 3.18 *a*). A significant reduction in relative expression of the 22 kDa band is observed with WDR47 siRNA treatment [31.9 ± 11.2 % (P < 0.05)] compared to control cells, but not compared to control siRNA-treated cells [62.3 ± 22.8 %] (Figure 3.18 *b*). However, a non-significant trend for decreased 22 kDa SCG10 with WDR47 siRNA treatment compared to control siRNA-treated cells is observed.
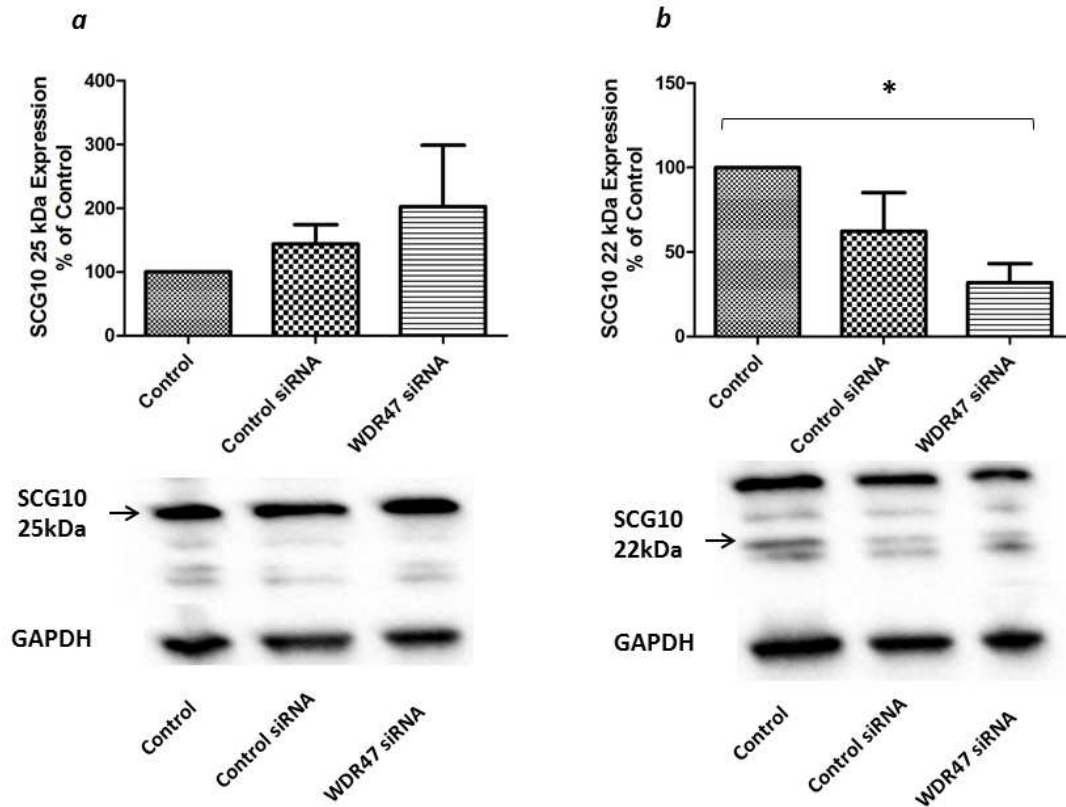
Figure 3.18: SCG10 relative expression following WDR47 siRNA treatment. Two major bands are detected. *a:* No significant differences are detected at the 22 kDa band of SCG10. *b:* WDR47 siRNA treatment significantly reduces SCG10 expression at the 25 kDa band compared to control cells (n = 4; P < 0.05 vs control).

3.7.2 Total Tau Relative Expression Levels

Western blot analysis of Tau protein was performed as an indirect indicator of microtubule function with WDR47 siRNA treatment. There is no significant difference in total tau levels between control, control siRNA-treated cells [99.9 ± 23.5 %], or WDR47 siRNA-treated cells [119.4 ± 39.0 % (Figure 3.19 *a*)].

3.7.3 Acetylated Tubulin Relative Expression Levels

Tubulin acetylation is an indication of microtubule stability (Al-Bassam J & Corbett KD, 2012). Western blot analysis of acetylated tubulin was performed to determine whether WDR47 siRNA-treatment is able to influence tubulin stability. There is no significant difference in acetylated tubulin levels between control, control siRNA-treated cells [119.2 ± 9.0 %], or WDR47 siRNA-treated cells [138.9 ± 15.4 %]. However, a non-significant trend for increased acetylated tubulin levels following WDR47 siRNA treatment is observed (Figure 3.19 *b*).
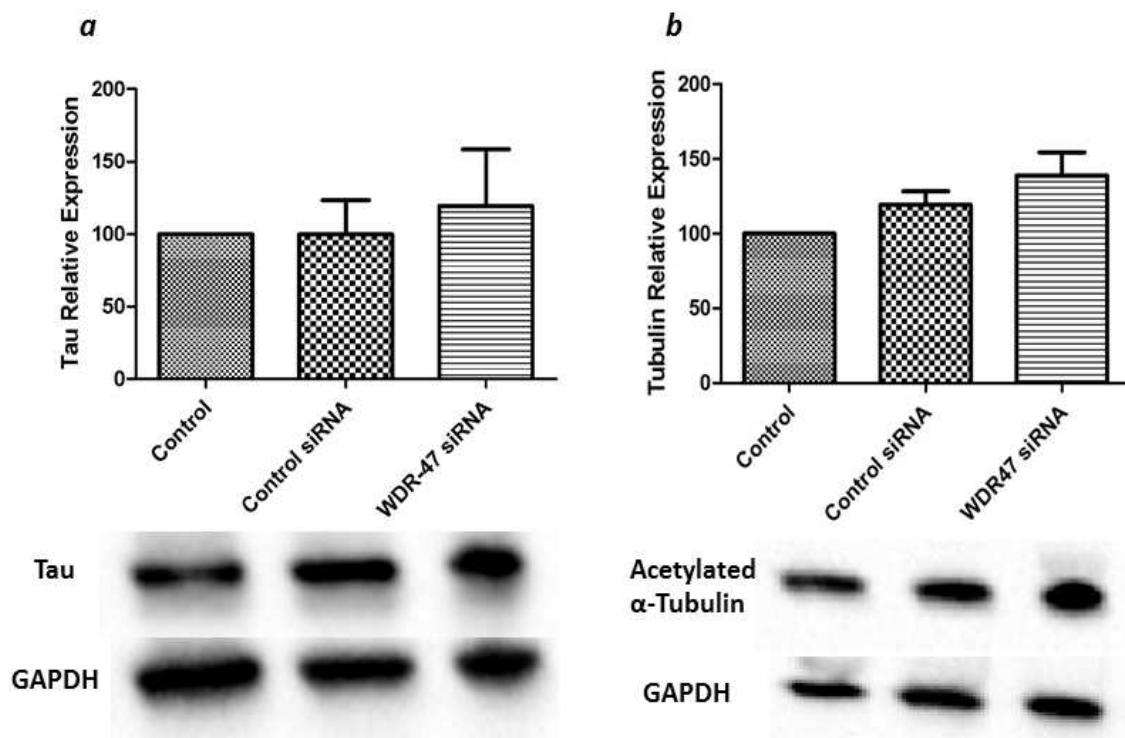
Figure 3.19: Total tau and acetylated tubulin relative expression following WDR47 siRNA treatment. *a:* No significant differences are observed in total tau levels. *b:* No significant differences are observed in acetylated tubulin levels. A non-significant trend for increased acetylated tubulin with WDR47 siRNA treatment is observed.

3.8 Cellular Localization and Distribution of WDR7 in GT1-7 Neurons

In order to assess the intracellular localization of WDR47 beyond the limit of resolution achieved with confocal microscopy, immuno-fluorescence and SR-SIM analysis was performed. SR-SIM reveals a predominantly cytoplasmic distribution of WDR47; however some fluorescence signal is detected in the nuclear region. Within the cytosol there are spherical vacuole-like regions where fluorescence signal is substantially decreased, however the cytoplasmic distribution of WDR47 appears to be largely homogenous (Figure 3.20).
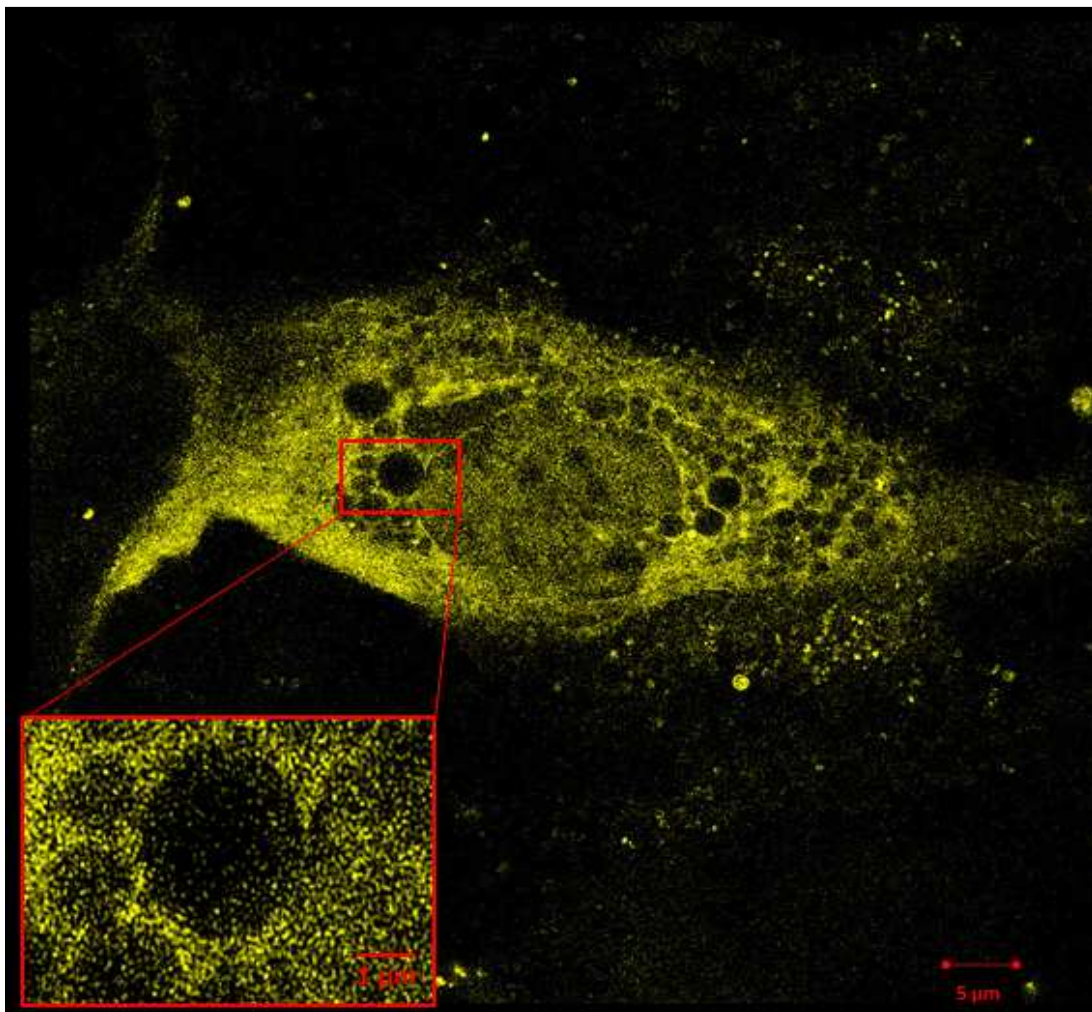
Figure 3.20: Representative SR-SIM fluorescent micrograph of WDR47-YFP transfected cell. WDR47 is predominantly cytoplasmic and homogenously distributed (n = 2; scale bars: 1 µm and 5 µm).

3.9 The Effect of WDR47 on LC3 Distribution and Acetylated Tubulin Network

To determine whether WDR47 siRNA treatment effects LC3 and/or acetylated tubulin distribution and network, immuno-fluorescence and confocal microscopy of cells co-stained with LC3 and acetylated tubulin was performed. LC3 positive punctae appear reduced in WDR47 siRNA treated cells, and acetylated tubulin fluorescence signal appears to be increased, particularly in the perinuclear region compared to control and control siRNA-treated cells (Figure 3.21 – 3.22). SR-SIM analysis was performed to further investigate the effect of WDR47 siRNA treatment on acetylated tubulin. In comparison to control and control siRNA treated cells (Figure 3.23 – 3.25), WDR47 siRNA-treated cells are characterised by accumulation of highly convoluted acetylated tubulin networks in the perinuclear region (Figure 3.25).
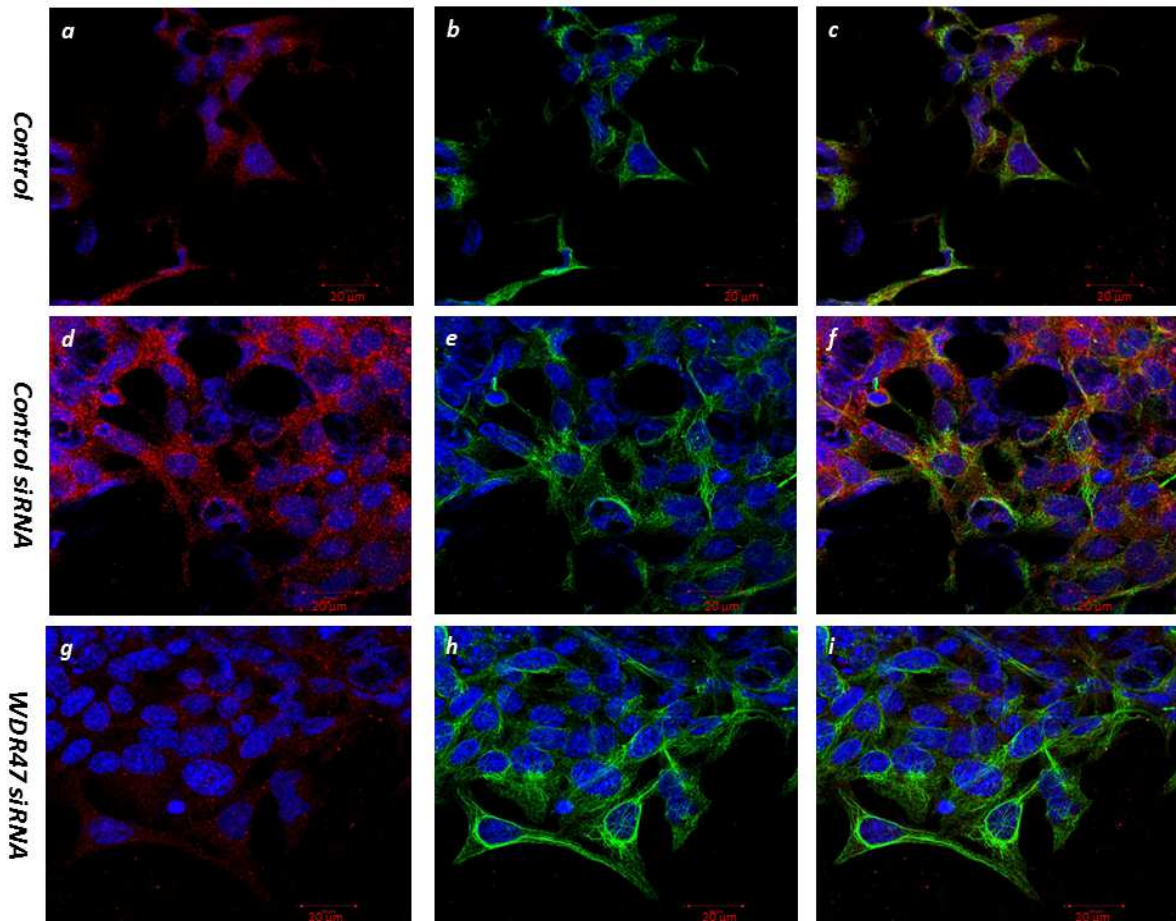
Figure 3.21: Representative confocal fluorescent micrographs of cells co-stained with LC3 (red) and acetylated tubulin (green). *a – c:* control cells; *d – f:* control siRNA-treated cells; *g – i:* WDR47 siRNA-treated cells. Nuclei are counterstained in blue with Hoechst 33342. LC3 fluorescence signal appears reduced, and acetylated tubulin fluorescence signal appears increased (particularly in the perinuclear region) in WDR47 siRNA-treated cells compared to control and control siRNA-treated cells (scale bar: 20 µm).
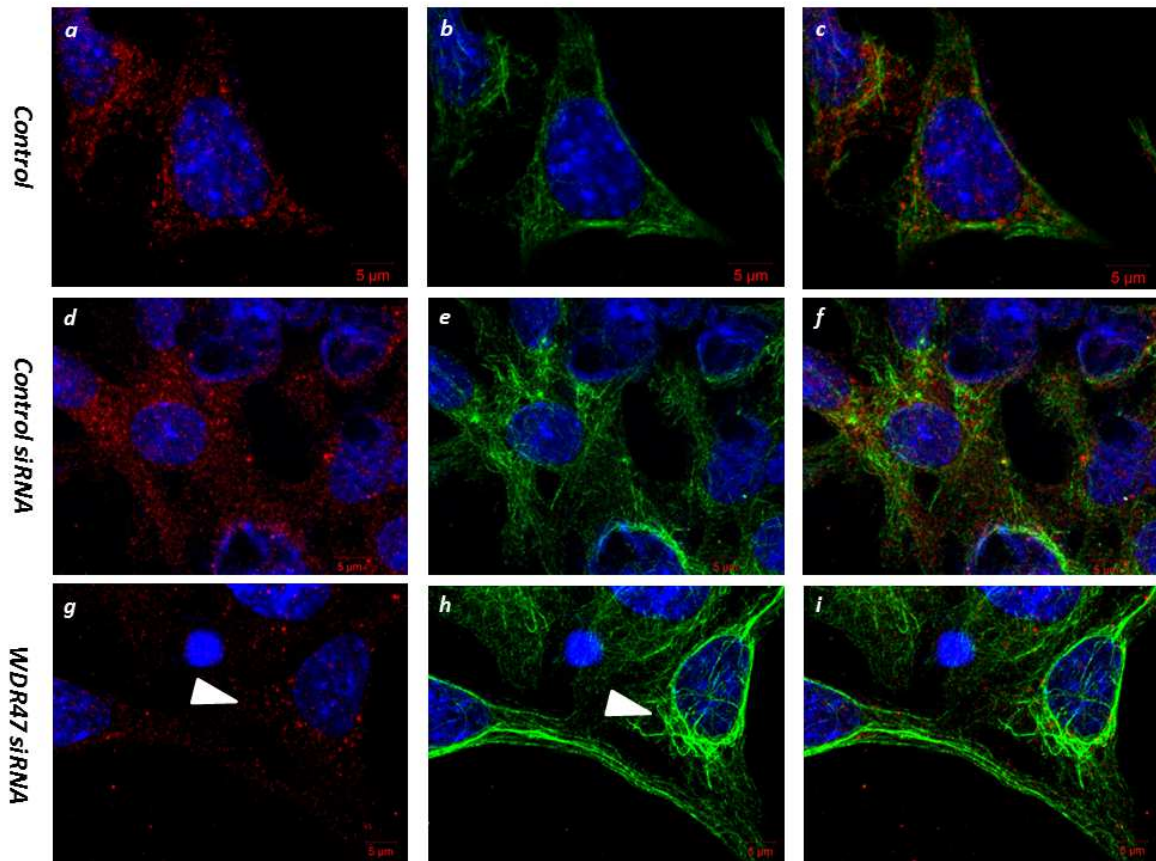
Figure 3.22: Representative confocal fluorescent micrographs of cells co-stained with LC3 (red) and acetylated tubulin (green): zoomed view. *a − c:* control cells; *d − f:* control siRNA-treated cells; *g − i:* WDR47 siRNA-treated cells. Nuclei are counterstained in blue with Hoechst 33342. LC3 fluorescence signal appears reduced, and acetylated tubulin appears more convoluted and concentrated in the perinuclear region in WDR47 siRNA-treated cells compared to control and control siRNA-treated cells (scale bar: 5 µm).
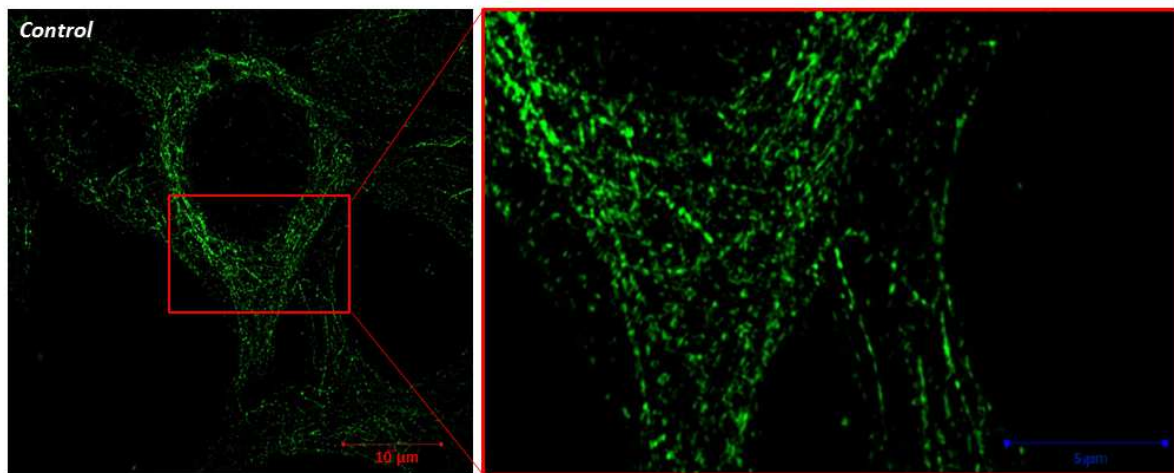
Figure 3.23: Representative SR-SIM fluorescent micrograph of acetylated tubulin in control cells (scale bars: 10 µm and 5 µm).
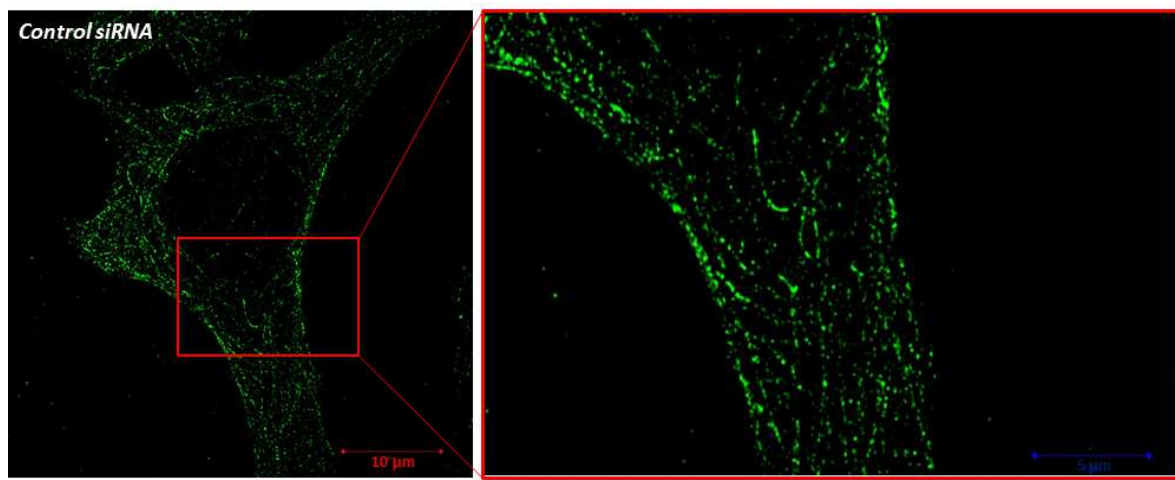
Figure 3.24: Representative SR-SIM fluorescent micrograph of acetylated tubulin in control siRNA-treated cells (scale bars: 10 µm and 5 µm).
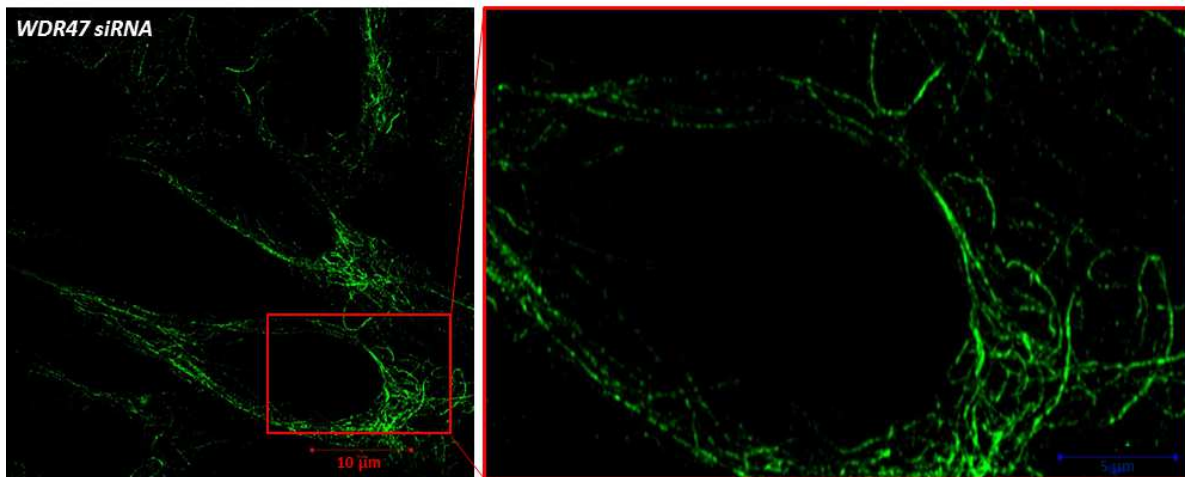
Figure 3.25: Representative SR-SIM fluorescent micrograph of acetylated tubulin in WDR47 siRNA-treated cells. Acetylated tubulin appears to robustly organize in the perinuclear region, forming a highly dense and convoluted network (scale bars: 10 µm and 5 µm).

3.10 Co-Localization of WDR47 with LC3 and of WDR47 with Acetylated Tubulin

Immuno-fluorescence and confocal microscopy of WDR47, LC3, and acetylated tubulin was performed in order to determine whether WDR47 co-localizes with LC3 and/or acetylated tubulin. A moderate degree of co-localization is observed between WDR47 and LC3 (Figure 3.26 – 3.27), particularly in the perinuclear region. A more pronounced degree of co-localization is observed between WDR47 and acetylated tubulin in the perinuclear region (Figure 3.28) as well as in extended processes (Figure 3.29).
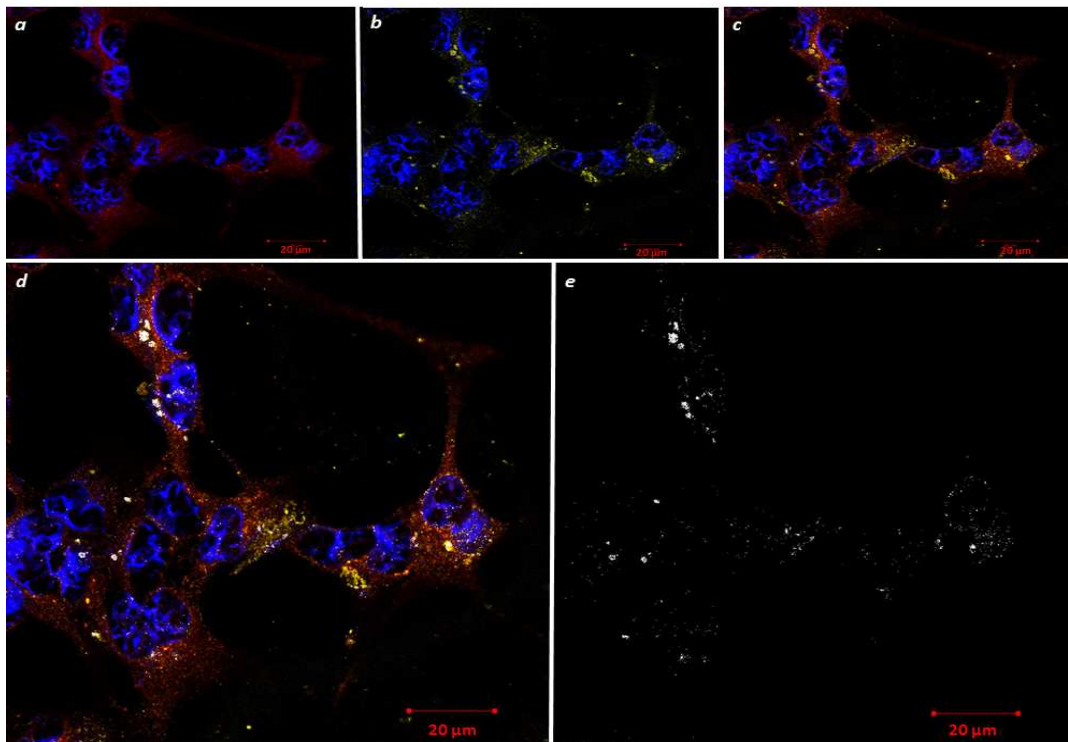
 Figure 3.26: Representative confocal fluorescent micrographs of WDR47 and LC3 co-localization. *a:* LC3 (red); *b:* WDR47 (yellow); *c:* overlay; *d:* co-localization (white) overlaid with fluorescence; *e:* co-localization only. A degree of co-localization is observed, particularly around the nucleus (nuclei are counterstained with Hoechst 33342) [scale bar: 20 μm].
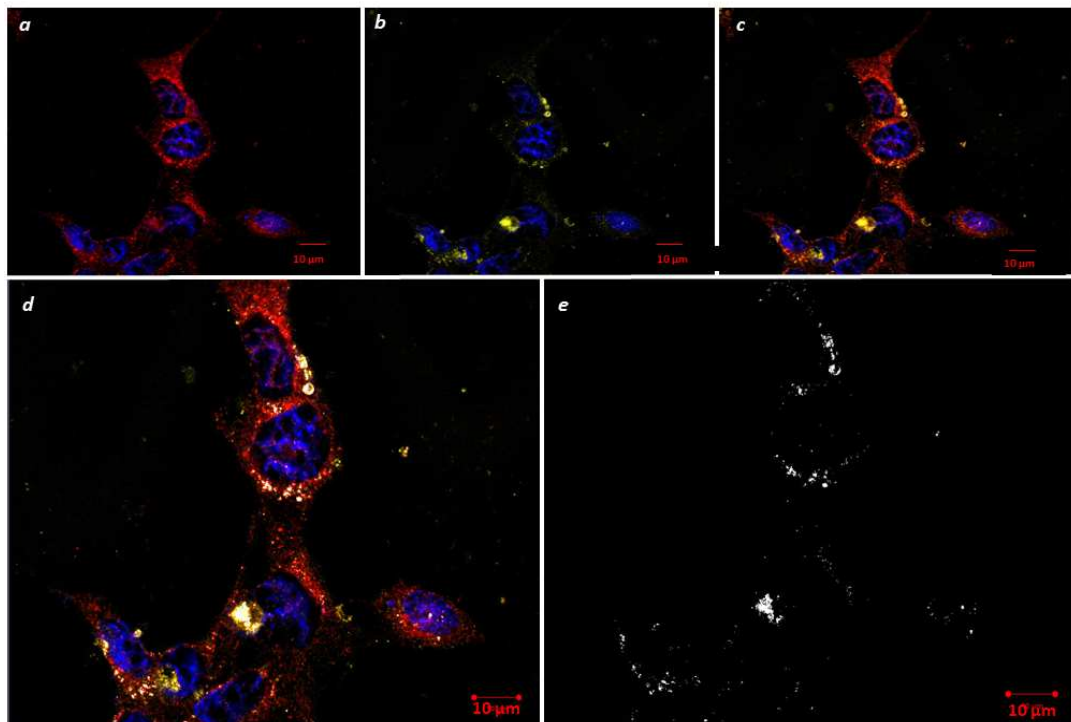
Figure 3.27: Representative confocal fluorescent micrographs of WDR47 and LC3 co-localization. *a:* LC3 (red); *b:* WDR47 (yellow); *c:* overlay; *d:* co-localization (white) overlaid with fluorescence; *e:* co-localization only (nuclei are counterstained with Hoechst 33342) [scale bar: 10 μm].
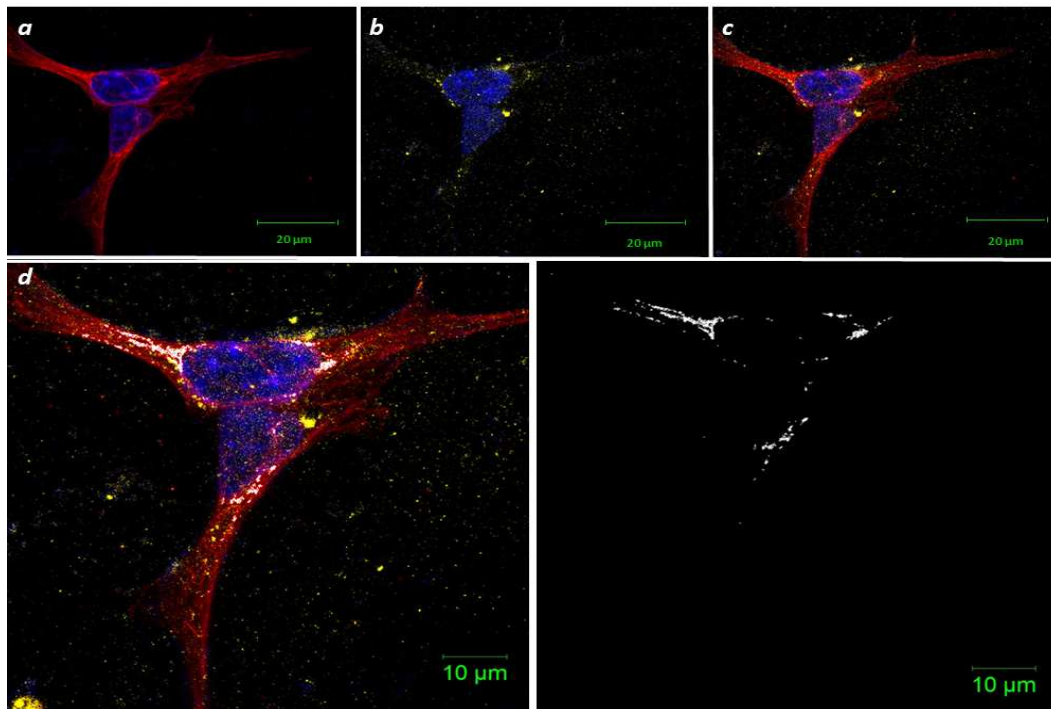
Figure 3.28: Representative confocal fluorescent micrographs of WDR47 and acetylated tubulin co-localization. *a:* tubulin (red); *b:* WDR47 (yellow); *c:* overlay; *d:* co-localization (white) overlaid with fluorescence; *e:* co-localization only. Co-localization is observed around the nucleus (nuclei are counterstained with Hoechst 33342)   [scale bars: (*a,b,c*) 20 µm; (*d,e*) 10 µm].
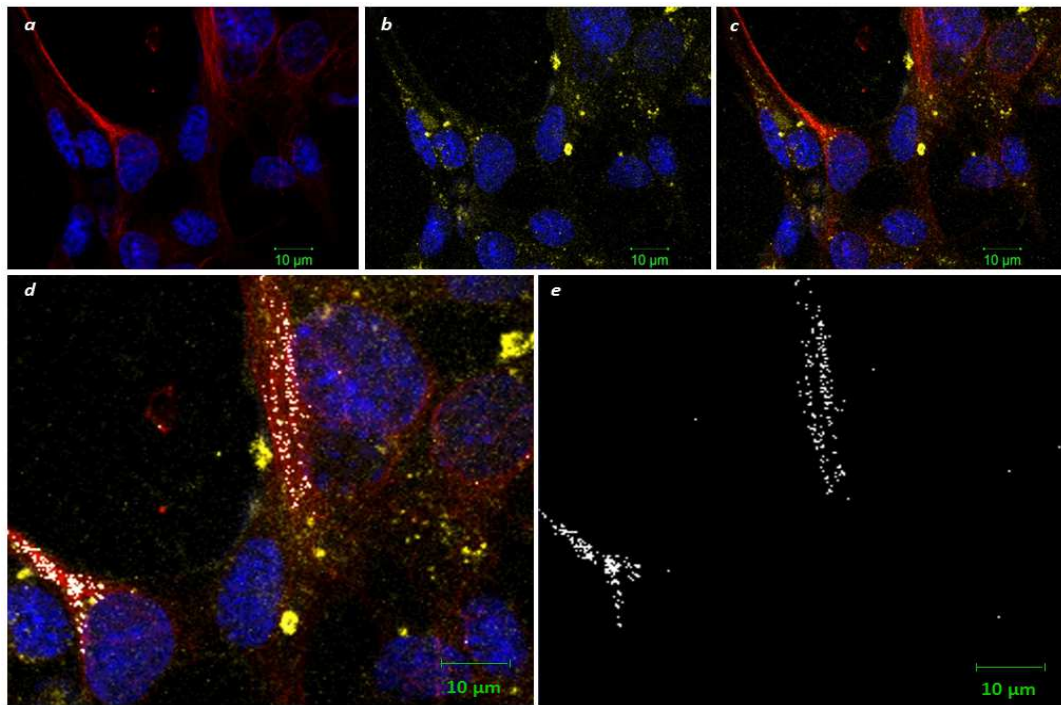
Figure 3.29: Representative confocal fluorescent micrographs of WDR47 and acetylated tubulin co-localization. *a:* LC3 (red); *b:* WDR47 (yellow); *c:* overlay; *d:* co-localization (white) overlaid with fluorescence; *e:* co-localization only. Co-localization is observed in neuronal processes (nuclei are counterstained with Hoechst 33342) [scale bars 10 μm].

3.11 FRAP analysis of WDR47 in YFP Transfected Cells

FRAP analysis was performed In order to assess mobile and immobile fraction of the WDR47 protein. Results for FRAP analysis are shown in figure 3.30 – 3.31. The microscope was incapable of generating a sufficient laser power to effectively bleach the WDR47-YFP fluorescence. The results observed may likely be a combination of a rapid fluorescence recovery of WDR47-YFP, a high expression of WDR47 in GT1-7 cells, and therefore insufficient bleaching power of the microscope lasers. WDR47-YFP FRAP analysis therefore requires optimization which is beyond the scope of this project; here we show results for a preliminary setup of experimental procedures.
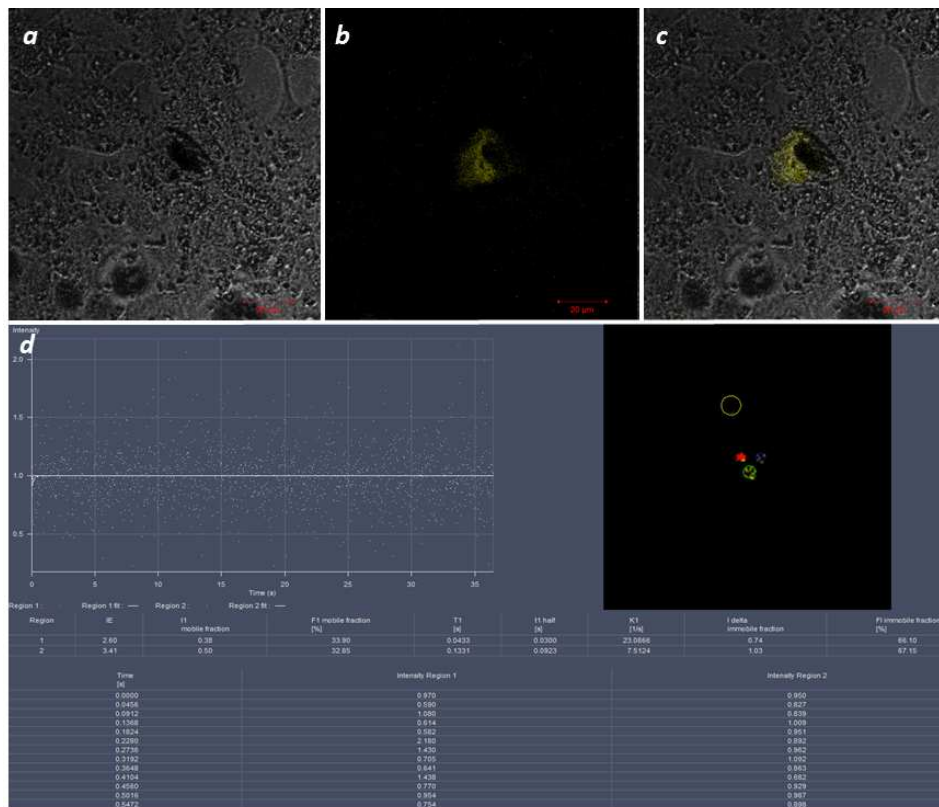
Figure 3.30: Fluorescence recovery after photo-bleaching (FRAP) of WDR47-YFP transfected cells. *a:* normal light (transmission); *b:* WDR47-YFP fluorescence; *c:* overlay; *d:* recovery curve (fluorescence intensity over time) after bleaching cytoplasmic regions. Background measurements were obtained from an extracellular region and the nucleus. A small increment in fluorescence intensity is observed approximately 1 second after bleaching, after which the intensity plateaus (scale bar: 20 μm).

97
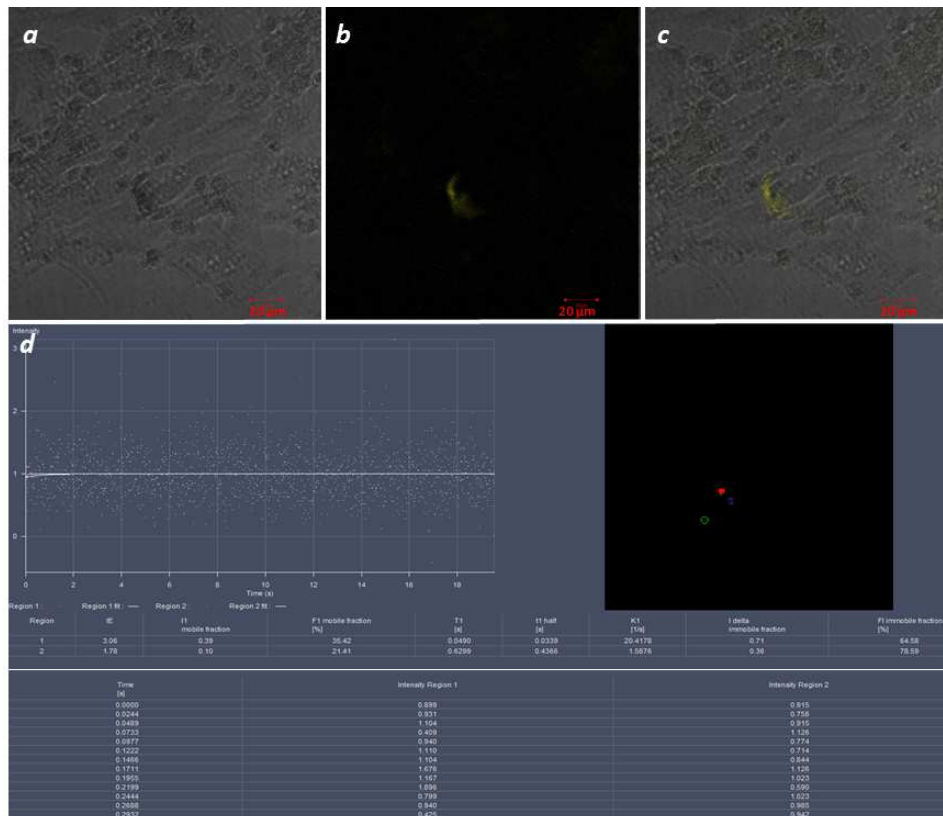
Figure 3.31: Fluorescence recovery after photo-bleaching (FRAP) of WDR47-YFP transfected cells. *a:* normal light (transmission); *b:* WDR47-YFP fluorescence; *c:* overlay; *d:* recovery curve (fluorescence intensity over time) after bleaching cytoplasmic regions. Background measurements were obtained from an extracellular region and the nucleus. A small increment in fluorescence intensity is observed approximately 1 second after bleaching, after which the intensity plateaus (scale bar: 20 µm).

Chapter 4: Discussion

WDR47 belongs to the functionally diverse WD40 family of proteins. Each member of the WD40 family houses a variable number of WD40 repeats that form a domain serving to create a platform for multiple protein complex assembly (Sun *et al.,* 2011). Previously identified interacting partners of WDR47 include Reelin (Kinnear, 2007), SCG10 (McGillewie, 2009), and MAP1S (Wang *et al.,* 2012). Although these interactions are indicative of a microtubule-regulating role of WDR47, the function of WDR47 in microtubule-dependent processes has not been previously investigated. We hypothesized that WDR47 is able to regulate microtubule-dependent processes such as neuronal migration and autophagy. We knocked down WDR47 in GT1-7 neuronal cells and performed a neuronal migration scratch assay to assess directed migration, and performed SEM to assess process formation and surface adhesion of migrating neurons. To assess autophagy we performed Western blot analysis of LC3 and P62 with and without Bafilomycin A1 treatment, confocal fluorescence microscopy of LC3, and co-localization analysis of WDR47 with LC3. TEM analysis was used to assess neuronal ultra-structure. To determine whether WDR47 affects microtubule dynamics, we performed acetylated tubulin SR-SIM 3-D analysis, co-localization of WDR47 with acetylated tubulin, as well as Western blot analysis of microtubule-regulating proteins SCG10 and Tau. Here, we first explore explanations for each result separately, after which we conclude by combining and interpreting all our results in light of potential previously identified interacting partners of WDR47.

4.1 The Effect of WDR47 on Neuronal Migration

4.1.1 WDR47 Knock-Down Decreases Migration Distance and Migration Velocity

Our results reveal that WDR47 siRNA treatment significantly reduces the average migration distance and the migration velocity (Figure 3.2), as well as the percentage and rate of wound closure (Figure 3.3). Furthermore WDR47 siRNA-treated cells appear to be characterised by a somewhat disrupted migration pattern, a compromised ability to form extended processes in the direction of migration (perpendicular to the wound edge), suggesting an overall compromised wound healing ability (Figure 3.4 – Figure 3.12).

Several plausible scenarios may contribute to the neuronal migration defects observed. For example, WDR47 and Lis1 may be regulating neuronal migration by a similar mechanism, given the remarkable similar domain structures of the proteins. Using mouse cortical slice migration assays and confocal time laps video-microscopy, Youn *et al.* (2009) demonstrated that a reduction of Lis1 levels considerably decreased migration velocity in a dose-dependent manner, with complete loss of Lis1 culminating in the total inability of neurons to migrate. The authors further demonstrated that leading process length was affected by the loss of Lis1: decreased Lis1 levels resulted in unusually lengthened leading processes, while complete loss of Lis1 lead to significantly shortened leading processes. The reported decrease in motility of Lis1 deficient migrating cells is consistent with several reports (Moon and Wynshaw-Boris, 2013; Tsai and Gleeson, 2006). Our results demonstrate that, like Lis1, a reduction in WDR47 protein levels significantly impairs neuronal migration velocity, and appears to affect leading process orientation (see SEM data below for more detail on leading process morphology).

We have demonstrated that WDR47 knock-down significantly reduces neuronal migration. An interaction between WDR47 and MAP1S, based on data presented by Wang *et al.* (2012), may contribute to the neuronal migration perturbations observed with WDR47 siRNA treatment. Over-expression of MAP1S is associated with excess formation of stable microtubules (Xie *et al.,* 2011), and excessive microtubule stability has, in turn, been shown to result in decreased neuronal migration velocity (Umeshima *et al.,* 2007). Furthermore, Kalny and Propst (2008) demonstrated that MAP1S affects cell migration: an *in vitro* wound healing assay was performed using cultured fibroblasts isolated from MAP1S knock-out mice. Compared to cells isolated from wild-type mice, MAP1S-deficient cells presented with a significantly decreased percentage of wound closure at 30 hours post scratch introduction. Additionally, MAP1S-deficient cells were reported to migrate slower than wild-type cells, taking considerably longer to heal the wound. Although the functional interactions of MAP1S with other proteins is still relatively unclear compared to other members of the MAP1 family, MAP1S is known to interact with NMDA receptor subunits (Wang *et al.,* 2012; Xie *et al.,* 2011). The main function of NMDA receptors is to regulate cellular calcium uptake, which is necessary for synapse formation (Lakatosova and Ostanikova). Interestingly, the NMDA receptors have also been reported to influence neuronal migration.

Manent *et al.,* (2005) demonstrated that treating hippocampal neuronal slices with NMDA receptor antagonists markedly decreased neuronal migration. Together, these results suggest that MAP1S may affect neuronal migration via an interaction with the NMDA receptors. An interaction between WDR47 and MAP1S may be a potential contributing factor to the decreased migration distances and velocity observed with WDR47 siRNA treatment, by affecting microtubule stability, and/or by interfering with NMDA receptor function.

Other contributing factors that may explain the aberrant migration associated with WDR47 siRNA treatment include disrupted migration direction (section 4.1.2), impaired filopodia extension and defective leading process extension (section 4.1.3), all of which may be a result of altered microtubule stability (Guerrier *et al.,* 2009; Myers *et al.,* 2006).

4.1.2 WDR47 Disrupts the Direction of Migration

To test whether WDR47 affects the direction of migration, we performed a 24 hour neuronal migration assay, manually tracking individual migrating neurons, and displaying data as rose diagrams. Compared to that of the control, Mitomycin control, and control siRNA groups, rose diagrams of WDR47 siRNA-treated neurons are characterised by a higher central plot density and data points falling in distinct quadrants, suggesting that several neurons are extending shorter processes in a less directed fashion (Figure 3.13). However, several data points do extend into the top left and bottom right quadrants, suggesting that migration direction is unaffected in a number of WDR47 siRNA-treated cells. This may be explained by the fact that, although WDR47 protein levels are significantly reduced following siRNA treatment, not all cells are affected by the knock-down. Furthermore, rose diagrams of the different groups appear overall similar, extending primarily into the top left and bottom right quadrants. A general feature of a rose diagram from any given group is that one arm is often longer than the other, suggesting that neurons on one side of the wound migrate further than neurons on the other side, likely as a result of neuronal density being greater in certain regions, or due to the angle of the pipette tip that introduced the wound creating differential injury on either side of the wound. Taken together these results suggest that WDR47 may play a role in regulating migration direction, and that this may contribute to the shorter migration distance observed, but with a degree of directionality

maintained. Thus, abnormalities in migration direction is likely not the only cause of the observed defects in neuronal migration distance and velocity.

Radially migrating projection neurons do not always follow a straight migratory path. Under normal conditions, the leading process may often undergo morphological changes as the neuron migrates through different cortical zones, transiting between a bipolar and multipolar state. Additionally, migrating neurons often temporarily pause or even reverse as they migrate past precursor neurons (Kwan *et al.,* 2012; Marín *et al.,* 2010). We observed these morphological and dynamic features: several migrating neurons temporarily altered their polarity, paused, or reversed. These features made comparing individually tracked migrating neurons a challenging task, and may explain the lack of a more pronounced effect of WDR47 siRNA treatment on migration direction. Although we do detect moderate perturbations using this method of assessing migration direction, a different approach, such as analysing growth cone turning, is recommended to confirm a potential role for WDR47 in regulating migration direction (Myers *et al.,* 2006).

Directed migration relies heavily on growth cone steering. Situated at the leading edge of a migrating cell, the growth cone dynamically explores the micro-environment to navigate the cell in the direction of migration (Geraldo and Gordon-Weeks, 2009; Mori *et al.,* 2006). Dujardin *et al.* (2003) demonstrated that both dynein and Lis1 are enriched in growth cones of migrating NIH3T3 cultured fibroblasts, and that interfering with either dynein function, by injecting cells with anti-dynein antibodies or by over-expressing dynactin, or Lis1 function, by Lis1 cDNA over-expression, impaired the forward migration of cells in a wound healing assay, as assessed with time lapse microscopy. Myers *et al.* (2006) demonstrated that siRNA knock-down of the dynein heavy chain subunit severely impaired growth cone turning in neuronal cells, and that this effect was mediated by an inability of microtubules to enter filopodia (discussed in further detail in section 4.1.3). Furthermore, dynein and Lis1 have been shown to migrate co-dependently toward the leading edge of migrating cells (Yamada *et al.,* 2008). These results suggest that dynein and Lis1 play an important role in directed migration by localizing to the growth cone of migrating cells and affecting the ability of microtubules to enter filopodia. The WD40 repeat domain of Lis1 is responsible for recruiting multiple dynein motors, thereby regulating microtubule dynamics and neuronal migration (Wang *et al.,* 2012). Like Lis1, WDR47 has a WD40 repeat domain consisting of

seven WD40 repeats (McGillewie, 2009; Wang *et al.,* 2012), suggesting that WDR47 may likely interact with dynein to affect dynein-mediated processes such as directed migration.

Our results have shown that migration direction is affected with WDR47 knockdown. Migration direction is furthermore dependent on several additional features, such as the extension and retraction of leading process filopodia (Geraldo and Gordon-Weeks, 2009) and the dynamic instability of the microtubule cytoskeleton, a feature that allows the microtubule to explore three-dimensional space to facilitate growth cone turning (Mori *et al.,* 2006; Schober *et al.,* 2007; Vega *et al.,* 2006). Drugs that suppress microtubule dynamics, such as Taxol and Nocodazole, are known to inhibit growth cone turning (Grenningloh *et al.,* 2004). The domain structure of WDR47 and the reported localization of WDR47 to microtubules *in vivo* are highly suggestive of a microtubule-regulating role of WDR47 (Wang *et al.,* 2012). Additionally, putative interactions between WDR47 and MAP1S (Wang *et al.,* 2012) and WDR47 and SCG10 (McGillewie, 2009) support a role for WDR47 in regulating microtubule stability. The observed effect of WDR47 siRNA treatment on neuronal migration direction may therefore likely be related to a role of WDR47 in regulating the dynamic instability of the microtubule network.

Given that the migration distance measurements were obtained by measuring the perpendicular distance of migrating neurons from the demarcated wound area (Figure 2.1), shorter leading processes extending in non-perpendicular directions of WDR47 siRNA-treated cells (Figure 3.12) may greatly contribute to significant effects observed in migration distance and velocity measurements.

4.1.3 WDR47 Affects Process Formation and Surface Adhesion of Migrating Neurons

SEM image data revealed that relative to control and control siRNA-treated migrating neurons, WDR47 siRNA-treated migrating neurons are defined by a shorter, thicker leading process, smoother surfaces characterised by a lack of filopodia-like extensions, poorly defined regions of surface adhesion, and a blunted, swollen leading edge (Figure 3.14 *g - i*). In contrast, control and control siRNA-treated neurons extend relatively long processes with defined regions of surface adhesion, several filopodia-like extensions, and a sharper leading edge of a comparatively smaller diameter (Figure 3.14 *a - f*).

Shorter and thicker neurites as observed in WDR47 siRNA-treated neurons may manifest due to defective microtubule regulation. Dynamic instability of microtubules is a cellular feature that enables leading process extension during neuronal migration, and is controlled by several microtubule-regulating proteins (Mori *et al.,* 2006; Schober *et al.,* 2007; Vega *et al.,* 2006). SCG10 is a microtubule-destabilizing protein that plays a key role in enhancing microtubule dynamics to enable neurite extension: Mori *et al.* (2006) used immunocytochemistry and rat hippocampal cultured neurons to demonstrate that reducing SCG10 expression by siRNA treatment inhibited neurite extension, while over-expressing SCG10 by poly-arganine protein transduction enhanced neurite extension. These results indicate that dynamic instability of the microtubule network is correlated with the length of extended neuronal processes, and that SCG10 is an important regulator of microtubule dynamics. The ability of WDR47 siRNA-treated neurons to extend a long leading process may be compromised as a result of a disturbance in dynamic instability, due to dysfunction of the microtubule-regulating protein SCG10. Our SCG10 protein analysis results support this scenario, knocking down WDR47 significantly reduces 22 kDa SCG10 protein levels (further discussed in section 4.4.4).

Our results suggest that knocking down WDR47 affects filopodia formation. Kholmanskikh *et al.* (2006) demonstrated that *Lis1+/–* mouse hippocampal neurons displayed fewer and shorter filopodia compared to wild-type neurons, indicating that Lis1 plays a role in filopodia formation. Although filopodia are extensions of the actin cytoskeleton (Guerrier *et al.,* 2009; Schaar *et al.,* 2005), microtubules play a role in regulating filopodia formation by interacting with actin filaments in the process region (Geraldo and Gordon-Weeks, 2009; Schober *et al.,* 2007). Microtubules enter filopodia by motor-based transport of short microtubules across actin and microtubule networks (Myers *et al.,* 2006) or by polymerization (Schober *et al.,* 2007). Myers *et al.* (2006) demonstrated that siRNA knock-down of dynein heavy chain in neurons from rat cervical ganglia inhibits microtubules from entering filopodia, suggesting that dynein is involved in the transport of short microtubules into filopodia. The authors also demonstrated that the inability of microtubules to enter filopodia impairs growth cone turning, thereby further supporting a role for filopodia in regulating directed migration. Based on the similarity of WDR47 and Lis1, which regulates and binds to dynein motors, WDR47 siRNA treatment may disturb dynein activity, thereby affecting the ability of short

microtubules to be transported via dynein motors into filopodia. In turn, these effects may affect growth cone turning, explaining the altered migration direction observed in WDR47 siRNA-treated cells. Alternatively, a potential microtubule regulating role of WDR47 through interaction with SCG10 or MAP1S may be a further mechanism contributing to the observed decrease in filopodia-like extensions, especially given the important role that microtubules play in regulating filopodia formation (Geraldo and Gordon-Weeks, 2009; Myers *et al.,* 2006).

Defective microtubule dynamics and filopodia formation observed with WDR47 siRNA treatment are likely contributing to the affected surface adhesion of migrating neurons. The localization of microtubules to the periphery and the entry of peripheral microtubules into filopodia are known to enable to formation of surface adhesion sites in cultured fibroblasts (Schober *et al.,* 2007).

Altered leading edge morphology of migrating neurons subjected to WDR47 siRNA treatment may be a result of impaired microtubule motor-based transport. Ahmad *et al.,* (2006) showed that inhibiting dynein activity by micro-injecting cultured neurons with P50 Dynamitin (a component of the dynactin complex that, when over-expressed, leads to dissociation of the dynactin complex, thereby interfering with dynein activity) resulted in neurons displaying blunted, swollen axonal tips. The authors concluded that this phenotypic abnormality is likely mediated by an accumulation of organelles in the distal region of axons, as a result of impaired axonal transport by dynein motors. Blunted and swollen leading edges observed with migrating neurons subjected to WDR47 siRNA treatment (Figure 3.14 *g - i*) therefore further support a potential role for WDR47 in regulating dynein motor activity, resulting in accumulation of vesicles and organelles in the leading tips. Alternatively, such accumulation could result from motor based transport being impaired as an indirect consequence of a disturbance in microtubule regulation.

Our data reveal that WDR47 knock-down manifests in impaired process formation, less defined regions of surface adhesion, and altered leading edge morphology (Figure 3.14). Wang *et al.* (2012) showed that WDR47 localizes to the cytoskeleton *in vivo,* suggesting that WDR47 may be playing a role in regulating microtubule dynamics. WDR47 may therefore be affecting microtubule regulation via direct interaction with microtubules and/or

microtubule-regulating proteins such as dynein, SCG10, and MAP1S, thereby affecting features such as leading process length, filopodia extension, and leading edge morphology. Leading process filopodia facilitate directed migration as well as surface adhesion of migrating neurons (Guerrier *et al.,* 2009; Schaar *et al.,* 2005). Decreased filopodia number may thus be contributing to the observed effects of WDR47 siRNA treatment on migration direction and/or surface adhesion. These factors likely all contribute to the overall decrease in the migration distance and velocity of WDR47 siRNA-treated migrating neurons.

4.2 WDR47 Knock-Down Increases Autophagic Flux

4.2.1 WDR47 Knock-Down Decreases LC3-II Protein Levels and LC3 Positive Punctae

Our results show that WDR47 siRNA treatment significantly reduces LC3-II protein levels compared to control and control siRNA-treated cells (Figure 3.16 *a*). In conjunction with Bafilomycin A1 treatment, which inhibits the H^+ ATPase and subsequently the fusion of autophagosomes with lysosomes, WDR47 siRNA treatment significantly increases LC3-II protein levels compared to control and control siRNA-treated cells (Figure 3.16 *b*). These data demonstrate that WDR knockdown significantly increases autophagic flux, i.e. the degradation rate of autophagosomes. Similar to LC3 protein level analysis, fluorescence microscopy reveals a decrease in LC3 positive punctae in WDR47 siRNA-treated cells compared to control and control siRNA-treated cells (Figure 3.21). These results further demonstrate that autophagic flux is increased with WDR47 siRNA treatment (Rubensztein *et al.,* 2009), suggesting that WDR47 is involved in regulating the rate of autophagosome and lysosome fusion.

4.2.2 WDR47 Affects P62 Protein Levels

We analysed P62 protein levels to further investigate the role of WDR47 in regulating autophagy and to assess whether WDR47 is able to particularly influence selective autophagy. P62 is an adaptor molecule that enables selective autophagy by targeting poly-ubiquitinated proteins toward the autolysosome for degradation through selective autophagy (Barth *et al.,* 2010).

In conjunction with Bafilomycin A1 treatment, P62 protein levels are significantly increased in the WDR47 siRNA group compared to the control group, and a non-significant trend for

increased P62 protein levels is observed compared to the control siRNA group (Figure 3.17 *b*). These results further support a role for WDR47 in regulating autophagy. However, no significant effects are observed in the absence of Bafilomycin A1 treatment (Figure 3.17 *a*), suggesting that WDR47 may be affecting macroautophagy and its machinery to a greater degree than selective autophagy, as P62 is a substrate that is itself degraded by macroautophagy. However, the response in P62 substrate level is not always immediately corresponding to changes in the overall autophagic flux (Bjørkøy *et al.,* 2009), and this demands further investigation.

4.2.3 WDR47 Co-Localizes with LC3 in the Perinuclear Region

We performed co-localization analysis of WDR47 and LC3 in an attempt to shed further light on the potential role of WDR47 in regulating autophagy. A moderate degree of co-localization is observed, particularly in the perinuclear region (Figure 3.26 – 3.27). A high degree of autophagosome and lysosome fusion occurs in the perinuclear region, as lysosomes are clustered near the centrosome (Katsumata *et al.,* 2010; Xie *et al.,* 2011). The CTLH domain of WDR47 shows sequence homology with RanBPM (Ran-binding protein in the microtubule-organizing centre), a protein reported to associate with the centrosome in mammalian cells (Kinnear, 2007; Tomaštíková *et al.,* 2012). These results may therefore suggest that WDR47 is potentially specifically involved in the autophagosome and lysosome fusion step of autophagy, which occurs predominantly in the perinuclear region. Another possibility is that, instead of directly interacting with LC3, WDR47 is affecting autophagy by interacting with autophagy-regulating proteins such as MAP1S and/or dynein motors (Wang *et al.,* 2012).

4.2.4 Potential Mechanisms to Explain how WDR47 Affects Autophagy

Our results indicate a profound effect of increased autophagic flux with WDR47 siRNA treatment. One explanation for the observed increase in autophagic flux may be altered microtubule stability associated with knocking down WDR47. Xie *et al.* (2010) demonstrated that interfering with microtubule stability by treating GFP-LC3-expressing HeLa cells with either the microtubule stabilizing drug paclitaxel or the destabilizing drug nocodazole impaired the conversion of LC3-I to LC3-II, without affecting autophagosome degradation. The authors reported that paclitaxel treatment, but not nocodazole treatment, caused an

increase GFP-LC3 positive punctae in mitotic cells, suggesting accumulation of LC3-II when microtubule stability is enhanced. Furthermore, immune-blot analysis revealed increased levels of LC3-I in both mitotic and interphase cells when treated with either paclitaxel or nocodazole, though LC3-II levels were unaffected, demonstrating that the effect of altered microtubule stability on autophagic markers LC3-I and –II is dependent on the cell cycle. Furthermore, Webb *et al.* (2004) reported that treating COS-7 cells with nocodazole interfered with autophagosome and lysosome fusion. The authors used immunofluorescence to demonstrate that nocodazole treatment resulted in accumulation of LC3-II. Furthermore, the authors performed Western blot analysis to demonstrate that nocodazole significantly decreased the expression of A53T synuclein, a protein known to be degraded by autophagy. Overall, the results from these studies demonstrate the effect that altered microtubule stability has on autophagy. The domain architecture of WDR47 (Kinnear, 2007), the putative interaction of WDR47 with MAP1S (Wang *et al.,* 2012) and of WDR47 with SCG10 (McGillewie, 2009), and the reported *in vivo* localization of WDR47 with the cytoskeleton (Wang *et al.,* 2012) all point toward a microtubule-regulating role of WDR47. The increased autophagic activity associated with WDR47 siRNA treatment may therefore be related to defective microtubule regulation.

Alternatively, a likely interaction between WDR47 and MAP1S (Wang *et al.,* 2012) may be responsible for the increased autophagic flux observed with WDR47 siRNA treatment. Xie *et al* (2011) showed that MAP1S regulates both basal autophagy and nutritive stress-induced autophagy, and that MAP1S binds to and recruits LC3-II-bound autophagosomes to microtubules. Western blot analysis revealed that knocking out MAP1S in mice reduced the autophagy markers Bcl-2, Bcl-xL, and P27 in brain, heart, and liver under basal conditions, and that subjecting these mice to nutritive stress lead to LC3-II accumulation, suggesting that MAP1S plays a role in autophagosome and lysosome fusion under nutritive stress-induced autophagy. Additionally, the authors used cultured HeLa cells and co-immunoprecipitation to demonstrate that MAP1S isoforms interact with LC3-I and LC3-II. Wang *et al* (2012) demonstrated that co-expression of WDR47 with the LC isoform of MAP1S leads to the localization of WDR47 along the microtubule cytoskeleton, and further showed by affinity pull-down analysis that the WD40 repeat domain of WDR47 interacts with the N-terminal of MAP1S. These results indicate that an interaction with MAP1S is a

potential mechanism to explain the increased autophagic flux observed with WDR47 siRNA treatment. However, this deserves further investigation.

Given the remarkably similar domain architecture of WDR47 and Lis1, which binds to and regulates dynein motor activity (McGillewie, 2009; Wang *et al.,* 2012), WDR47 may regulate autophagic flux by interacting with dynein motors. Kimura *et al.* (2008) made use of time lapse fluorescent microscopy and HeLa cells to show that autophagosomes tagged with GFP-LC3 move predominantly toward the centrosome, where lysosomes are gathered, in a dynein-dependent manner. The authors reduced dynein activity by microinjecting HeLa cells with anti-dynein antibodies or by over-expressing dynamitin, a component of the dynein-dynactin complex. Both interventions successfully interfered with dynein activity and significantly reduced autophagosome transport. Similarly, Katsumata *et al.* (2010) used cerebellar granule cells and time-lapse imaging of GFP-LC3 to confirm that autophagosomes move primarily toward the centrosome, and that dynein inhibition largely impairs the retrograde transport of autophagosomes. Additionally, Yamamoto *et al.* (2010) showed that chemical inhibition of dynein with Erythro-9-[3-(2-hydroxynonyl)] adenine in human glioma cells stably expressing GFP-LC3 markedly increased autophagosome number, while interfering with dynein function by over-expressing dynamitin inhibited the formation of autophagosomes. The authors suggest that different forms of dynein inhibition affect autophagy in distinct ways, and that the interaction of dynein and dynamitin is essential for autophagosome formation. In summary, dynein is emerging as a key role-player in regulating autophagic flux, and it is therefore conceivable that altered dynein motor activity may contribute to the observed increase in autophagic flux of WDR47 siRNA-treated cells.

Several likely interactions of WDR47 with autophagy- and microtubule-regulating components may therefore explain the observed increase in autophagic flux associated with WDR47 siRNA treatment. Further investigation is required in order to elucidate the precise mechanism by which WDR47 affects autophagic activity.

4.3 WDR47 Affects ER and Nuclear Envelope Ultra-Structure

TEM analysis of neuronal ultra-structure shed further insight on likely roles of WDR47 in regulating processes such as neuronal migration and autophagy. Relative to control and control siRNA-treated cells, WDR47 siRNA-treated cells are characterised by more abundant

membrane structures (Figure 3.15: first column), an increased prominence of ER structures (Figure 3.15: second column), and an expanded nuclear envelope characterized by a greater distance between the inner and outer nuclear membrane (Figure 3.15: third column). These morphological features may be explained by several possible scenarios.

Increased autophagic flux associated with WDR47 siRNA treatment may be linked to the ER ultra-structural aberrations observed with WDR47 siRNA treatment. We observed an increase in ER membrane structures, manifesting in a robust and prominent ER network morphology in WDR47 siRNA-treated cells. The ER is a continuous sheet of membranes that folds and packages proteins that enter the secretory pathway (Schuck *et al.,* 2009), and is a major site of autophagosome generation (Bartolomeo *et al.,* 2010; Loos *et al.,* 2013; Yu, 2014). The abundance of the ER is regulated to maintain ER homeostasis in response to cellular requirements. The volume of the ER is increased when unfolded proteins accumulate, a result of ER folding demand surpassing ER folding capacity (Bernales *et al.,* 2006). ER homeostasis is mainly achieved by a highly conserved cascade that is activated upon accumulation of unfolded proteins, called the unfolded protein response (Bernales *et al.,* 2006; Schuck *et al.,* 2009). Bernales *et al.* (2006) demonstrated that an extensive expansion of the ER occurs when cells are treated with dithiothretol to induce the unfolded protein response. The substantial increase in the amount of cytoplasmic membrane structures observed with WDR47 siRNA treatment may point toward an inability of the ER folding capacity to meet the substrate demand, so as to control the amount of cytoplasmic constituents, thus leading to a compensatory action whereby the ER expands. The expanded ER may allow the cell to achieve higher rates of autophagosome formation and fusion in an attempt to maintain homeostasis. On the contrary, up-regulated autophagy as a result of WDR47 siRNA treatment may be the cause of the observed expanded ER structures, as a compensatory mechanism whereby the cell is attempting to provide sufficient isolation membranes to meet an increased demand for protein degradation through autophagy.

The expanded nuclear envelope observed with WDR47 siRNA treatment may be structurally linked to the increased ER prominence. The outer membrane of the nuclear envelope is the site of origin of the perinuclear ER, which is continuous with the peripheral ER that extends into the cytoplasm (Schuck *et al.,* 2009). Alternatively, the expanded nuclear envelope observed with WDR47 siRNA treatment may be a result of defective microtubule regulation.

110

The microtubule cage that surrounds the nucleus of the migrating neuron is tightly associated with the nuclear envelope (Schaar and McConnel, 2005; Tsai and Gleeson, 2005). The microtubule cytoskeleton plays a critical role in nuclear movement, achieved by multiple protein complexes that link the outer nuclear membrane to the microtubule. These complexes consist of Lis1 and NudE homologues, dynein and motors, as well as several identified (e.g. UNC-83, UNC-84, Sad1, and ANC-1) and potentially unidentified proteins (Fridolfsson *et al.,* 2010). Dynein motors generate a pulling force to allow centrosome positioning and nuclear movement within the cell (Fridolfsson *et al.,* 2010; Tsai and Gleeson, 2005). Given that the domain structure of WDR47 is suggestive of a microtubule-regulating role as an adaptor protein capable of forming multiple protein complexes, our results suggest that WDR47 may be a component of the protein complex that couples the outer nuclear envelope to the microtubule cytoskeleton. WDR47 siRNA treatment may result in an expanded nuclear envelope due to defective coupling of the nucleus to the microtubule cytoskeleton. The aberrant neuronal migration observed with WDR47 siRNA treatment may therefore be further influenced by defective nucleokinesis as a result of an interaction between WDR47 and dynein.

4.4 The Effect of WDR47 on Microtubule Dynamics

4.4.1 WDR47Kcock-Down Affects Acetylated Tubulin Distribution and Protein Levels

We assessed acetylated tubulin networks through immune-fluorescence and Western blot analysis to determine whether WDR47 may play a role in regulating microtubule dynamics, as acetylated tubulin is indicative of increased tubulin stability (Al-Bassam and Corbett, 2012; Tökèsi *et al.,* 2010). A pronounced increase in fluorescence intensity of cells stained for acetylated tubulin through immuno-fluorescence is observed in the perinuclear region of cells treated with WDR47 siRNA compared to control and control siRNA-treated cells (Figure 3.21 -3.25). A non-significant trend is observed for increased acetylated tubulin protein levels, as detected by Western blot analysis, with WDR47 siRNA treatment (Figure 3.19 *b*). These results support a role for WDR47 in tubulin stability regulation by impacting microtubule dynamics.

Similar to the observed effect of WDR47 siRNA treatment on tubulin localization to the perinuclear region, Sasaki *et al.* (2000) used immuno-staining and fluorescence microscopy

to demonstrate that knocking down Lis1 in COS-7 cells lead to accumulation of β-tubulin and dynein heavy chain subunits in the perinuclear region. These results indicate that Lis1 plays a role in regulating the distribution of dynein and tubulin throughout the cell. It has been well-documented that Lis1 regulates dynein activity (Moon and Wynshaw-Boris, 2013; Manent and LoTurco; 2012), and that dynein motors regulate the movement of tubulin units and short transportable microtubules (Myers *et al.,* 2006; Yamada *et al.,* 2008). The increased perinuclear localization of tubulin as observed in this study may therefore be a result of dysfunctional dynein motor activity due to the absence of Lis1. Interestingly, dynein depletion has been reported to result in a similar accumulation of microtubules near the centrosome in cultured neurons, indicating a compromised ability of microtubules to extend into axonal processes (Ahmad *et al.,* 2006). The similarity in functional domain architecture between Lis1 and WDR47, as well as the observed similar effect of WDR47 on tubulin distribution, support the notion that WDR47 and Lis1 may play similar roles in neurodevelopment by binding to dynein motors to regulate microtubule dynamics.

The observed increase in fluorescence signal of acetylated microtubules with WDR47 siRNA-treatment cells may further support a role for WDR47 in regulating microtubule stability, a feature that is crucial to microtubule-dependent processes such as neuronal migration (Ayala *et al.,* 2007; Heng *et al.,* 2009). An interaction between WDR47 and SCG10 (McGillewie, 2009) and/or between WDR47 and MAP1S (Wang *et al.,* 2012) support this scenario, as SCG10 plays a crucial role in enhancing dynamic instability to enable microtubule remodelling (Alves *et al.,* 2010; Bondallaz *et al.,* 2006) and as accumulation of MAP1S leads to excessive stabilization of the microtubule cytoskeleton (Xie *et al.,* 2011).

4.4.2 WDR47 Affects Acetylated Tubulin Network Structure

Perinuclear acetylated tubulin networks are highly convoluted in WDR47 siRNA group cells compared to control and control siRNA group cells (Figure 3.21 -3.25), indicating that WDR47 affects tubulin dynamics and network structure. Several possible mechanisms of action exist for this observed feature.

Microtubule convoluting, referred to in literature descriptively as bending, buckling, bundling, or looping, are common features of microtubules in living cells, although the relevance of and mechanisms behind such features are largely unclear. A number of

mechanisms have been proposed to be responsible for such microtubule dynamics, including microtubule polymerization against an immobile end and the formation of crosslinks between microtubules via interactions with motor proteins such as dynein. Microtubule polymerization against a stationary, anchored end is thought to be largely responsible for generating the forces responsible for microtubule bending and buckling (Bicek *et al.* 2009). A stationary end may be achieved by microtubule crosslinking (Bicek *et al.* 2009; Hawkins *et al.,* 2010), or by centrosome anchoring (Mètin *et al.,* 2008), while microtubule polymerization is linked to dynein motor activity: dynein motors move from their site of synthesis to the plus-end of the microtubule, where short, transportable microtubule fragments are loaded onto dynein, after which the motors transport these microtubule fragments toward the minus-end of the cell (Yamada *et al.,* 2008). Dynein also plays a role in generating intracellular forces responsible for centrosome displacement, thereby affecting the ability of the centrosome to anchor microtubules (Vallee and Tsai, 2006). Several reports have demonstrated the involvement of dynein in microtubule dynamics: Brito *et al.* (2005) demonstrated that over-expression of dynein in *Dictyostelium* results in microtubule bending and buckling. In contrast, Malikov *et al.,* (2004) reported dynein regulates the organization of microtubule bundles into radial arrays by nucleating microtubules, similar to centrosomal microtubule nucleation. Additionally, Ahmad *et al.* (2006) demonstrated that siRNA knock-down of dynein heavy chain subunits in cultured neurons results in abnormally twisted and looped axonal microtubules, indicative of an inability of microtubules to align into radial arrays. Dynein therefore appears to play a critical role in microtubule dynamics, but the exact mechanisms by which dynein affects such features are not yet confirmed (Bicek *et al.,* 2009). Based on the similar domain architechture of WDR47 and Lis1, WDR47 may possibly affect dynein motor activity, which may affect both centrosome mobility and microtubule polymerization. Alternatively, WDR47 may directly impact centrosome anchoring and mobility via its CTLH domain, based on the finding that the CTLH domain likely plays a role at the centrosome (Wang *et al.,* 2012; Tomaštíková *et al.,* 2012). The observed microtubule convoluting in the perinuclear region described in our study may therefore be a result of dynein-mediated microtubule polymerization against a stationary centrosome.

By using an *in vitro* dynein motility assay, Yamada *et al.* (2008) demonstrated that antibody-mediated inhibition of Lis1 in cultured neurons impairs the minus-end-directed motor activity of dynein. The authors further demonstrated with imaging analysis that Lis1, dynein, and microtubules form a complex that is transported toward the growing tip of the microtubule. These findings indicate that Lis1 regulates the transport of short microtubules by dynein motors across microtubule tracks toward the dynamic plus end, where polymerization most frequently occurs (Conde and Cáceres, 2009). The similarity in domain architecture of WDR47 and Lis1 presents the likelihood that WDR47 may play a similar role in binding to dynein subunits to facilitate microtubule polymerization at the growing plus end. WDR47 siRNA treatment may result in impaired dynein function, resulting in an inability of dynein to transport short microtubules between the minus-end and the plus-end of the microtubule, with subsequent accumulation of microtubules in the perinuclear region. Such accumulation may result in microtubule polymerization, which may cause the highly convoluted microtubule structures observed in WDR47 siRNA-treated neurons. Alternatively, WDR47 may interact with microtubule-regulating proteins such as MAP1S (Wang e*t al.,* 2012) and/or SCG10 (McGillewie, 2009), thereby regulating microtubule stabilization and polymerization. WDR47 siRNA treatment may disrupt the dynamic instability of the microtubule system, leading to excessive polymerization and subsequent convoluting of microtubules in the perinuclear region. However, the potential link between WDR47 and microtubule-regulating proteins as well as the mechanism by which WDR47 affects such microtubule dynamics remains to be further elucidated.

4.4.3 WDR47 Co-localizes with Acetylated Tubulin

WDR47 and acetylated tubulin co-localizes, both in the perinuclear region and in extended processes (Figure 3.18 – 3.29). Wang *et al.* (2012) used immune-gold electron microscopy to demonstrate that WDR47 localised to the microtubule cytoskeleton *in vivo* in the axons, dendrites, and cell bodies of cortical neurons. The authors demonstrated that co-expression of WDR47 with the LC isoform of MAP1S in COS-7 cells lead to localization of WDR47 along the microtubule cytoskeleton, suggesting that MAP1S is an important mediator of the cytoskeletal localization of WDR47. Our results, in the context of the published data, strengthen the possibility of a role for WDR47 in interacting with the microtubule cytoskeleton. To our knowledge, our results are the first data indicating that WDR47 co-

localizes with specifically acetylated tubulin, suggesting a potential role for WDR47 in regulating microtubule stability.

4.4.4 WDR47 Affects the Relative Expression of the Microtubule-Destabilizing Protein SCG10

SCG10 is a crucial microtubule-destabilizing protein that has recently been identified as a putative binding partner of WDR47 (McGillewie, 2009). We therefore used Western blot analysis to assess whether knocking down WDR47 affects SCG10 protein levels. Our results show four bands in the molecular weight region of SCG10, with major bands detected at 22kDa and 25 kDa. This data is consistent with other reports (Bondallaz *et al.,* 2006; Westerlund *et al.,* 2011). A significant reduction in SCG10 protein levels at the 22 kDa band is observed with WDR47 siRNA treatment. Additionally, compared to the control and control siRNA groups, WDR47 siRNA-treated cells display a non-significant trend for increased SCG10 protein levels at the 25 kDa band ((Figure 3.18).

By binding to and sequestering tubulin dimers from the microtubule, SCG10 enhances microtubule dynamics and facilitates neurite outgrowth in undifferentiated neurons (Alves *et al.,* 2010; Bondallaz *et al.,* 2006; Vega *et al.,* 2006). The observed shift from a lower to a higher molecular weight is due to the phosphorylation of SCG10, and such phosphorylation decreases the microtubule destabilising activity of SCG10 (Grenningloh *et al.,* 2004; Vega *et al.,* 2006). These results therefore suggest that WDR47 siRNA treatment is culminating in a higher degree of SCG10 phosphorylation. Hence, WDR47 may play a role in regulating the phosphorylation state of SCG10, thereby affecting microtubule stability. These results may further explain the observed effects of WDR47 on acetylated tubulin networks.

Vega *et al.* (2006) demonstrated that total SCG10 protein levels are markedly decreased following either over-expression of Tau protein in COS-7 cells or treatment with Taxol, both of which result in excessive microtubule stabilization. The decrease in SCG10 protein levels was shown to be a result of increased Calpain-dependent degradation of SCG10. These results demonstrate that, in addition to phosphorylation, SCG10 activity is regulated by microtubule stabilization. The authors further propose that hyper-phosphorylated forms of SCG10, represented by high molecular weight species, may precede SCG10 degradation. WDR47 siRNA treatment appears to shift SCG10 protein levels from the lower molecular

weight species to high molecular weight species, indicating that the knock-down of WDR47 results in a higher degree of SCG10 phosphorylation. In light of the immuno-fluorescence and Western blot data summarized above, WDR47 siRNA treatment may result in excessive microtubule stabilization, leading to SCG10 phosphorylation.

An interaction between WDR47 and SCG10 (McGillewie, 2009) may contribute to the observed decreased neuronal migration of WDR47 siRNA-treated neurons: Westerlund *et al.* (2011) recently demonstrated that SCG10 plays a role in regulating neuronal migration. The authors transfected mouse cerebellar granule neurons with short hairpin RNA (sh-RNA) to knock down SCG10, and neuronal migration was assessed using Transwells. The authors first demonstrated that the knock-down of SCG10 increased neuronal migration rate in cultured neurons. The authors then electroporated mouse embryos at embryonic day 15 with SCG10 sh-RNA, and demonstrated that the knock-down of SCG10 similarly increased neuronal migration rate *in vivo*. As SCG10 facilitates dynamic instability by destabilising microtubules (Alves *et al.,* 2010; Bondallaz *et al.,* 2006), decreasing SCG10 levels likely resulted in excessive microtubule stabilisation, thereby increasing neuronal migration rate. An interaction between WDR47 and SCG10 may affect neuronal migration by regulating the microtubule-stabilizing activity of SCG10.

4.4.5 WDR47 Does Not Significantly Affect the Relative Expression of Tau Protein

Tau is a MAP of particular relevance to neuronal migration studies, as it facilitates neuronal process extension by recruiting tubulin dimers to the microtubule cytoskeleton (Lakatosova and Ostatnikova, 2012; Poulain and Sobel, 2010). Relative expression of Tau protein is not significantly affected by WDR47 siRNA treatment (Figure 3.19 *b*). These results indicate that the effects of WDR47 on neuronal migration, autophagic flux, and microtubule dynamics are not mediated by alterations in total Tau protein.

Taken together with the reported *in vivo* localization of WDR47 to the cytoskeleton when co-expressed with MAP1S (Wang *et al.,* 2012) and the putative interaction between WDR47 and SCG10 (McGillewie, 2009), our results strongly suggest a role for WDR47 in regulating microtubule stability in this in vitro model of neuronal migration. A likely role for WDR47 in regulating microtubule stability may greatly contribute to the observed defects in neuronal migration and increased autophagic flux associated with WDR47 siRNA treatment. These

effects may be further mediated by proteins that affect microtubule dynamics, autophagy, and/or neuronal migration, such as MAP1S and Dynein.

4.5 Possible Interactions Mediating the Role of WDR47

4.5.1 Dynein: A Common Regulator of Microtubule Dynamics, Neuronal Migration, and Autophagy

Dynein is not only the main minus-end-directed microtubule motor, but is also involved in several features of neuronal migration, autophagy, and microtubule dynamics. Nuclear displacement during neuronal migration requires a force generated by dynein motors, Lis1, and microtubules (Schaar and McConnel, 2005; Tsai and Gleeson, 2005). Specifically, a dynein-Lis1 complex is believed to generate a pulling force that acts on the perinuclear microtubules and NE to enable forward translocation of the nucleus during migration (Mètin *et al.,* 2008; Tsai and Gleeson, 2005), thus nuclear envelope morphological alterations, as observed with this study, may likely result from altered dynein activity. Dynein is involved in filopodia extension by facilitating the transport of short microtubules into filopodia (Myers *et al.,* 2006), which, in turn, play a crucial role in enabling surface adhesion of neuronal processes (Schober *et al.,* 2007) as well as directed migration (Geraldo and Gordon-Weeks, 2009). Directed migration, achieved by growth cone steering, is also directly affected by dynein activity (Dujardin *et al.,* 2003; Myers *et al.,* 2006). Our results reveal that knocking down WDR47 leads to a significant decrease in neuronal migration, as well as alterations in migration direction, filopodia formation, and surface adhesion. Dynein enables the relocation of organelles and cytosolic contents from the growing tip of the neuronal process back to the cell body, and interference with dynein function leads to swollen, blunt leading edges (Ahmad *et al.,* 2006), as observed in our study. Additionally, dynein motors are involved in transporting autophagosomes across the microtubule cytoskeleton, thus regulating autophagic flux (Katsumata *et al.,* 2010; Yamamoto *et al.,* 2010). Our results indicate that knocking down WDR47 leads to increased autophagic flux. Lastly, dynein is involved in microtubule polymerization and dynamics by transporting short microtubules throughout the cell (Ahmad *et al.,* 2006; Myers *et al.,* 2006). Our results suggest that knocking down WDR47 affects microtubule dynamics. Given that WDR47 and Lis1 both have a LisH domain at the N-terminal and seven WD40 repeats at the C-terminal, and that the

seven WD40 repeats of Lis1 recruit and assemble multiple dynein complexes (Kinnear, 2007; McGillewie, 2009; Wang *et al.,* 2012), it is conceivable that WDR47 regulates dynein activity. Additionally, cells deficient in Lis1 are characterised by increased localization of microtubules to the perinuclear region along with decreased localization to the leading process (Sasaki *et al.,* 2000), reduced migration velocity, and fewer leading process filopodia (Moon and Wynshaw-Boris, 2013), a phenotype very similar to that which we observed in cells treated with WDR47 siRNA, thus strongly suggesting that WDR47 and Lis1 both regulate dynein. Many of the observed effects of WDR47 siRNA treatment may be explained by a model in which WDR47 affects dynein activity: An interaction between dynein and WDR47 would explain the effect of WDR47 siRNA treatment on neuronal migration and migration direction, filopodia formation, surface adhesion, and leading edge morphology of migrating neurons, autophagic flux, nuclear envelope expansion, and altered microtubule dynamics. One possibility is that WDR47 may bind to dynein in order to facilitate the association of dynein with microtubules, thus affecting the ability of dynein to regulate processes such as neuronal migration and autophagy (Figure 4.1). The possible interaction between WDR47 and dynein and the mechanisms discussed here deserve further investigation.

4.5.2 MAP1S: A Common Regulator of Microtubule Stability and Autophagy

The function of MAP1S in the context of microtubule-dependent processes is relatively less understood than that of other members of the MAP1 family. However, MAP1S has been reported to affect autophagy by binding to and recruiting autophagosome-associated LC3-I and -II to microtubules. MAP1S knock-out mice display dysfunction in nutritive stress-induced autophagy as well as basal autophagy (Xie *et al.,* 2011). Furthermore, MAP1S may play a role in neuronal migration, as it has been shown to affect fibroblast migration (Kalny and Propst, 2008) and to interact with the NMDA receptor (Wang *et al.,* 2012; Xie *et al.,* 2011), which regulates neuronal migration and leading process extension (Manent *et al.,* 2005). However, whether MAP1S is involved in regulating neuronal migration has not yet been fully investigated. Additionally, overexpression of MAP1S results in excessively stable microtubules (Wang *et al.,* 2012; Xie *et al.,* 2011).

A novel interaction between WDR47 (termed nemitin by the authors) and MAP1S has been shown to enable localization of WDR47 to the microtubule cytoskeleton (Wang *et al.,* 2012). An interaction between WDR47 and MAP1S may therefore contribute to the increased autophagic flux observed in our study, the altered microtubule dynamics, and possibly also the neuronal migration defects associated with WDR47 siRNA treatment. An interaction between WDR47 and MAP1S may potentially be essential for the autophagosome-recruiting function of MAP1S, the MAP1S-NMDA receptor interaction, or the microtubule-stability regulating role of MAP1S, thereby affecting both autophagy and migration.

4.5.6 Multiple Interaction Partners May Mediate the Role of WDR47 in Neurodevelopment

How can the role of WDR47 be understood in the context of recently identified putative interacting partners? Our results suggest that WDR47 is involved in regulating directed neuronal migration, autophagic flux, and microtubule dynamics. It is possible that WDR47 may interact simultaneously with dynein and MAP1S, both of which may affect microtubule dynamics and thereby neuronal migration, and both of which have been shown to interact with autophagosomes. In the context of autophagy, MAP1S may recruit autophagosomes to the microtubule cytoskeleton, and WDR47 may serve as an adaptor protein to allow MAP1S-bound autophagosomes to bind to dynein for transport to lysosomes. The CTLH domain of WDR47 suggests that WDR47 associates with the centrosome (Kinnear, 2007; Tomaštíková *et al.,* 2012), a region where a high rate of autophagosome and lysosome fusion occurs (Katsumata *et al.,* 2010; Xie *et al.,* 2011). WDR47 may be recruiting MAP1S-autophagosome complexes to the acetylated microtubules in the centrosomal region, thereby regulating autophagosome and lysosome fusion. Another possibility is that WDR47 may be facilitating the interaction of dynein with microtubules, thus affecting microtubule-dependent processes. WDR47 could also be interacting with MAP1S to either affect its microtubule stability-regulating role or its interaction with the NMDA receptor, thereby affecting microtubule dynamics or migration, both of which we have observed in the present study. Additionally, WDR47 may be recruiting SCG10 to microtubules to modulate microtubule stability (McGillewie, 2009), thereby affecting both neuronal migration and autophagy (Figure 4.2). A combination of these molecular mechanisms may also explain the effects of WDR47 siRNA treatment on neuronal migration, autophagic flux, and microtubule dynamics. Lastly, the significance of an interaction between WDR47 and Reelin (Kinnear, 2007) may

now be revealed even further, as Reelin becomes internalised for lysosomal degradation upon completion of its function of activating the Reelin cascade (Lakatosova and Ostatnikova, 2012). WDR47 may recruit Reelin to autophagosomes, thus facilitating lysosomal degradation (Figure 4.1). As Reelin exerts its function of regulating neuronal migration by binding to extracellular receptors, and as the relevance of Reelin internalization is currently believed to be related to its intracellular degradation (Folsom and Fatemi, 2013; Lakatosova and Ostatnikova, 2012), a scenario whereby WDR47 interacts with Reelin to enable lysosomal degradation seems most reasonable. The context of Reelin in relation to autophagic flux requires further investigation.
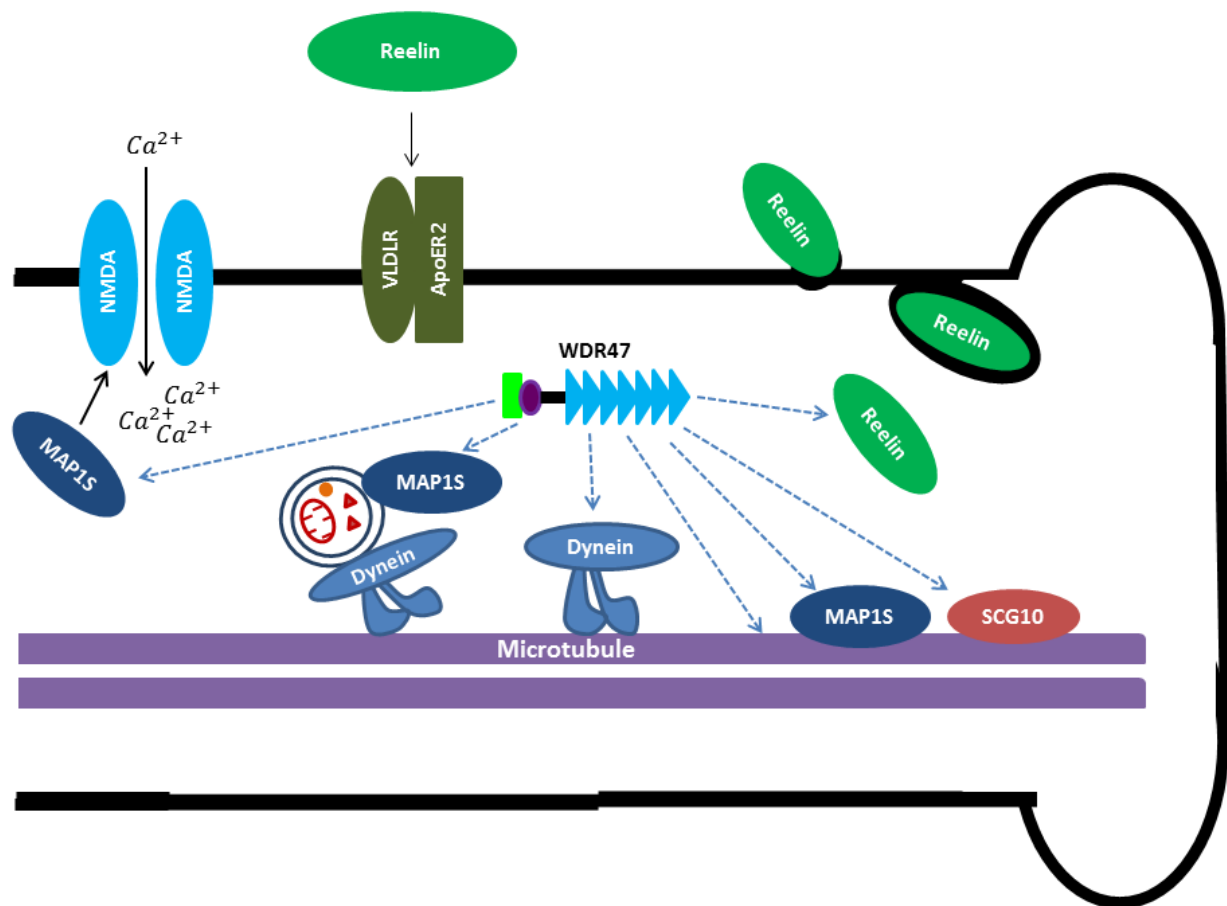
Figure 4.1: Protein interactions that may mediate the effect of WDR47 on neuronal migration, autophagy, and microtubule dynamics. From left to right: WDR47 may regulate MAP1S interaction with NMDA receptor subunits, which facilitates neuronal migration. WDR47 may recruit MAP1S-autophagosome complexes to the microtubules, possibly to enable dynein-autophagosome complex formation, thereby enabling autophagic flux. WDR47 may be interacting with and regulating dynein motors, thereby affecting neuronal migration,

autophagic flux, and microtubule polymerization. WDR47 may recruit MAP1S and/or SCG10 to the microtubules, thereby regulating microtubule stability and microtubule-dependent processes. Lastly, the putative interaction between WDR47 and Reelin may be explained by internalized Reelin being recruited by WDR47 for lysosomal degradation.

4.6 Conclusion

Neuronal migration and autophagy are both important processes for neurodevelopment (Kwan *et al.,* 2012; Ban *et al.,* 3013), and a number of neurological disorders have been attributed to defects in WD40 repeat proteins that regulate these processes. Humans deficient in Lis1, a WD40 repeat protein that is crucial to neuronal migration, suffer from the severe brain malformation disorder lissencephaly (Manent and LoTurco; 2012; Moon and Wynshaw-Boris, 2013), while humans deficient in WDR45, a WD40 repeat family that has recently emerged as a key autophagy-regulating protein, suffer from static encephalopathy of childhood with neurodegeneration in adulthood (SENDA) (Ozawa *et al.,*2014; Saitsu *et al.,* 2013). Problems such as whether the regulations of migration and autophagy overlap and whether/how these processes influence one another remain unanswered. Although it is evident that both neuronal migration and autophagy are microtubule dependent processes linked by common microtubule-regulating proteins such as MAP1S and dynein, and that dysfunctional microtubule regulation may affect both neuronal migration and autophagy, the role of WDR47 in this context remains unclear (Kimura *et al.,* 2008; Manent and LoTurco; 2012; Xie *et al.,* 2011). Our results indicate that WDR47 regulates directed neuronal migration, along with surface morphological features such as filopodia formation and surface adhesion of migrating neurons. Such surface morphological features are likely contributing to the role of WDR47 in regulating neuronal migration. Furthermore we provide evidence that WDR47 affects autophagic flux as well as neuronal ultra-structure. Ultra-structural effects, such as increased abundance of cytoplasmic membrane structures and an increased ER prominence, support a role for WDR47 in regulating autophagic flux. Lastly, our results show that WDR47 co-localizes with acetylated tubulin and that WDR47 affects microtubule dynamics, acetylated tubulin protein levels and the relative expression of the microtubule-destabilising protein SCG10. This microtubule-regulating role of WDR47 may contribute to the effects of WDR47 on directed neuronal migration, filopodia

formation, surface adhesion of migrating neurons, and autophagic flux. Furthermore, it is highly likely that interactions between WDR47 and SCG10, dynein, and/or MAP1S may contribute to these profound effects (Figure 4.2). In conclusion, the results presented here suggest that WDR47 is involved in regulating directed neuronal migration, neuronal process formation and surface adhesion, autophagic flux, ER prominence, nuclear envelope expansion, microtubule networking dynamics, and SCG10 protein levels. We therefore provide insight into functions of WDR47 in neurodevelopment, contributing to the extensive, growing body of research aimed at understanding the numerous different genes and proteins that regulate brain formation.
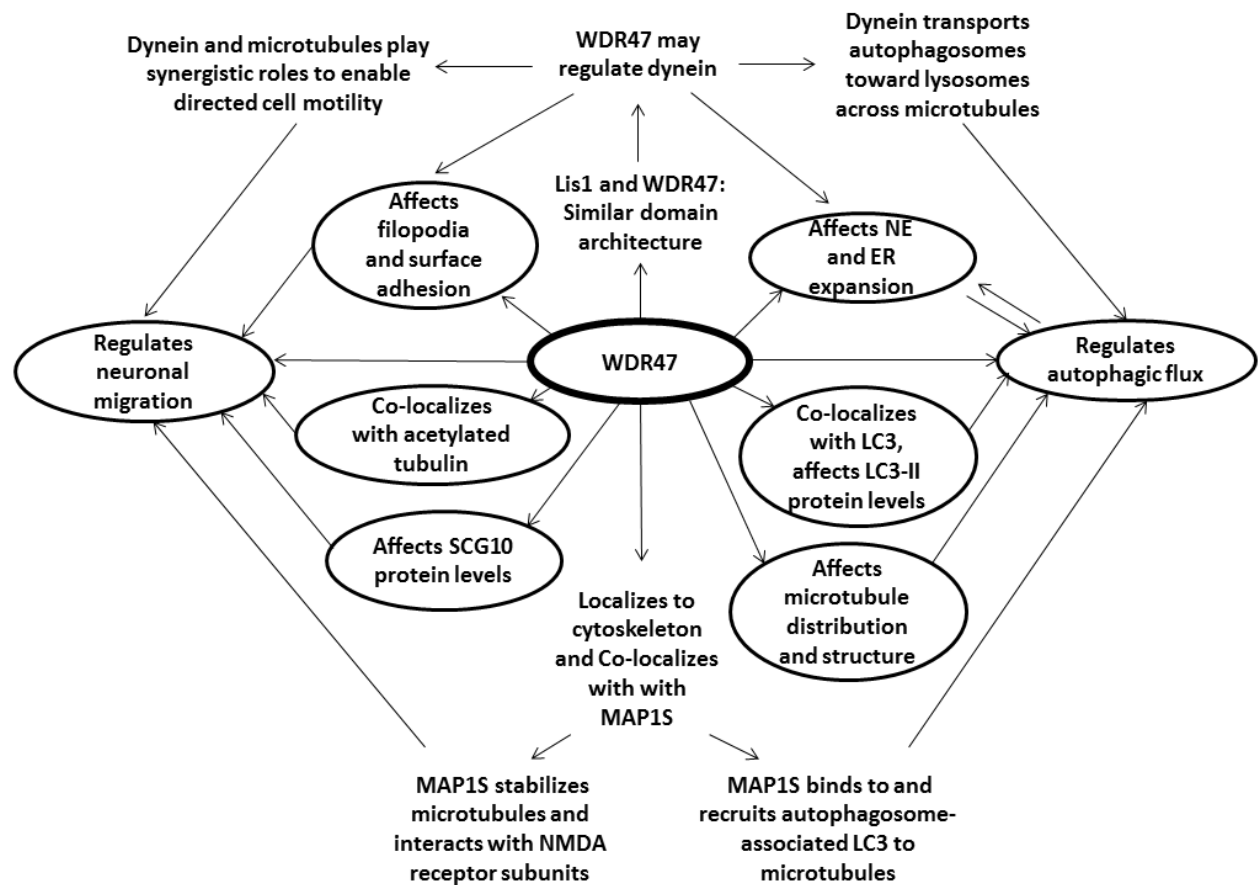
Figure 4.2: Integration of the results obtained from this study (in circles) with key literary observations. WDR47 affects filopodia formation and surface adhesion of migrating neurons, co-localizes with acetylated tubulin, and affects SSCG10 protein levels, all of which may contribute to the observed effects of WDR47 on neuronal migration. We have also shown the WDR47 affects ER volume, colocalizes with LC3, affects LC3-II protein levels, and affects microtubule distribution and structure, all of which may contribute to the observed effect of WDR47 on autophagic flux. Furthermore, literary sources suggest that WDR47 regulates MAP1S and likely interacts with dynein, both of which may affect neuronal migration, autophagy, and/or microtubule dynamics.

4.7 Future Recommendations

In light of our findings, an *in vivo* model investigating the effects of WDR47 on behaviour and brain structure may be of great interest, as it may reveal neurodevelopmental perturbations, or may be linked to specific neurological diseases. Such a model is essential in order to confirm a regulatory role of WDR47 in microtubule-dependent processes such as neuronal migration and autophagy. An approach whereby neuronal migration is assessed using embryonic cortical slices may provide imperative insight. Further molecular studies are required to determine the mechanisms behind the perturbed neuronal migration, increased autophagic flux, and altered microtubule dynamics observed with WDR47 siRNA treatment. Additionally, it would be useful to determine the role of WDR47 in starvation-induced autophagy.

It may be of great interest to determine whether WDR47 is able to interact with or regulate dynein, as such an effect may explain many of the observed effects of WDR47 siRNA treatment on neuronal cells. Further investigation of the interactions between WDR47 and MAP1S, as well as between WDR47 and SCG10 may provide useful insight into potential mechanisms of WDR47 in regulating microtubule-dependent processes.

In light of our results, it may be useful to investigate whether WDR47 is able to influence kinases responsible for SCG10 phosphorylation, such as JNK-1 and MAPK, thereby regulating the microtubule stabilizing activity of SCG10.

References

Ahmad FJ, He Y, Myers KA, Hasaka TP, Francis F, Black MM *et al*. Effects of Dynactin Disruption and Dynein Depletion on Axonal Microtubules. Traffic. 2006; 7: 524 – 537.

Al-Bassam J and Corbett KD. α-Tubulin acetylation from the inside out. PNAS. 2012; 109 (48): 19515 – 19516.

Alves MM, Burzynski G, Delalande J-M, Osinga J, van der Groot A, Dolgas AM *et al*. KBP interacts with SCG10, linking Goldberg – Scprintzen syndrome to microtubule dynamics and neuronal differentiation. Hum. Mol. Gen. 2010; 19 (18): 3642 – 3651.

Ayala R, Shu T and Tsai L-H. Trekking across the brain: The journey of neuronal migration. Cell. 2007; 128: 29 – 43.

Baas P and Qiang L. Neuronal microtubules: when the MAP is the roadblock. TRENDS in Cell Biology. 2005; 15 (4): 183 – 187.

Ban B, Jun M, Ryu H, Jang D, Ahmad ST and Lee J. Autophagy negatively regulates early axon growth in cortical neurons. Mol. Cell. Biol. 2013; doi: 10.1128/MCB.00627 – 13.

Barth S, Glick D and Macleod KF. Autophagy: assays and artifacts. J Pathol. 2010; 221 (2): 117 – 124.

Bartolomeo SB, Corazzari M, Nazio F, Oliverio S, Lisi G, Antonioli M *et al*. The dynamic interaction of AMBRA1 with the dynein motor complex regulates mammalian autophagy. JCB. 2010; 191 (1): 155 – 168.

Bernales S, McDonald KL and Walter P. Autophagy Counterbalances Endoplasmic Reticulum Expansion during the Unfolded Protein Response. PLoS Biology. 2006; 4 (12): 2311 - 2344.

Bicek AD, Tüzel E, Demtchouk A, Uppalapati M, Hancock WO, Kroll DM *et al*. Anterograde Microtubule Transport Drives Microtubule Bending in LLC-PK1 Epithelial Cells. Mol Biol Cell. 2009; 20: 2943 – 2953.

Bondallaz P, Barbier A, Soehrman S, Grenningloh G and Riederer BM. The Control of Microtubule Stability In Vitro and in Transfected Cells by MAP1B and SCG10. Cell Motil Cytoskelleton. 2006; 63: 681 – 695.

Bjørkøy G, Lamark T, Pankiv S, øvervatn A, Brech A and Johansen T. Monitoring Autophagy Degradation of p62/SQSTM1. Methods Enzymol. 2009; 452: 181 – 197.

Brito DA, Strauss J, Magidson V, Tikhonenko I Khodjakov A and Koonce MP. Pushing forces drive the comet-like motility of microtubule arrays in *Dictyostelium*. Mol Biol Cell. 2005; 16: 3334 – 3340.

Cecconi F, Bartolomeo SD, Nardacci R, Fuoco C, Corazzari M, Guinta L *et al.* A Novel Role for Autophagy in neurodevelopment. Autophagy. 2007; 3 (5): 506 – 508.

Collins PY, Patel V, Joestl SS, March D, Insel TR and Daar AS. Grand challenges in global mental health. Nature. 2011; 479: 27 – 30.

Conde C and Cáceres A. Microtubule assembly, organization, and dynamic in axons and dendrites. Nat Rev Neurosci. 2009; 10: 319 – 332.

Cuervo AM. Autophagy in sickness and in health. Tends Cell Biol. 2004; 14: 70 – 77.

Dujardin DL, Barnhart LE, Stehman SA, Gomes ER, Gundersen GG and Vallee RB. A role for cytoplasmic dynein and LIS1 in directed cell movement. J Cell Biol. 2003; 163: 1205 – 1211.

Ehninger D, Li W, Fox K, Stryker MP and Silva, AJ. Reversing neurodevelopmental disorders in adults. Neuron. 2008; 60 (6): 950 – 960.

Eriksson M, Samuelsson H, Samuelsson E-B, Liu L, McKeehan WL, Benedikz E and Sundström E. The NMDAR subunit NR3A interacts with microtubule-associated protein 1S in the brain. Biochem. Biophys. Res. Commun. 2007; 361: 127 – 132.

Falconer DS. Two new mutants, 'trembler' and 'reeler', with neurological actions in the house mouse (Mus musculus L.). J Genet. 1951; 50: 192–201.

Faller EM, Villeneuve TS and Brown DL. MAP1a associate light chain 3 increases microtubule stability by suppressing microtubule dynamics. Mol Cell Neurosci. 2009; 41: 85 – 93.

Folsom TD and Fatemi SH. The involvement of Reelin in neurodevelopmental disorders. Neuropharmacology. 2013; 68: 122 – 135.

Fridolfsson HN, Ly N, Meyerzon M and Starr DA. UNC-83 coordinates kinesin-1 and dynein at the nuclear envelope during nuclear migration. Dev Biol. 2010; 338: 237 – 250.

Gaiano N. Strange Bedfellows: Reelin and Notch Signalling Interact to Regulate Cell Migration in the Developing Neocortex. Neuron. 2008; 60: 189 – 191.

Gaspard N and Vanderhaeghen P. From stem cells to neural networks: recent advances and perspectives for neurodevelopmental disorders. Dev Med Child Neurol. 2010; 53: 13 – 17.

Geraldo S and Gordon-Weeks PR. Cytoskeletal dynamics in growth-cone steering. J Cell Sci. 2009; 122: 3595 – 3604.

Guerrier S, Coutinho-Budd J, Sassa T, Gresset A, Jordan VC and Chen K. The F-BAR Domain of srGAP2 Induces Membrane Protrusions Required for Neuronal Migration and Morphogenesis. Cell. 2009; 138: 990 – 1004.

Hanson TE and Johansen T. Following autophagy step by step. BMC Biology. 2011; 9 (39): 1 – 4.

Hawkins T, Mirigian M, Yasar MS and Ross JL. Mechanics of Microtubules. J Biomech. 2010; 43:23 – 30.

Hara Tm, Nakamura K, Matsui M, Yamomoto A, Nakahara Y, Suzuki-Migishima R *et al.* Suppression of basal autophagy in neural cells causes neurodegenerative disease in mice. Nature. 2006; 441: 885 – 889.

Heng JI, Chariot A and Nguyen L. Molecular layers underlying cytoskeletal remodelling during cortical development. Trends in Neuroscience. 2009; 33(1): 38 – 44.

Heintzmann R and Cremer CG. Laterally modulated excitation microscopy: improvement of resolution by using a diffraction grating. BigioJJ, Schneckenburger H, Slavik J, Svanberg K, Viallet PM, editors. SPIE digital Library. 1999; 185 – 196.

Herz J and Chen Y. Reelin, lipoprotein receptors and synaptic plasticity. Nat Neurosci. 2006; 7: 850 – 859.

Kalny MI and Propst F. In Vivo and in Vitro Characterization of MAP1S Function. 2008. PhD thesis.

Kato M and Dobyns WB. Lissencephaly and the neuronal molecular basis of neuronal migration. Hum. Mol. Genet. 2003; 12: 89 – 96.

Katsumata K, Nishiyama J, Inoue T, Mizushima N, Tajeda J and Yuzaki M. Dynein- and activity-dependent retrograde transport of autophagosomes in neuronal axons. Autophagy. 2010; 6 (3): 378 – 385.

Kholmanskikh SS, Koeller HB, Wynshaw-Boris A, Gomez T, Letoumeau PC and Ross ME. Calcium dependent interaction of Lis1 with IQGAP1 and Cd42 promotes neuronal motility. Nat Neurosci. 2006; 9: 50 – 57.

Kimura S, Noda T and Yoshimori T. Dynein-Dependent Movement of Autophagosomes Mediates Efficient Encounters with Lysosomes. Cell Struct Funct. 2008; 33: 109 – 122.

Kinnear CJ. Molecular genetic strategies to identify Obsessive-compulsive disorder (OCD) and schizophrenia candidate genes in a South African sub-population group. 2007; PhD thesis, Stellenbosch University, South Africa.

Klionsky DJ. The molecular machinery of autophagy: unanswered questions. J Cell Sci. 2005; 118: 7 – 18.

Komatsu M, Waguri S,Chiba T, murata S, Iwata J, Tanida I *et al.* Loss of autophagy in the central nervous system causes neurodegeneration in mice. Nature. 2006; 441 (15): 880 – 884.

Kumada T, Lakshmana MK and Komuro H. Reversal of Neuronal Migration in a Mouse Model of Fetal Alcohol Syndrome by Controlling Second-Messenger Signalings. J Neurosci. 2006; 26 (3): 742 – 756.

Kwan KY, Sestan N and Anton ES. Transcriptional co-regulation of neuronal migration and laminar identity in the neocortex. Development. 2012; 139: 1535 – 1546.

Lakatosova S and Ostatnikova D. Reelin and its complex involvement in brain development and function. The Int J Biochem Cell Biol. 2012; 44: 1501 – 1504.

Lee K, Hwang S and Lee J. Neuronal Autophagy and Neurodevelopmental disorders. Exp Neurobiol. 2012; 22(3): 133 – 142.

Leemhuis J, Bouche E, Frotscher M, Henle F, Hein L, Herz J *et al.* Reelin Signals through Apolipoprotein E Receptor 2 and Cdc42 to Increase Growth Cone Motility and Filopodia Formation. J Neurosci. 2010; 30 (44): 14759 – 14772.

Li Y-H, Ghavampur S, Bondallaz P, Will L, Grenningloh G and Püschel AW. Rnd1 Regulates Axon Extension by Enhancing the Microtubule Destabilising Activity of SCG10. J. Biol. Chem. 2009; 284: 363 - 371.

Liang C-C, Park AY and Guan J-L. *In vitro* scratch assay: a convenient and inexpensive method for analysis of cell migration *in vitro.* Nature Protocols. 2007; 2: 329 – 333.

Loos B, Engelbrecht A-M, Lockshin RA, Klionsky DJ and Zakeri Z. The variability of autophagy and cell death susceptibility. Autophagy. 2013; 9(9): 1270 – 1285.

Malikov V, Kashina A and Rodionov V. Cytoplasmic Dynein Nucleates Microtubules to Organize Them into Radial Arrays In Vivo. Mol Biol Cell. 2004; 15: 2742 – 2749.

Manent J-B and LoTurco J. Reversing disorders of neuronal migration and differentiation in animal models. Jasper's Basic Mechanisms of the Epilepsies. 2012; Fourth Edition.

Manent J-B, Demarque M, Jorquera I, Pellegrino C, Ben-Ari Y, Aniksztein L *et al.* A Noncanonical Release of GABA and Glutamate Modulates Neuronal Migration. J Neurosci. 2005; 25 (19): 4755 – 4765.

Marín O, Valiente M, Ge X and Tsai L. Guiding Neuronal Cell Migrations. Cold Spring Harb Perspect Biol. 2010; 2:a001834.

May PA, Gossage JP, Marais A-S, Adnams CM, Hoyme HE, Jones KL *et al.* The epidemiology of fetal alcohol syndrome and partial FAS in a South African Community. Drug Alcohol Depend. 2007; 88: 259 – 271.

McGillewie L. Identification of novel ligands of WDR47, using yeast two-hybrid analysis. 2009. MSc thesis, Stellenbosch University, South Africa.

Mètin C, Vallee RB, Rakic P and Pradeep GB. Modes and Mishaps of Neuronal Migration in the Mammalian Brain. J Neurosci. 2008; 28 (46): 11746 – 11752.

Moon H.M. and Wynshaw-Boris A. Cytoskeleton in action: lissencephaly, a neuronal migration disorder. WIREs Dev Biol. 2013; 2: 229–245.

Morii H, Shiraishi-Yamaguchi Y and Mori N. SCG10, a Microtubule Destabilising Factor, Stimulates the Neurite Outgrowth by Modulating Microtubule Dynamics in Rat Hippocampal Primary Cultured Neurons. J Neurobiol. 2006; DOI 10.1002/neu: 1101 – 1250.

Myers KA, Tint I, Nadar CV, He Y, Black MM and Baas PW. Antagonistic forces generated by cytoplasmic dynein and myosin-II during growth cone turning and axonal retraction. Traffic. 2006; 7: 1333 – 1351.

Nocker SV and Ludwig P. The WD-repeat protein superfamily in Arabidopsis: conservation and divergence in structure and function. BMC Genomics. 2003; 4 (50): 1471 – 2164.

Osborn DPJ. The poor physical health of people with mental illness. Western J Med. 2001; 175: 329 – 333.

Ozawa T, Koide R, Nakata Y, Saitsu H, Matsumoto N, Takahashi K *et al.* A Novel WDR45 mutation in a patient with static encephalopathy of childhood with neurodegeneration in adulthood (SENDA). Am J Med Genet Part A. 2014; 9999: 1 – 3.

Petralia RS, Schwartz CM, Wang XY, Kawamoto EM, Mattson MP and Yao PJ. Sonic hedgehog promotes autophagy in hippocampal neurons. Biology Open. 2013; 2: 499 – 504.

Poulain FE and Sobel A. The microtubule network and neuronal morphogenesis: Dynamic and coordinated orchestration through multiple players. Mol Cell Neurosci. 2010; 43: 15 – 32.

Prince M, Patel V, Saxena S, Mai M, Maselko J, Phillips MR and Rahman A. No health without mental health. Global Mental Health 1. 2007; 370: 859 – 877.

Richards LJ. Axonal pathfinding mechanisms at the cortical midline in the development of the corpus callosum. Braz J Med Biol Res. 2002; 35: 1431 – 1439.

Rubensztein DC, Cuervo AM, Ravikumar B, Sarkar S, Korolchuk V and Klionsky DJ. In search of an "autophagometer". Autophagy. 2009; 5 (5): 585 – 589.

Saitsu H, Nishimura T, Muramatsu K, Kodera H, Kumada S, Sugai K *et al. De novo* mutations in the autophagy gene WDR45 cause static encephalopathy of childhood with neurodegeneration in adulthood. Nat Gen. 2013; 45 (4): 445 – 449.

Sasaki S, Shionoya A, Ishida M, Gambello MJ, Yingling J, Wynshaw-Boris A *et al.* A LIS1/NUDEL/Cytoplasmic Dynein Heavy Chain Complx in the Developing and Adult Nervous System. Neuron. 2000; 28: 681 – 696.

Schaar BT and McConnel SK. Cytoskeletal coordination during neuronal migration. PNAS. 2005; 102 (38): 13652 – 13657.

Schober JM, Komarova YA, Chagai OY, Akhmanova A and Borisy GG. Microtubule-targeting-dependent reorganization of filopodia. J Cell Sci. 2007; 120: 1235 – 1244.

Schuck S, Prinz WA, Thorn KS, Voss C and Walter P. Membrane expansion alleviates endoplasmic reticulum stress independently of the unfolded protein response. JCB. 2009; 187 (4): 525 – 536.

Shehata M, Matsumura H, Okubo-Suzuki R, Ohkawa N and Inokuchi K. Neuronal Stimulation Induces Autophagy in Hippocampal Neurons That Is Involved in AMPA Receptor Degradation after Chemical Long-Term Depression. J Neurosci. 2012; 32 (30): 10413 – 10422.

Smith TF, Gaitatzes C, Saxena K and Neer EJ. The WD repeat: a common architecture for diverse functions. Trends in Biochem Sci. 1999; 24: 181 – 185.
.
Solecki DJ, Model L, Gaetz J, Kapoor TM and Hatten ME. Pas6 signalling controls glial-guided neuronal migration. Nat Neurosci. 2004; 7 (11): 1195 – 1203.

Stirnimann CU, Petsalaki E, Russel RB and Muller CW. WD40 proteins propel cellular networks. Trends Biochem Sci. 2010; 35: 565 – 574.

Tanaka T, Semeo FF, Higgins C, Gambello MJ, Wynshaw-Boris A and Gleeson JG. Lis1 and doublecortin function with dynein to mediate coupling of the nucleus to the centrosome in neuronal migration. J Cell Biol. 2004; 165: 709 – 721.

Tanida I, Ueno T and Kominami E. LC3 conjugation system in mammalian autophagy. The Int J Biochem Cell Biol. 2004; 36: 2503 – 2518.

Tökèsi N, Lehotzky A, Horvath I, Szabo B, Olah J, Lau P *et al.* TPPP/p25 Promotes Tubulin Acetylation by Inhibiting Histone Deacetylase 6. J Biol Chem. 2010; 285 (23): 17896 – 17906.

Tomaštíková E, Cenklová V, Kohoutová L, Petrovská B, Váchová L, Halada P *et al.* Interactions of an Arabidopsis RanBPM homologue with LisH-CTLH domain proteins revealed high conservation of CTLH complexes in eukaryotes. BMC Plant Biology. 2012; 12 (83): 1 – 14.

Tomlinson M, Rudan I, Saxena S, Swartz L, Tsai A and Patel V. Setting priorities for global mental health research. Bull World Health Organ. 2009; 87: 438 – 446.

Tsai L-H and Gleeson JG. Nucleokinesis in Neuronal Migration. Neuron. 2005; 46: 383 – 388.

Ueda K and Komano T. Sequence-specific DNA damage induced by reduced Mitomycin C and 7-N-(*p*-hydroxyphenyl) Mitomycin C. Nucleic Acids Res. 1984; 12: 6673 – 6683.

Umeshima H, Hirano T and Kengaku M. Microtubule-based nuclear movement occurs independently of centrosome positioning in migrating neurons. PNAS. 2007; 104 (41): 16182 – 16187.

Vallee RB and Tsai L-H. The cellular roles of the lissencephaly gene LIS1, and what they tell us about brain development. Genes and Dev. 2006; 20: 1384 – 1393.

Vega IE, Hamano T, Propost JA, Grenningloh G and Yen S-H. Taxol and tau overexpression induced calpain-dependent degradation of the microtubule-destabilising protein SCG10. Exp Neurol. 2006; 202: 152 – 160.

Wang W, Lundin VF, Millan I, Zeng A, Chen X, Yang J *et al.* Nemitin, a Novel Map8/Map1s Interacting Protein with WD40 Repeats. PLoS ONE. 2012; 7 (4): e33094.

Webb JL, Ravikumar B and Rubinsztein DC. Microtubule disruption inhibits autophagosome-lysosome fusion: implications for studying the roles of aggresomes in polyglutamine diseases. The Int J Biochem Cell Biol. 2004; 36: 2541 – 2550.

Westerlund N, Zdrojewska J, Padzik A, Komulainen E, Bjorkblom B, Ranniko E *et al.* Phosphorylation of SCG10/stathmin-2 determines multipolar stage exit and neuronal migration rate. Nat Neurosci. 2011; 14 (3): 305 – 315.

Wolrd Health Organization (WHO). Mental Health Atlas, South Africa: 2011; Department of Mental Health and Substance Abuse.

Wynshaw-Boris A, Pramparo T, Youn YH and Hirotsune S. Lissencephaly: Mechanistic insights from animal models and potential therapeutic strategies. Semin Cell Develo Biol. 2010; 21: 823 – 830.

Xie R, Nguyen S, McKeehan WL and Liu L. Acetylated microtubules are required for fusion of autophagosoms with lysosomes. BMC Cell Biology. 2010; 11 (89): 1 – 12.

Xie Rui, Nguyen S, McKeehan K, Wang F, McKeehan WL and Liu L. Microtubule-associated Protein 1S (MAP1S) Bridges Autophagic Components with Microtubules and Mitochondria to Affect Autophagosomal Biogenesis and Degradation. J Biol Chem. 2011; 286 (12): 10367 – 10377.

Yamada M, Yoshida Y, Mori D, Takotoh T, Kengaku M, Umeshima H *et al.* Inhibition of calpain increases LIS1 expression and partially rescues in vivo phenotypes in a mouse model of lissencephaly. Nat Med. 2009; 15: 1202 – 1207.

Yamada M, Toba Sm Yoshida Y, Haratani K, mori D, Yano Y *et al.* Lis1 and NDE1 coordinate the plus-end-directed transport of cytoplasmic dynein. EMBO Journal. 2008; 27: 2471 – 2483.

Yamamoto M, Suzuki SO and Himeno M. The effects of dynein inhibition on the autophagic pathway in glioma cells. Neuropathology. 2010; 30: 1 – 6.

Youn YH, Pramparo T, Hirotsune S and Wynshaw-Boris A. Distinct Dose-Dependent Cortical Neuronal Migration and Neurite Extension Defects in *Lis1* and *Ndel1* Mutant Mice. J Neurosci. 2009; 29 (49): 15520 –15530.

Yamamoto M, Suzuki SO and Himeno M. The effects of dynein inhibition on the autophagic pathway in glioma cells. Neuropathology. 2010; 30: 1 – 6.

Yu L. Recent progress in autophagy. Cell Research. 2014; 24: 1 – 2.

Zhao Y, Huang Q, Yang J, Lou M, Wang A, Dong J *et al.* Autophagy impairment inhibits differentiation of glioma stem/progenitor cells. Brain Research. 2010; 1313: 250 – 258.

Addendum

In-house Sequence Alignment of WDR47 and Nemitin

In-house sequence alignment of WDR47 and Nemitin were performed in order to confirm whether WDR47 and Nemitin are the same protein or highly similar proteins. The results indicate that WDR47 and Nemitin are in fact the same protein (Figure A1).

```
WDR47     MTAEETVNVKEVEIIKLILDFLNSKKLHISMLALEKESGVINGLFSDDMLFLRQLILDGQ     60
Nemitin   MTAEETVNVKEVEIIKLILDFLNSKKLHISMLALEKESGVINGLFSDDMLFLRQLILDGQ     60
          ************************************************************


WDR47     WDEVLQFIQPLECMEKFDKKRFRYIILKQKFLEALCVNNAMSAEDEPQHLEFTMQEAVQC    120
Nemitin   WDEVLQFIQPLECMEKFDKKRFRYIILKQKFLEALCVNNAMSAEDEPQHLEFTMQEAVQC    120
          ************************************************************


WDR47     LHALEEYCPSKDDYSKLCLLLTLPRLTNHAEFKDWNPSTARVHCFEEACVMVAEFIPADR    180
Nemitin   LHALEEYCPSKDDYSKLCLLLTLPRLTNHAEFKDWNPSTARVHCFEEACVMVAEFIPADR    180
          ************************************************************


WDR47     KLSEAGFKASNNRLFQLVMKGLLYECCVEFCQSKATGEEITESEVLLGIDLLCGNGCDDL    240
Nemitin   KLSEAGFKASNNRLFQLVMKGLLYECCVEFCQSKATGEEITESEVLLGIDLLCGNGCDDL    240
          ************************************************************


WDR47     DLSLLSWLQNLPSSVFSCAFEQKMLNIHVDKLLKPTKAAYADLLTPLISKLSPYPSSPMR    300
Nemitin   DLSLLSWLQNLPSSVFSCAFEQKMLNIHVDKLLKPTKAAYADLLTPLISKLSPYPSSPMR    300
          ************************************************************


WDR47     RPQSADAYMTRSLNPALDGLTCGLTSHDKRISDLGNKTSPMSHSFANFHYPGVQNLSRSL    360
Nemitin   RPQSADAYMTRSLNPALDGLTCGLTSHDKRISDLGNKTSPMSHSFANFHYPGVQNLSRSL    360
          ************************************************************


WDR47     MLENTECHSIYEESPERDTPVDAQRPIGSEILGQSSVSEKEPANGAQNPGPAKQEKNELR    420
Nemitin   MLENTECHSIYEESPERDTPVDAQRPIGSEILGQSSVSEKEPANGAQNPGPAKQEKNELR    420
          ************************************************************


WDR47     DSTEQFQEYYRQRLRYQQHLEQKEQQRQIYQQMLLEGGVNQEDGPDQQQNLTEQFLNRSI    480
Nemitin   DSTEQFQEYYRQRLRYQQHLEQKEQQRQIYQQMLLEGGVNQEDGPDQQQNLTEQFLNRSI    480
          ************************************************************


WDR47     QKLGELNIGMDGLGNEVSALNQQCNGSKGNGSNGSSVTSFTTPPQDSSQRLTHDASNIHT    540
Nemitin   QKLGELNIGMDGLGNEVSALNQQCNGSKGNGSNGSSVTSFTTPPQDSSQRLTHDASNIHT    540
          ************************************************************


WDR47     STPRNPGSTNHIPFLEESPCGSQISSEHSVIKPPLGDSPGSLSRSKGEEDDKSKKQFVCI    600
Nemitin   STPRNPGSTNHIPFLEESPCGSQISSEHSVIKPPLGDSPGSLSRSKGEEDDKSKKQFVCI    600
          ************************************************************


WDR47     NILEDTQAVRAVAFHPAGGLYAVGSNSKTLRVCAYPDVIDPSAHETPKQPVVRFKRNKHH    660
Nemitin   NILEDTQAVRAVAFHPAGGLYAVGSNSKTLRVCAYPDVIDPSAHETPKQPVVRFKRNKHH    660
          ************************************************************


WDR47     KGSIYCVAWSPCGQLLATGSNDKYVKVLPFNAETCNATGPDLEFSMHDGTIRDLAFMEGP    720
```

134

```
Nemitin     KGSIYCVAWSPCGQLLATGSNDKYVKVLPFNAETCNATGPDLEFSMHDGTIRDLAFMEGP   720
            ************************************************************

WDR47       ESGGAILISAGAGDCNIYTTDCQRGQGLHALSGHTGHILALYTWSGWMIASGSQDKTVRF   780
Nemitin     ESGGAILISAGAGDCNIYTTDCQRGQGLHALSGHTGHILALYTWSGWMIASGSQDKTVRF   780
            ************************************************************

WDR47       WDLRVPSCVRVVGTTFHGTGSAVASVAVDPSGRLLATGQEDSSCMLYDIRGGRMVQSYHP   840
Nemitin     WDLRVPSCVRVVGTTFHGTGSAVASVAVDPSGRLLATGQEDSSCMLYDIRGGRMVQSYHP   840
            ************************************************************

WDR47       HSSDVRSVRFSPGAHYLLTGSYDMKIKVTDLQGDLTKQLPIMVVGEHKDKVIQCRWHTQD   900
Nemitin     HSSDVRSVRFSPGAHYLLTGSYDMKIKVTDLQGDLTKQLPIMVVGEHKDKVIQCRWHTQD   900
            ************************************************************

WDR47       LSFLSSSADRTVTLWTYNG          919
Nemitin     LSFLSSSADRTVTLWTYNG          919
            ******************
```

Figure A1: In-house sequence alignment confirming that WDR47 is Nemitin.

Mitomycin C Assessment

Prior to the execution of the neuronal migration assay, an experiment using Mitomycin C and Hoechst 33342 nuclear stain was performed in order to verify that the Mitomycin C concentration of 10 µg/ml is sufficient to inhibit neuronal proliferation. Two groups existed: an untreated control group, and a Mitomycin C group, treated with 10 µg/ml of Mitomycin C. The choice for this concentration was guided by the manufacturer's protocol (Sigma-Aldrich). Three random fields of view per group were captured at 0 hours and 24 hours after treatment (Figure A2). Cell counts were performed and the percentage increase in cell number over the 24 h period was determined for each group (Figure A3). These results indicate that 10 µg/ml of Mitomycin C successfully inhibits GT1-7 neuronal proliferation.
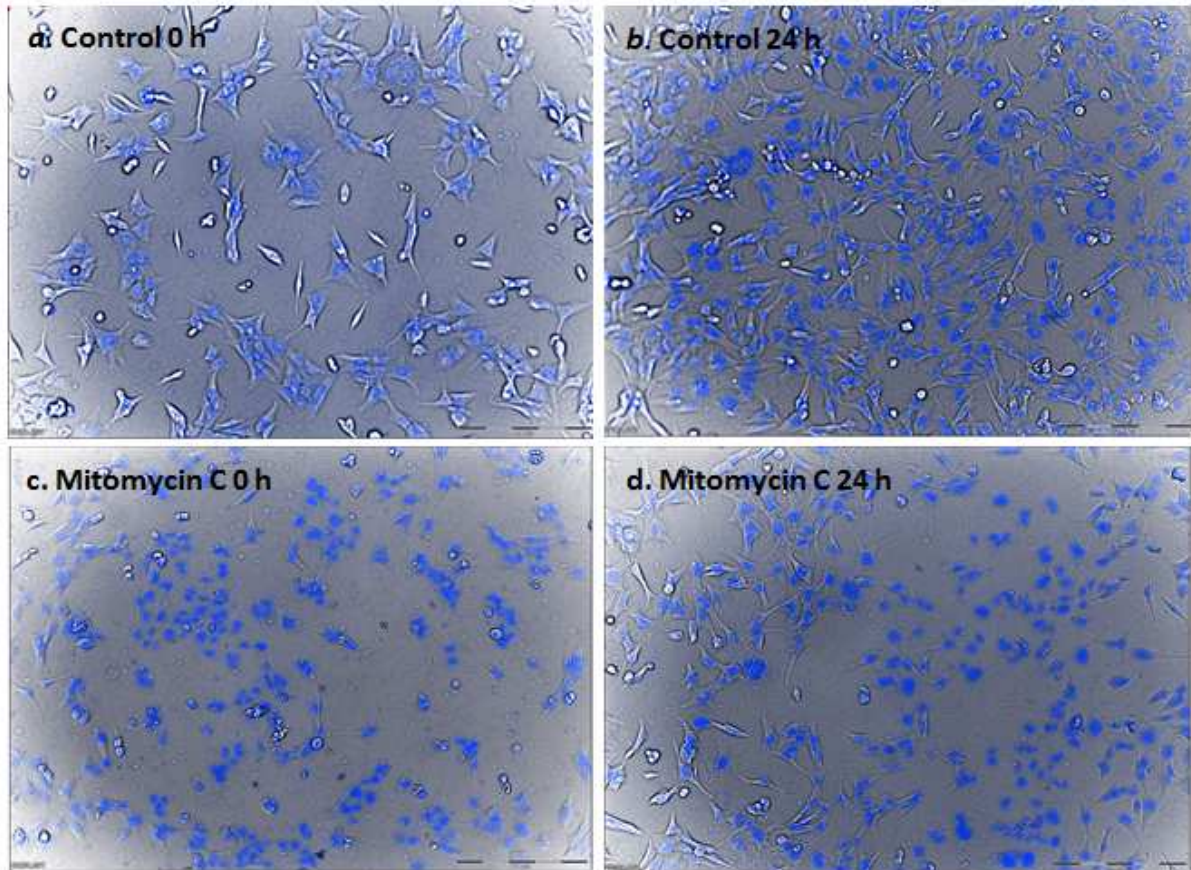
Figure A2: Representative images of Mitomycin C assessment. Nuclei were counterstained with Hoechst 33342 for nuclear counts. Images of control and Mitomcyin C-treated cells were captured at 0 hours (*a, c*) and 24 hours (*b, d*) after treatment. Scale bar: 200 μm.
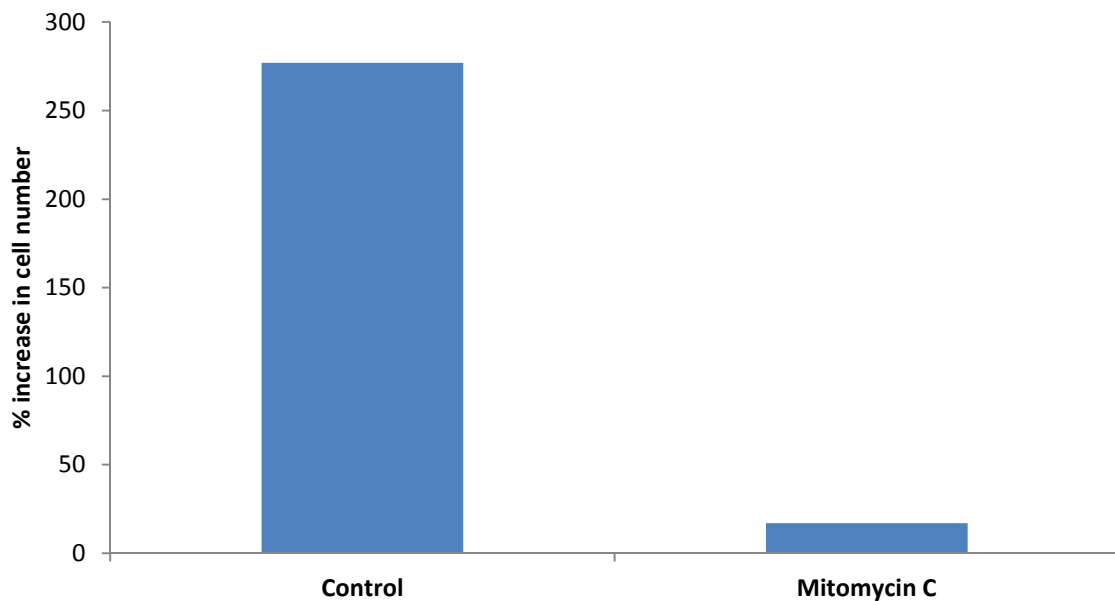

Figure A3: Percentage Increase in cell number 24 hours after treatment with 10 μg/ml Mitomycin C. Control cells increased by 277% while cells treated with Mitomycin C increased by 17%.

136